University of Cape Town

Department of Civil Engineering

# Extension and verification of the PWM_SA model to incorporate SANI-specific bioprocesses using experimental data from the Hong Kong SANI saline sewage treatment pilot plant.

Hope Thendo Mudau

Supervisor: A.Prof. David Ikumi


Submitted in partial fulfilment of the requirements for the degree of Master's of Science, Civil Engineering, specialising in Water Quality Engineering

April 2025

# Declaration:

1. I know that plagiarism is wrong. Plagiarism is to use another's work and to pretend that it is one's own.

2. I have not allowed, and will not allow, anyone to copy my work with the intention of passing it off as his or her own work.

3. This project is my own work.

4. I have included internet articles, books, or other material references used for this project.

Signed: Signed by candidate

Date: 2025-04-08

# Extension and verification of the PWM_SA model to incorporate SANI-specific bioprocesses using experimental data from the Hong Kong SANI saline sewage treatment pilot plant.

## Abstract

This study addresses water scarcity in South Africa's coastal regions, exacerbated by climatic, demographic, and pollution challenges. Cape Town's 2018 "Day Zero" crisis highlighted the need for innovative solutions. Adapting Hong Kong's SANI system, proven effective for saline wastewater treatment, offers a sustainable approach to conserve freshwater and enhance resilience. This study extends the Plant Wide Model for South Africa (PWM_SA) by integrating SANI-specific bioprocesses to evaluate its applicability in addressing these challenges.

The study's primary objectives included adapting the PWM_SA model to incorporate sulfate reduction, autotrophic denitrification, and nitrification processes characteristic of the SANI system, focusing on achieving accurate mass balance across key chemical species and overall internal consistency. Specifically, the model extension aimed to ensure mass balance verification across Chemical Oxygen Demand (COD), Sulfur (S), Phosphorus (P), and Nitrogen (N), and to verify the extended model using empirical data from the Hong Kong SANI pilot plant.

The methodology involved an extension of the PWM_SA model using the existing Gujer matrix framework, with the addition of a steady-state model to represent Biological Sulfate Reduction (BSR). This model component employed COD-based kinetics to capture the removal of biodegradable COD and sulfate, with sewage sludge serving as the carbon source. The model structure includes three key components: (1) a COD-based

anaerobic hydrolysis kinetics module that simulates the removal of biodegradable COD and sulfate under varying Hydraulic Retention Times (HRT) and Sludge Retention Times (SRT); (2) a stoichiometric module that balances key elements (C, H, O, N, P, S), COD, and charge, which enables the prediction of concentrations for essential parameters—including alkalinity, COD, sulfate ($SO_4^{2-}$), sulfide ($H_2S$), nitrate ($NO_3^-$), and Free Saline Ammonia (FSA)—across sulfate reduction and autotrophic denitrification stages; and (3) a mixed weak acid/base chemistry module, which accounts for inorganic carbon ($HCO_3^-$) and sulfide species ($H_2S/HS^-$), ensuring accurate pH predictions.

The biochemical processes for sulfate reduction and autotrophic denitrification were integrated into the matrix along with their corresponding stoichiometric and kinetic parameters, offering a detailed representation of the biochemical interactions and transformations occurring in the system. The Gujer matrix structure allowed for the systematic classification of components based on solubility, degradability, and organic or inorganic characteristics, facilitating model verification and consistency through elemental mass balance. The extended model was implemented and verified in the WEST software, utilizing experimental data from the SANI pilot plant in Hong Kong to align the model with real-world treatment conditions and verify the accuracy of kinetic rates and parameters. This approach established a reliable basis for modelling saline wastewater treatment within the PWM_SA framework.

The overall results of this study demonstrated that the adapted PWM _SA model, now incorporating SANI-specific bioprocesses achieved high accuracy in simulating COD, S, N, and P transformations within the treatment system, closely mirroring empirical data and ensuring robust mass balance across key elements. With a COD mass balance reaching 100% compared to a measured balance of 90%, the model shows strong consistency in predicting organic matter utilization, and component transformations through sulfate reduction, autotrophic denitrification, and nitrification. Additionally, the effluent COD values supported the model's predictive accuracy, although minor deviations underscored inher-

ent limitations in the steady-state approach for capturing dynamic effluent characteristics.

In conclusion, this study successfully integrated the SANI system's bioprocesses into the PWM_SA model, creating a robust framework for saline wastewater treatment in South Africa. Although the steady-state model provided meaningful insights, some limitations highlight the potential for future dynamic modelling to capture transient fluctuations and real-time responses to influent variability. This research establishes a critical foundation for the implementation of SANI-based saline sewage treatment in South Africa, supporting efforts to enhance water sustainability and manage pollution effectively in saline and water-stressed environments.

# Acknowledgements

This study is the culmination of effort and support from many individuals, and I would like to express my deepest gratitude to everyone who contributed to its completion. I would like to thank:

- My Lord and personal saviour, Jesus Christ, for His guidance, grace, and unfailing love throughout this journey. It is through His strength and wisdom that I have been able to complete this dissertation, and I give Him all the glory.
- I am deeply grateful to my supervisor, A/Prof. David Ikumi, for his mentorship, patience, and insightful feedback. Your support and encouragement have been invaluable in shaping the direction of this work.
- To my family, thank you for your unconditional love, prayers, and encouragement. Your faith in me and your sacrifices have made this achievement possible. To my friends and colleagues, I am grateful for your companionship, understanding, and motivation during the highs and lows of this process.
- I would also like to acknowledge The University of Cape Town for the resources and opportunities provided, and to the Department of Water and Sanitation (DWS) for their support and funding.
- Finally, I dedicate this work to everyone who believed in me and inspired me to persevere. I am eternally thankful to Jesus Christ, whose strength made my weakness perfect and this journey worthwhile.

# Contents

# List of Figures

# List of Tables

# List of Abbreviations

**WWTP** Waste Water Treatment Plant

**SANI** Sulfate Reduction, Autotrophic Denitrification, and Nitrification Integrated

**WAS** Waste Activated Sludge

**RAS** Return Activated Sludge

**SWTF** Sea Water Toilet Flushing

**AS** Activated Sludge

**IFAS** Integrated Fixed-film Activated Sludge

**AGS** Aerobic Granular Sludge

**SRB** Sulfate Reducing Bacteria

**SOB** Sulfur Oxidizing Bacteria

**BNR** Biological Nutrient Removal

**UV** Ultraviolet

**COD** Chemical Oxygen Demand

**SRUSB** Sulfate-Reducing Upflow Sludge Bed

**CHONPS** Carbon, Hydrogen, Oxygen, Nitrogen, Phosphorus, and Sulfur

**ASM2-3P** three-phase activated sludge model No.2

**IWA** International Water Association

**OHO** Ordinary Heterotrophic Organisms

**PAO** Polyphosphate Accumulating Organisms

**ANO** Ammonia Oxidising Organism

**PP** polyphosphate

**PHA** poly-3-hydroxyalkanoates

**BEPR** Biological Excess Phosphorus Removal

**TN** Total Nitrogen

**HRT** Hydraulic Retention Time

**TSS** Total Suspended Solids

**TOC** Total Organic Carbon

**AS** Acetotrophic Sulfidogens

**HS** Hydrogenotrophic Sulfidogens

**ADN** Autotrophic Denitrifiers

**BPO** Biodegradable Particulate Organics

**ASM** Activated Sludge Model

**DNA** Deoxyribonucleic Acid

**PCA** Principal Component Analysis

**GHG** Greenhouse Gas

**CBNR** Conventional Biological Nutrient Removal

**UPO** Unbiodegradable Particulate Organics

**SRT** solids retention time

**DO** Dissolved Oxygen

**STSTW** Sha Tin Sewage Treatment Works

**CAS** conventional activated sludge

**PE** Population Equivalents

**FMS** Fine Mesh Sieves

**MBBR** Moving Bed Biofilm Reactor

**BAF** Bed Biological Aerobic/Anoxic Filters

**ASM2-3P** Three-Phase Activated Sludge Model No. 2

**SDM-3P** Three-Phase Anaerobic Digestion Model

**IWA** International Water Association

**ISS** Inorganic Settleable Solids

**VFA** Volatile Fatty acids

**FBSO** Fermentable Biodegradable Soluble Organics

**FSA** Free and Saline Ammonia

**SCFA** Short-Chain Fatty Acids

**HDN** Heterotrophic Denitrifiers

**RBCOD** Readily Biodegradable COD

**SBCOD** Slowly Biodegradable COD

**USO** Unbiodegradable Soluble Organics

**WERF** Water Environment Research Foundation

**MBBR** Moving Bed Biofilm Reactor

# Chapter 1: Introduction

## 1.1 Background

Sustainable urban water management is a critical challenge faced by densely populated coastal cities around the world. Rapid urbanization, coupled with limited land resources and dwindling supplies of fresh water, necessitates innovative approaches to meet the water demands of urban populations while minimizing environmental impacts. This challenge is particularly acute in densely populated coastal cities like Hong Kong, which face unique constraints in terms of space and freshwater availability.[78] To address these challenges, Hong Kong has implemented alternative water supply strategies, including Sea Water Toilet Flushing (SWTF), since the 1950s.[79]

Seawater toilet flushing is a pioneering approach that has been practised in Hong Kong for over half a century. This approach involves using seawater for toilet flushing, resulting in the generation of saline sewage. Due to the usage of seawater, saline sewage has high Sulfur (S) content.[78] Therefore, it is necessary to develop a wastewater treatment technology based on the microbiology of the S cycle. The traditional Acetotrophic Sulfidogens (AS) method requires a substantial volume and generates excessive sludge[33,37] while processes like the Moving Bed Biofilm Reactor (MBBR)[52], Integrated Fixed-film Activated Sludge (IFAS)[65], and Aerobic Granular Sludge (AGS)[58] have been successfully implemented at full scale, however, they still face the issue of high sludge production. Furthermore, various conventional sludge treatment techniques, such as mechanical, ultrasonic, thermal, and ozone pre-treatment for excess sludge disintegration can be combined with sewage treatment processes to reduce sludge, however, they are often energy-intensive, costly, or require a significant amount of space.[25,55]

As a result of this predicament, there has been a growing trend in utilizing anaerobic and autotrophic slow-growing bacteria in mainstream treatment due to their benefits in

sludge reduction, space efficiency, and energy savings.[6,12,11] This led to the development of the Sulfate Reduction, Autotrophic Denitrification, and Nitrification Integrated (SANI) process, which has gained prominence in wastewater treatment research.[78] The SANI process is an innovative wastewater treatment method that leverages the properties of saline sewage to efficiently remove organic matter and contents like nitrate ($NO_3^-$) and S. It operates under anaerobic and anoxic conditions, employing Sulfate Reducing Bacteria (SRB) and autotrophic denitrifiers to achieve these objectives. This process utilizes sulfate in sewage, integrating the S cycle into the mainstream treatment between organic Carbon (C) and Nitrogen (N) removal steps.[10] The SANI process involves three biological reactions. In the first reaction which occurs in the anaerobic reactor, sulfate ($SO_4^{2-}$) is reduced to sulfide ($H_2S$) by SRB, while organic C is oxidized to carbon dioxide ($CO_2$) (which dissolves as bicarbonate ($HCO_3^-$)). The second reaction occurs in the anoxic reactor, ($H_2S$) is subsequently oxidized back to ($SO_4^{2-}$) by Sulfur Oxidizing Bacteria (SOB), while $NO_3^-$ is autotrophically reduced to $N_2$. This is followed by the third reaction which occurs in the aerobic reactor whereby ammonia ($NH_4^+$) is oxidized to $NO_3^-$ by autotrophic nitrifiers. This unique process, developed in response to the challenges posed by SWTF, has since demonstrated its potential for sustainable wastewater treatment and resource recovery.

The challenges and successes of the SWTF system in Hong Kong provide valuable insights for addressing water stress in other coastal cities, including those in South Africa. As South Africa faces its own water management challenges, there is a compelling need to explore the potential for implementing similar alternative water supply strategies. This research aims to expand upon the existing knowledge by investigating the feasibility of implementing a system-wide model that includes and tracks S and simulates the SANI process.

## 1.2 Problem Statement

Water scarcity is a critical problem in Cape Town and other coastal regions of South Africa.[24] Cape Town's "Day Zero" crisis in 2018 starkly demonstrated the severe impact of water shortages and highlighted the limitations of the city's existing water management systems.[50] The escalating water scarcity in South Africa is further exacerbated by pollution, overexploitation of resources, and the degradation of river catchments.[50] Factors such as rapid urbanization, industrial activities, agriculture, energy demands, and unintentional pollution place significant strain on the nation's water systems.[15] According to the 2018 National Water and Sanitation Master Plan, the country faces a projected $17\%$ water supply deficit by 2030 if sustainable solutions are not implemented.[41] Coastal regions are particularly affected, with many communities experiencing unreliable access to clean and sustainable freshwater sources.

Traditional freshwater supply systems are increasingly inadequate to meet the demands of rapidly growing urban populations, while energy-intensive alternatives such as desalination pose financial and environmental challenges. Without urgent intervention, water scarcity in South Africa will continue to intensify, jeopardizing the sustainability of urban water systems, the health of communities, and economic stability. This growing crisis underscores the need for innovative and sustainable water management strategies tailored to the unique challenges of South Africa's coastal regions.

The success of Hong Kong's SWTF system demonstrates its effectiveness in conserving freshwater.[46] This model could be replicated in South Africa's coastal regions, where freshwater is particularly scarce, especially during periods of drought. Implementing SWTF in cities like Cape Town, Durban, and Port Elizabeth could lead to significant freshwater savings while minimizing the environmental impact of water extraction from natural sources.

## 1.3 Aims and Objectives

The objective of this study is to refine the Plant Wide Model of South Africa (PWM _SA), which incorporates S-related processes, using empirical data from a SANI saline sewage treatment system, such as that used in the Hong Kong SANI pilot plant.[61] Key bio-processes, along with their necessary parameters, components, and kinetic rates, will be integrated into the existing PWM_SA model and implemented within the WEST (Mike powered by DHI) software for simulations.

**The project objectives are as follows:**

1. **Extend the PWM_SA model to include SANI processes:** This objective focuses on incorporating all relevant bioprocesses of the SANI system into the PWM_SA model in the WEST Software, encompassing key processes like sulfate reduction, autotrophic denitrification, and nitrification.

2. **Application of elemental mass and charge balances to evaluate the model for internal consistency:** This step involves performing a mass balance check on core elements, including Carbon, Hydrogen, Oxygen, Nitrogen, Phosphorus, and Sulfur (CHONPS), alongside Chemical Oxygen Demand (COD) and ionic charges. The verification process ensures that each bioprocess and reactor within the model maintains an elemental balance and consistency across the system.[30]

3. **Run simulations and verify the model consistency:** This involves evaluating the capability of the extended PWM_SA model in predicting the SANI system's performance by comparing its predictive outputs to previous results measured from a pilot scale SANI system.

## 1.4 Scope & Limitations

The primary aim of this project is to construct a mathematical model using the WEST wastewater treatment modelling software for the SANI system. This model builds upon

the existing PWM_SA model by incorporating essential elements such as BSR, autotrophic denitrification within the anoxic reactor, and nitrification and sulfide oxidation in the aerobic reactor. These additions are intended to enhance the model's functionality and improve its accuracy in simulating the bioprocesses unique to the SANI system.

The scope of this model is defined by its focus on steady-state conditions, wherein the system's behaviour and parameters reach stable equilibrium. This approach assumes that environmental conditions and operational variables remain constant over time, allowing for an in-depth assessment of the system's long-term performance under idealized stable conditions. Such steady-state models are particularly valuable for understanding typical system behaviour, guiding system design, and optimizing operational parameters under stable and predictable conditions.

However, the steady-state focus presents notable limitations. This model does not account for transient responses or dynamic fluctuations that occur in real wastewater treatment operations, such as variations in influent quality, flow rates, and environmental factors. Although steady-state models provide foundational insights, they lack the flexibility to represent the system's responsiveness to sudden changes or daily operational variability. Consequently, while this project aims to establish a reliable baseline model, it does not fully capture the complex dynamics of a live treatment plant environment. Furthermore, this study is a desk-based research project focused on developing a model of the SANI processes using the WEST platform. The experimental data for model verification is sourced from literature studies on the Hong Kong SANI system.[46] This data is reconciled and preprocessed using Microsoft Excel before being applied to verify the model developed in WEST.

The findings from this project serve as a groundwork for the future development of dynamic models, which would allow for a more comprehensive understanding by simulating the system's responses to fluctuating conditions. Developing such dynamic models is essential for applications where real-time variability plays a critical role in performance

assessment and control. Therefore, this project is constrained to steady-state simulations, aligning to establish a consistent and stable representation of the SANI system, but it emphasizes the need for future work to extend beyond steady-state assumptions for a more holistic analysis of wastewater treatment processes.

## 1.5 Dissertation Outline & Mind Map

This study begins with an introductory section that is divided into key segments: background, problem statement, aims and objectives, scope and limitations, and a study outline. The background provides the theoretical foundation for the study, establishing the context and purpose of the research. The problem statement then outlines the rationale for extending the PWM_SA model using empirical data from the SANI saline sewage treatment system at the Hong Kong SANI pilot plant. This is followed by a detailed outline of the project's aims and objectives, which guide the research focus. The scope and limitations section clarifies the project's boundaries, and the study outline summarizes the structure of the work.

The literature review follows the introductory chapter, providing a theoretical framework for the research. This review is organized into several chapters covering the SANI model's processes, its biological components, and development timeline, as well as highlighting existing gaps and potential areas for future enhancement. Additionally, the literature review explores the PWM_SA, setting a comparative basis for the study.

The methodology section then details the approach taken in this research, including the use of WEST software, the verification processes, and the confidence measures applied. This section provides a comprehensive account of the research design and methodological choices, ensuring clarity on how the study was conducted.

Following the methodology, the results and discussion section presents and interprets the study's findings. This section includes data analysis, discussion of results, and insights drawn from the findings, addressing the project's objectives and the implications of the

results. The dissertation concludes with a final section on conclusions and future recommendations, where the achievements of the research are evaluated, outcomes summarized, and potential directions for further investigation outlined. A visual representation of the dissertation outline is depicted in Figure 1.1.

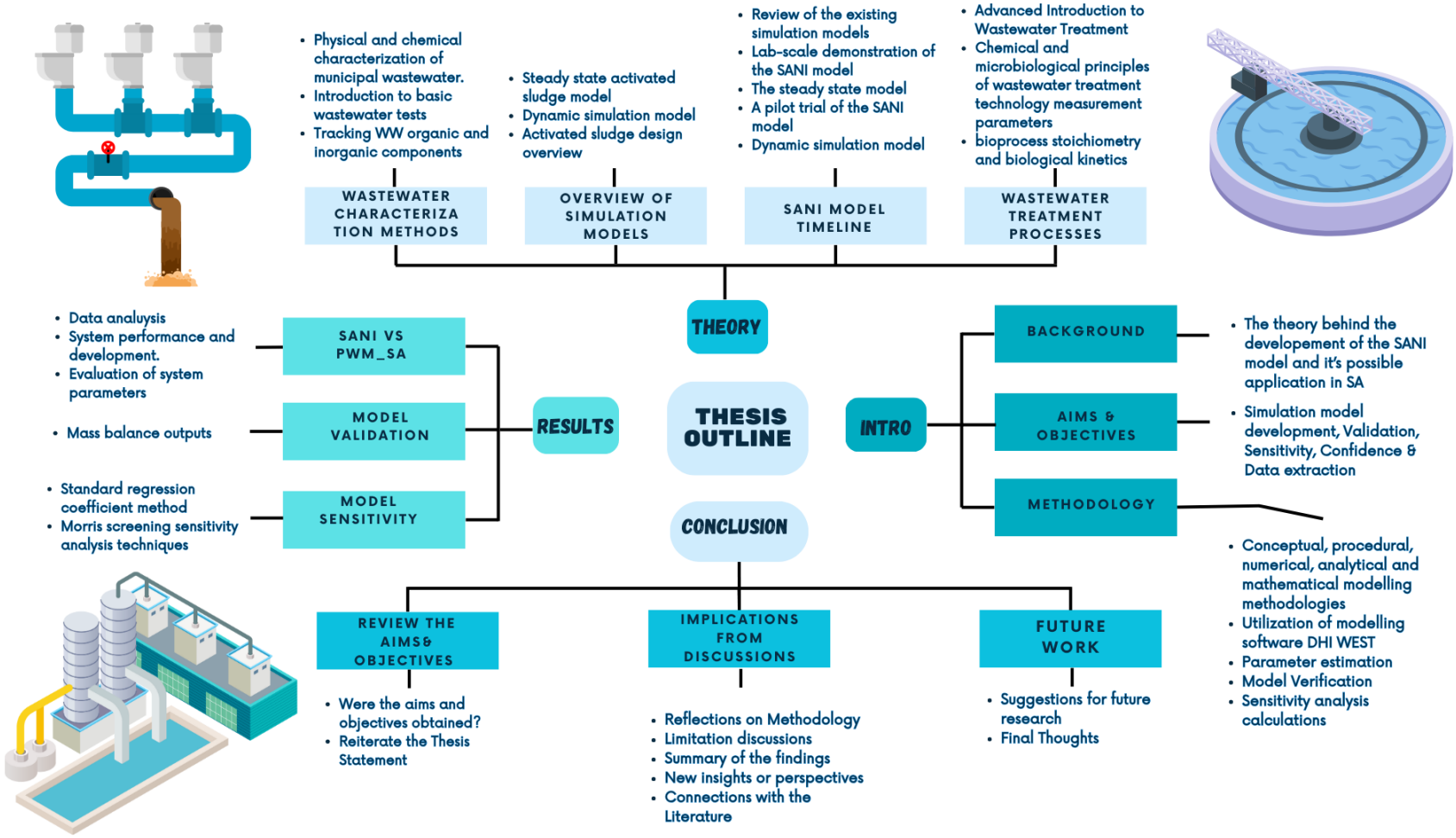


Figure 1.1 A visual representation of the dissertation structure.

# Chapter 2: Literature Review

This section explores the critical advancements in wastewater treatment technologies, focusing on the innovative SANI system. The review begins with an overview of conventional wastewater treatment processes, including preliminary, primary, and secondary treatments, to provide a foundational understanding of the challenges in managing saline wastewater. It then delves into the SANI model, highlighting its unique biochemical processes and environmental benefits, such as reduced sludge production and energy efficiency.

The review further examines existing studies on the SANI system, including lab-scale demonstrations, pilot trials, and modelling approaches, to evaluate its performance under varying conditions. Additionally, the PWM _SA is discussed as a basis for extending and adapting to the SANI system to address water management challenges in South Africa. Finally, the review identifies research gaps and prospective areas for enhancing the implementation and modelling of such systems, paving the way for sustainable and resilient wastewater treatment solutions.

## 2.1 Overview of a Waste Water Treatment Plant ( WWTP)

In a time characterized by fast urban growth and industrial expansion, handling wastewater has become a significant environmental concern.[51] The release of untreated or poorly treated wastewater into natural water sources poses serious risks to ecosystems and public well-being, underscoring the growing importance of wastewater treatment facilities.

This section delves into a brief exploration of a Waste Water Treatment Plant (WWTP). It offers a simple analysis of the various components, processes, and technologies employed in these facilities to effectively treat and purify wastewater before its discharge into receiving waters.

### 2.1.1 Preliminary and Primary Treatment

Preliminary treatment in a WWTP involves the initial steps to remove large debris and solids from the incoming wastewater.[72] This process typically includes screening, grit removal, and odour control.[14] Preliminary treatment helps protect downstream equipment and processes and ensures a smoother treatment of wastewater.

The screening process uses screens to sift through incoming wastewater, removing large solid items such as branches, plastics, and debris to prevent their entry into the treatment system.[72] Furthermore, comminutors, which are equipped with cutting mechanisms, are employed to disintegrate solids and incorporate them back into the wastewater flow. Following this step, the grit removal process utilizes grit chambers, facilitating the settling of heavier particulate matter that doesn't easily decompose or break down, while enabling the lighter organic solids to proceed to the next treatment unit.[67] This procedure minimizes pipe blockages and safeguards moving mechanical equipment from abrasion, wear, and downstream buildup. The subsequent stage addresses odour control through a combination of methods, including vapour-phase, liquid-phase, and operational techniques.[72] These approaches encompass activated carbon adsorption, the introduction of chemicals (such as chlorine), and operational enhancements, such as improved housekeeping practices.[28]

Primary treatment involves sedimentation and flotation.[62] The influent from screens and/or grit removal systems flows into a primary clarifier also known as a primary settling tank that is employed to remove solids (sludge) from the influent by sedimentation, remove scum from the influent by flotation and thicken solids for removal and further treatment.[64]

### 2.1.2 Secondary Treatment

The primary function of secondary wastewater treatment is to further purify and clean the wastewater that has undergone primary treatment.[72] This phase primarily relies on

biological processes and additional physical processes to remove dissolved and suspended organic matter, nutrients (like N and P), and remaining contaminants from the wastewater. Common secondary treatment methods include AS systems and trickling filters, which use microorganisms to break down pollutants.[63] The ultimate goal is to produce treated effluent that is significantly cleaner and less harmful to the environment, reducing the potential for pollution when discharged into natural water bodies.

In the AS process, wastewater is mixed with a culture of microorganisms in aeration tanks. These microorganisms, including bacteria and protozoa, form what is known as activated sludge.[62] Aeration is provided to ensure a continuous supply of O, promoting the growth and activity of these microorganisms. They metabolize and consume organic matter, transforming it into microbial biomass and harmless byproducts like $CO_2$ and water ($H_2O$). Afterwards, the activated sludge is separated from the treated water by settling in clarifiers. Some of the activated sludge is returned to the aeration tank to maintain a healthy microbial population and this is known as Return Activated Sludge (RAS), while the excess can be wasted or processed further and this is known as Waste Activated Sludge (WAS).

The AS process is composed of essential components that facilitate biological wastewater treatment. Within this process, biological reactors serve as the primary tanks where aerobic, anaerobic, or anoxic conditions are carefully controlled to cultivate a healthy mixed liquor.[67] This mixed liquor is pivotal in the biological treatment processes, targeting the removal of organic matter and potentially ($NH_4^+$), N, and P, depending on permit requirements. To support these biological reactions, a blower and diffuser system are integral, providing the necessary O for microorganisms to carry out their work efficiently. This system also promotes mixing, ensuring continuous contact between microorganisms and their food source, while keeping flocculated microorganisms in suspension, and aeration can be achieved through either mechanical means or diffused air. Additionally, secondary clarifiers are employed to separate and remove settleable solids from the wastewater, en-

suring clarified effluent.

In trickling filters, wastewater is distributed over a bed of porous media (like rocks or plastic material) where a biofilm of microorganisms develops.[1] As the wastewater trickles through this biofilm, microorganisms adhere to the media and consume the organic matter. Oxygen diffuses through the biofilm, supporting the microbial metabolism. Over time, this process reduces the organic content of the wastewater. Periodically, the biofilm may need to be scraped or otherwise managed to prevent it from becoming too thick, which could impede its effectiveness.[1]

### 2.1.3 Post-Secondary Treatment Processes

The secondary treatment plays a critical role in reducing the concentration of pollutants.[1] However, to achieve stringent water quality standards and meet specific treatment goals, further treatment steps are often required. This section explores the post-secondary treatment processes employed in wastewater treatment, addressing their significance, implementation, and safeguarding environmental and public health.[7]

Tertiary treatment emerges as an advanced echelon of purification that transcends secondary treatment. Its primary focus lies in the removal of precise contaminants, mostly heavy metals, and chemical contaminants - with most of the N and (P) removed in secondary treatment.[7] Moreover, tertiary treatment often encompasses the deployment of advanced filtration methods and supplementary disinfection procedures to ensure that the treated water aligns seamlessly with the most exacting water quality regulations.[8] These tactical interventions are judiciously tailored to improve contaminant removal or enhance settling properties within the wastewater, aligning treatment strategies with the distinctive composition of the effluent.

While disinfection is a salient component of secondary treatment, the tertiary stage may warrant supplementary disinfection measures to ensure the treated water is devoid of harmful microorganisms. Techniques such as chlorination, Ultraviolet (UV) radiation, and

ozonation are strategically applied to guarantee the microbiological safety of the effluent.[7]

In scenarios where wastewater is earmarked for non-potable reuse, encompassing applications like irrigation, industrial processes, or groundwater recharge, advanced treatment processes come to the fore.[39] These sophisticated methodologies span reverse osmosis, UV disinfection, activated carbon adsorption, and a gamut of specialized techniques.[7] These endeavours are undertaken with precision to meet the stringent quality standards mandated by intended reuse applications. The culminating phase in the wastewater treatment odyssey entails the responsible distribution of the treated water. This may involve compliant discharge into a receiving water body, meticulously adhering to stringent environmental regulations. Conversely, it may involve the orchestrated allocation of treated water for specific reuse applications, a decision contingent upon local policies and the specific objectives of the treatment facility.

## 2.2 The Sulfate Reduction, Autotrophic Denitrification and Nitrification Integrated (SANI) Model

Saline sewage produced through seawater flushing is a distinctive type of wastewater characterized by its high salt content.[44] Saline sewage originates from the utilization of seawater for flushing toilets, a practice employed in some coastal regions, such as Hong Kong, to conserve freshwater resources.[59] It contains a significantly elevated concentration of dissolved salts which gives it its characteristic salinity. Additionally, this type of sewage often exhibits a unique ratio of COD to S, with a typical value of 2.4 mg COD/mg S.[78] The presence of such high salinity levels in this sewage necessitates specialized treatment processes before it can be safely discharged or reused, as its high salt content can be detrimental to the environment and conventional wastewater treatment systems.

The SANI configuration can be particularly effective in treating saline sewage, especially because it contains high S content.[45] It is designed to efficiently remove multiple contaminants from wastewater in a single integrated system. The SANI model combines

three key biological processes: sulfate reduction, autotrophic denitrification, and nitrification, all working together to treat wastewater effectively as illustrated in Figure 2.2.[78]

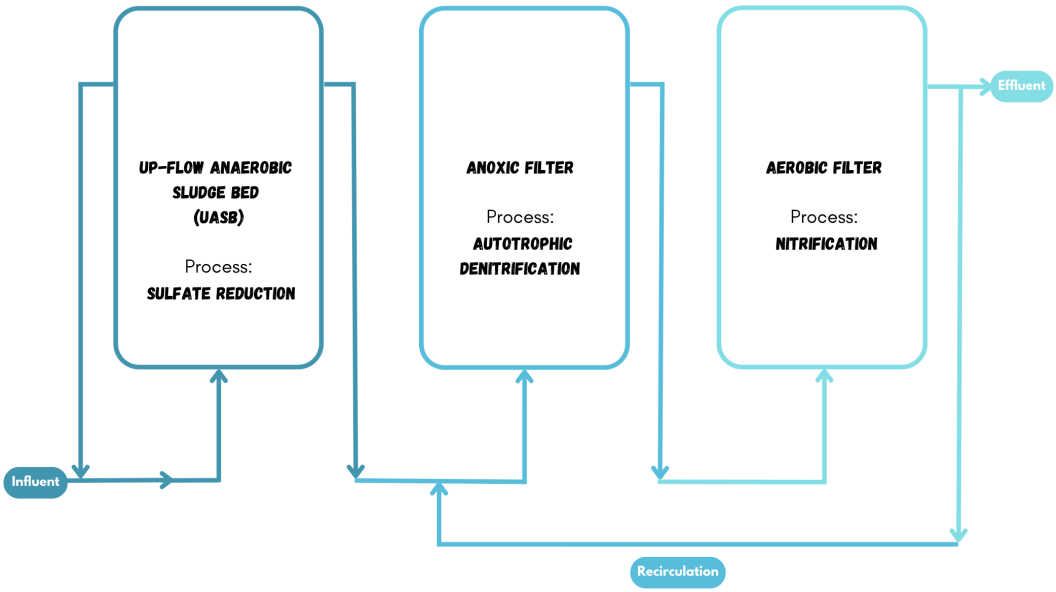


Figure 2.1 A simplified illustration of the SANI process.[78]

This configuration is well-suited for such scenarios because it leverages microbial processes that specialize in handling high salinity and elevated S levels. The SRB within the SANI system plays a crucial role by converting $SO_4^{2-}$ into $H_2S$, which not only reduces the $SO_4^{2-}$ concentration but also facilitates the removal of other contaminants. Furthermore, the integrated design of the SANI incorporates autotrophic denitrification and nitrification processes, enabling the efficient removal of N compounds, which are often found in sewage. Therefore, the SANI model offers a comprehensive and environmentally sustainable solution for the treatment of saline sewage, effectively addressing both the salinity and S challenges inherent in this type of wastewater.[46] Detailed descriptions of the processes involved in the SANI system are provided in the chapters below and more explicitly in Section 2.3.

The SANI model integrates these three processes into a single treatment system, creating a synergistic effect that enhances the removal of various contaminants, including S, N compounds, and other organic matter. This integrated approach offers several advantages,

such as reduced energy consumption, improved treatment efficiency, and a smaller physical footprint compared to traditional wastewater treatment methods.[78] Overall, the SANI configuration represents an innovative and sustainable solution for wastewater treatment, addressing multiple water quality challenges simultaneously while minimizing environmental impacts.[79] It has the potential to play a significant role in advancing the field of wastewater treatment and promoting environmentally responsible practices.[43]

Saline sewage generated through seawater flushing is a unique type of wastewater with high salt content.[44] This type of sewage is produced by using seawater for toilet flushing, a method applied in some coastal areas, such as Hong Kong, to conserve freshwater resources.[59] Saline sewage is characterized by its elevated concentration of dissolved salts, giving it a distinct salinity profile. Additionally, it typically exhibits a specific COD to S ratio, commonly around 2.4 mg COD/mg S.[78] Due to its high salt concentration, saline sewage requires specialized treatment processes before safe discharge or reuse, as conventional wastewater treatment systems are often not equipped to handle such high salinity levels, which can be harmful to the environment.

The SANI configuration is especially effective for treating saline sewage, particularly due to its ability to process the high S content typically found in this wastewater.[45] The SANI system integrates three biological processes—sulfate reduction, autotrophic denitrification, and nitrification—into a single treatment framework, as shown in Figure 2.2.[78]

This configuration is particularly well-suited for treating saline sewage, as it uses microbial processes optimized for environments with high salinity and S levels. Within the SANI system, SRB convert $SO_4^{2-}$ into $H_2S$, reducing the $SO_4^{2-}$ concentration and facilitating the removal of other contaminants. The inclusion of autotrophic denitrification and nitrification in the SANI system further enables the efficient removal of N compounds, which are often present in sewage. Consequently, the SANI model provides a comprehensive and sustainable solution for saline sewage treatment, effectively addressing both salinity and S content issues.[46]. This integrated approach offers several advantages, such

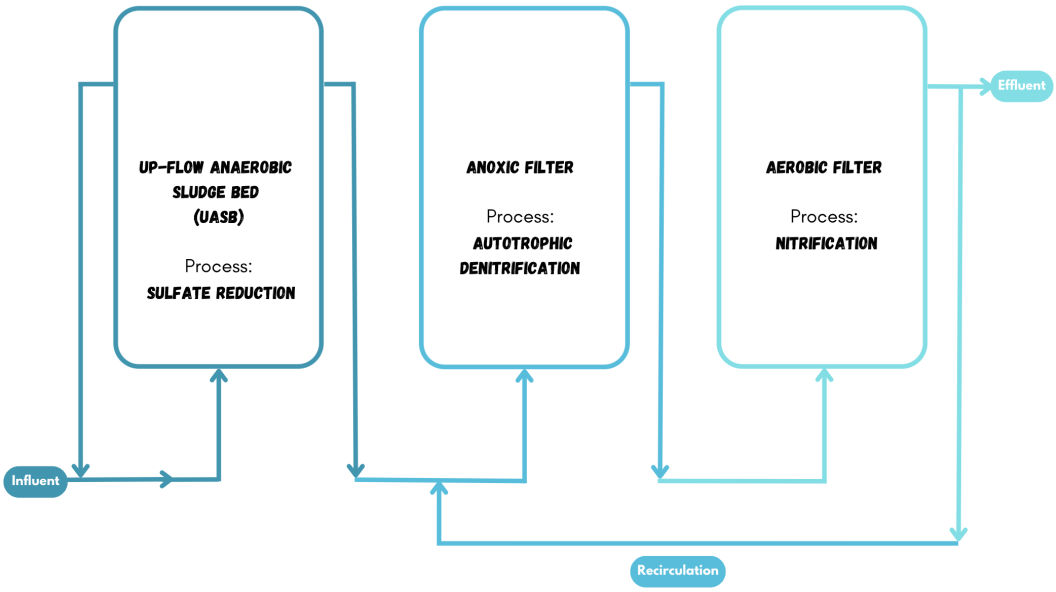


Figure 2.2 A simplified illustration of the SANI process.[78]

as reduced energy consumption, improved treatment efficiency, and a smaller physical footprint than conventional wastewater treatment methods.[78] Overall, the SANI configuration presents an innovative and environmentally sustainable solution for wastewater treatment, addressing diverse water quality challenges while minimizing environmental impact.[79] This model has significant potential to advance wastewater treatment practices and promote environmentally responsible approaches in the field.[43] Detailed descriptions of these processes are provided in the following chapters, particularly in section 2.3

### 2.2.1 Sulfate-Reducing Upflow Sludge Bed (SRUSB)

The SRUSB is an anaerobic wastewater treatment component in the SANI configuration in which microorganisms break down organic matter, it operates by directing wastewater upward.[81] As wastewater flows against gravity, solid particles settle to form a sludge bed at the bottom of the reactor. Anaerobic bacteria attached to this sludge bed digest organic compounds in the wastewater. This reactor offers efficient organic pollutant removal, reduced energy consumption compared to aerobic systems, and the valuable byproduct of biogas generation.[28]

Within the SRUSB's anaerobic environment, SRB play a crucial role in sulfate reduction.[60] These specialized microorganisms utilize the $SO_4^{2-}$ present in the influent wastewater as an electron acceptor in the absence of O.[56] As organic matter flows upward through the reactor, SRB enzymatically reduce $SO_4^{2-}$ ions, breaking them down into sulfide ions ($S^{2-}$). This conversion of $SO_4^{2-}$ to $S^{2-}$ not only aids in $SO_4^{2-}$ removal from the wastewater but also leads to the precipitation of other compounds in the wastewater. The generated $S^{2-}$ interacts with metal ions and forms insoluble metal sulfides, effectively reducing the concentrations of both $SO_4^{2-}$ and certain metals in the treated wastewater.[71] Thus, sulfate reduction in the SRUSB reactor contributes to the removal of $SO_4^{2-}$ contaminants while also facilitating the anaerobic digestion of organic matter, making it a valuable component of the wastewater treatment process. The sulfide-rich effluent from the SRUSB can be beneficially utilized in the subsequent anoxic reactor of a wastewater treatment system.[56]

### 2.2.2 Anoxic Reactor

An anoxic reactor is a specialized component within wastewater treatment systems, intentionally designed to foster an environment devoid of molecular O, a condition known as anoxic.[44] This deliberate absence of O is crucial for enabling the efficient removal of N compounds, specifically $NO_3^-$ and $NO_2^-$.[29] In contrast to aerobic conditions characterized by abundant O presence, an anoxic reactor sustains conditions where O is intentionally minimized or absent altogether.

Anoxic reactors host a diverse community of microorganisms, including denitrifying bacteria. These bacteria are responsible for the denitrification process, which involves the conversion of $NO_3^-$ and $NO_2^-$ ions into harmless $N_2$ or, in some cases, nitrous oxide ($N_2O$) gas.[42] To fuel this reduction process, $S^{2-}$ from the SRUSB influent acts as a natural electron donor, particularly in environments with low organic carbon content. As denitrification progresses, ($N_2$) is released into the atmosphere, effectively eliminating N compounds from the wastewater. Anoxic reactors contribute significantly to enhancing the quality of treated

wastewater by reducing the concentration of N compounds, making them indispensable in wastewater treatment facilities aiming to meet environmental regulations and safeguard aquatic ecosystems from N-related pollution.[19]

### 2.2.3 Aerobic Reactor

The purpose of the aerobic reactor is to promote the biological conversion of $NH_4^+$ and $NO_2^-$ and then into $NO_3^-$ through aeration and the activity of specific bacteria, reducing harmful N compounds in wastewater and improving effluent quality for discharge or further treatment.[29] The process begins with ammonia-oxidizing bacteria that utilize O from aeration to oxidize $NH_4^+$ present in the wastewater. This oxidation reaction transforms $NH_4^+$ into $NO_2^-$, releasing energy that sustains the bacteria's growth and activity. The chemical reaction is shown below:[44]

$$\mathrm{NH_4^+\,(Ammonia) + 1.5\,O_2\,(Oxygen)\ \rightarrow NO_2^-\,(Nitrite) + H_2O\,(Water) + H^+\,(Hydrogen\,ions)} \tag{2.1}$$

In the second step, nitrite-oxidizing bacteria further oxidize $NO_2^-$ to $NO_3^-$ within the biofilm. This step is crucial because it removes the intermediate $NO_2^-$ compound, which can be toxic to aquatic life, and converts it into $NO_3^-$, which is less harmful.[45] The chemical reaction of the second step is shown below:[44]

$$\mathrm{NO_2^-\,(Nitrite) + 0.5\,O_2\,(Oxygen)\ \rightarrow NO_3^-\,(Nitrate)} \tag{2.2}$$

Aeration is a critical aspect of the nitrification aerobic reactor.[56] It ensures a continuous supply of O to support the aerobic bacteria responsible for $NH_4^+$ and $NO_2^-$ oxidation. Adequate O levels are essential to maintain the metabolic activity of these bacteria and the progression of nitrification reactions.

Maintaining the appropriate pH level within the reactor is essential for optimal nitrification. Nitrification is most efficient within a specific pH range, typically around 7-8.[44]

Operators may adjust pH levels as needed to create suitable conditions for nitrifying bacteria and continually monitor the nitrification process in the aerobic reactor. Parameters such as $NH_4^+$, $NO_2^-$, and $NO_3^-$ concentrations are regularly measured, and adjustments to aeration rates, pH, and other operating parameters may be made to optimize nitrification performance. The treated effluent from the nitrification aerobic reactor is typically suitable for discharge into receiving waters or for further treatment, depending on regulatory requirements.[80,57]

## 2.3 Review Of The Existing SANI Models

In this chapter, we delve into an exploration of the various modelling approaches developed for the SANI system, conducting a comprehensive review and analysis of the lab-scale demonstration, pilot-plant SANI model, steady-state simulation model, and the advancements in the dynamic simulation model. The examination of the methodologies, results, conclusions, and identified gaps within each of these modelling frameworks is aimed at offering a comprehensive overview of the progress, challenges, and future directions in the field of SANI system modelling.

The primary obstacles encountered during the SANI process encompass five key areas: (1) the efficiency of sulfate reduction,[78] (2) the effectiveness of autotrophic denitrification using dissolved $H_2S$[45], (3) the process's performance in terms of COD and Total Nitrogen (TN) removal, as well as the production of excess sludge,[46] (4) the impact of recirculation flow on autotrophic denitrification, and (5) the accumulation of S within the system.[25] An exhaustive investigation was undertaken to address these challenges, which was structured into three distinct phases: (1) a laboratory-scale demonstration of the process utilizing synthetic saline wastewater[78], (2) the development of a steady-state model for process evaluation[45], and (3) a pilot trial of the process involving genuine saline sewage.[46] Figure 2.3 illustrates the timeline of when these studies were completed.

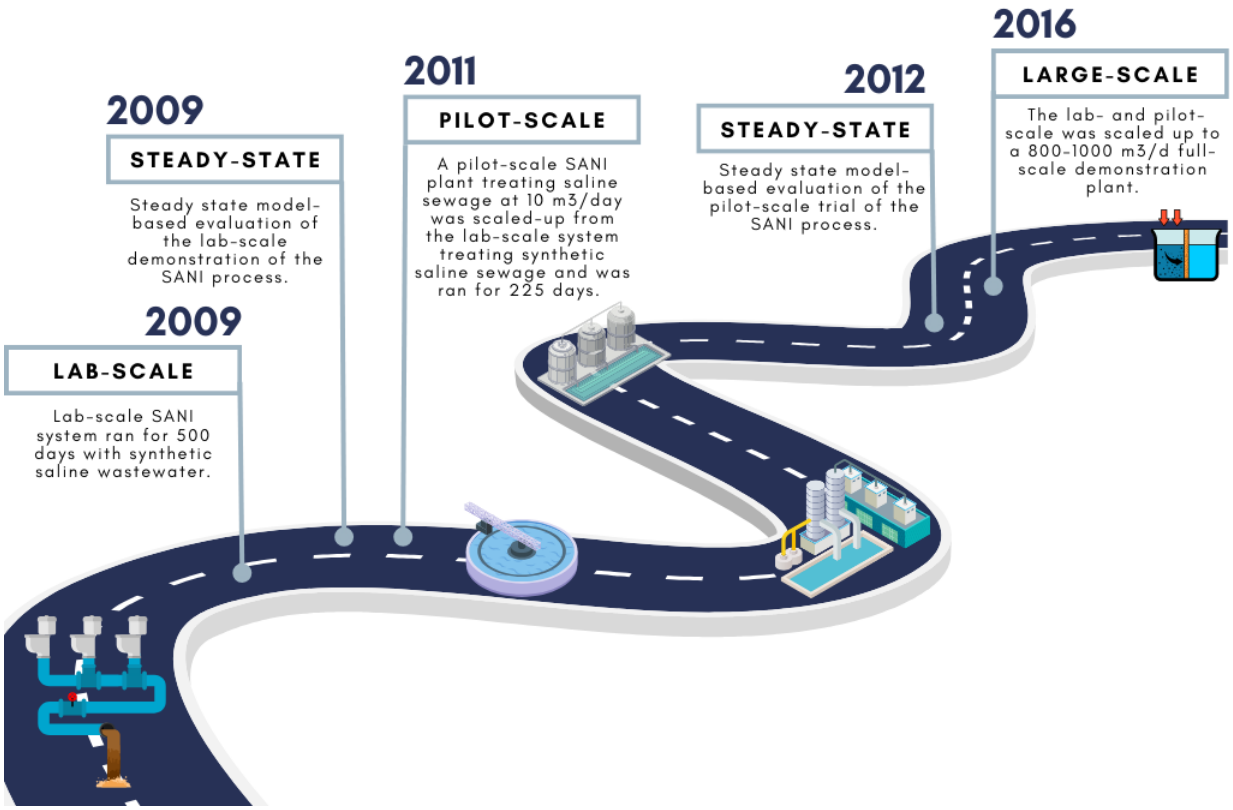


Figure 2.3 A timeline of the studies performed on the SANI system.[78,46,45,79]

### 2.3.1 Lab-Scale Demonstration of the SANI Model

A study was conducted in 2009 to evaluate a lab-scale SANI system, utilizing synthetic saline wastewater (a stock solution that was prepared to simulate the characteristics of Hong Kong's sewage in terms of salinity and sulfate concentration) under varying operational conditions.[78] The investigation spanned over 500 days and focused on assessing performance metrics, such as COD and N removal efficiency, while also examining the impact of Hydraulic Retention Time (HRT), $NO_3^-$ concentrations, dissolved O levels, and recirculation ratios.

The rationale behind performing this study was to resolve the sludge problem (reduction in the volume of sewage sludge production) in Hong Kong by combining sulfate reduc-

tion and denitrification based on $H_2S$ which should lead to low net sludge production with low costs since the growth yield of autotrophic denitrifiers is low.[78] This novel Biological Nutrient Removal (BNR) method offers a notable reduction in surplus sludge generation due to the inherently low growth yields of the three primary microbial groups involved: SRB, autotrophic denitrifiers, and nitrifiers. In this particular approach, the majority of COD is converted into $CO_2$ during the sulfate reduction process mediated by SRB. When considering the comprehensive system design, the estimations suggested that the overall cost savings could exceed 50% for a sewage treatment facility with a daily capacity of 10,000 cubic meters.[78] Figure 2.4 shows an illustrative representation of the experimental setup for the SANI system. The setup comprised of three main components, an anaerobic section designed for the removal of COD via SRB; a subsequent anoxic compartment dedicated to the autotrophic denitrification of $NO_3^-$, employing the dissolved $H_2S$ generated during sulfate reduction; and an aerobic area responsible for the nitrification of ($NH_4^+$) and the recirculation of $NO_3^-$ back to the anoxic region to facilitate denitrification. The

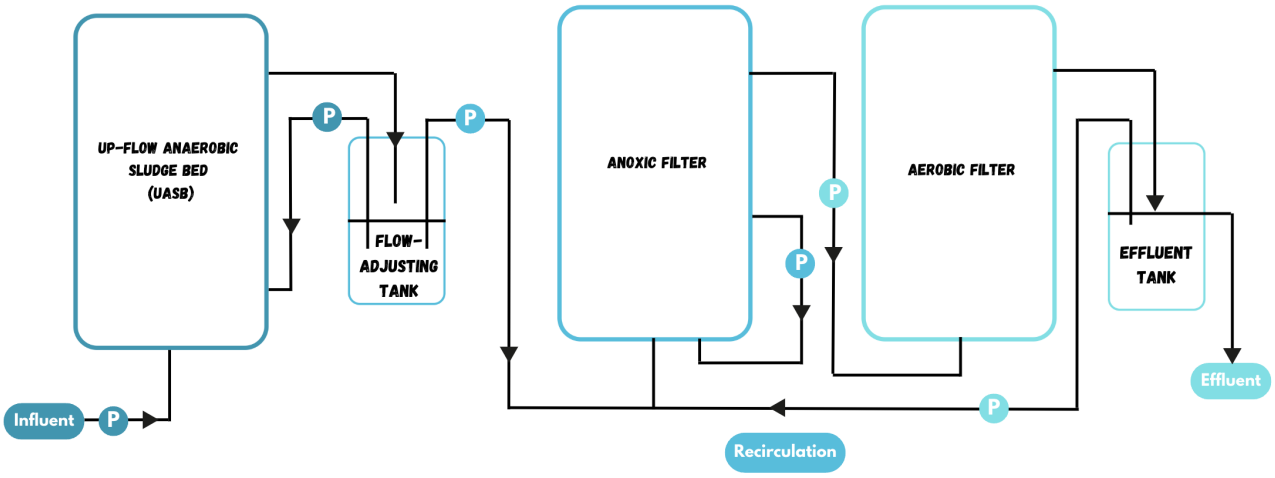


Figure 2.4 An illustration of the experimental setup of the lab-scale SANI system.[78]

complete SANI system received a continuous supply of synthetic saline wastewater and mixing within all three reactors was achieved through dedicated internal recirculation systems (as illustrated in Figure 2.4). To ensure a consistent source of dissolved $H_2S$ for the

anoxic filter, the SRUSB was initially operated with a fixed HRT of 6 hours during the SANI system's startup phase. The comprehensive evaluation of the SANI system's performance, encompassing organic and N removal as well as the production of surplus sludge, was conducted under varying recirculation ratios between the anoxic and aerobic filters, with the aim of enhancing the overall N removal efficiency of the system. Table 2.1 shows the performance of the lab-scale demonstration SANI model under various recirculation ratios.

Table 2.1 Performance of the Lab-Scale Demonstration SANI model (Q is the influent flow rate of the system).[78]

| Parameters | I | II | III | IV |
|---|---|---|---|---|
| Anoxic filter / Aerobic filter recirculation rate | 1Q | 2Q | 3Q | 4Q |
| Influent COD of anoxic filter (mg/L) | 31.8 ± 1.5 | 15.5 ± 0.8 | 25.9 ± 1.3 | 21.4 ± 1.0 |
| Effluent COD of the system (mg/L) | 14.1 ± 0.7 | 8.1 ± 0.4 | 14.7 ± 0.6 | 11.7 ± 0.6 |
| TN influent of SRUSB (mg N/L) | 30 ± 1.5 | 30 ± 1.3 | 30 ± 1.5 | 29 ± 1.5 |
| TN effluent of aerobic filter (mg N/L) | 16 ± 0.8 | 10 ± 0.5 | 8 ± 0.4 | 19 ± 0.9 |
| Nitrate Removal in anoxic filter (%) | 99 ± 4.1 | 99 ± 4.5 | 97 ± 4.6 | 8 ± 0.4 |
| Nitrification Efficiency in aerobic filter (%) | 98 ± 4.1 | 99 ± 4.5 | 93 ± 4.5 | 17 ± 0.8 |
| TN removal efficiency (%) | 49 ± 2.4 | 65 ± 3.2 | 74 ± 3.7 | 35 ± 1.7 |
| COD Removal Efficiency (%) | 94.4 ± 4.7 | 96.9 ± 4.8 | 94.3 ± 4.7 | 94.2 ± 4.7 |

Based on the conclusions made from this study[78], the lab-scale SANI process has proven to be a promising solution for efficiently removing COD and N from saline wastewater while keeping sludge production to a minimum. The extensive 500-day experimental investigation revealed impressive results, including high removal rates for COD (95%) and N (99% $NO_3^-$, 74% TN) without the need for sludge withdrawal. With average Total Suspended Solids (TSS) concentrations in the effluent as low as 1.1 mg/L, the system demonstrated its effectiveness.

Furthermore, it was established that the COD-to-sulfate ratio in saline wastewater had no detrimental effect on $H_2S$ production for autotrophic denitrification. More than 80% of the COD was effectively removed through sulfate reduction.

To optimize the system, it was determined that a minimum S/N ratio of 1.6 in the

anoxic filter influent is required for achieving more than 90% $NO_3^-$ removal through autotrophic denitrification, which plays a vital role in total N removal within the SANI process.

Additionally, S balance analyses confirmed that the system effectively managed S accumulation and minimized losses of $H_2S$. These findings collectively emphasize the robustness and potential of the lab-scale SANI process for the treatment of saline wastewater, offering significant implications for sustainable and efficient wastewater management.

### 2.3.2 The Steady State Model Based on the Lab-scale Demonstration

To elucidate and validate the findings of the lab-scale demonstration of the SANI system, a steady-state model was developed, integrating COD, N, and S mass and charge balances based on stoichiometric considerations of the sulfate reduction, autotrophic denitrification, and autotrophic nitrification processes.[44]

The steady-state model was formulated to represent BSR, employing primary sewage sludge as the primary substrate. In order to explore the sludge generation within the SANI system from a stoichiometric perspective, their approach was employed to model the three biological reactions inherent to the SANI process, which encompass BSR, autotrophic denitrification, and nitrification. The model's predictions closely aligned with observed data on COD, nitrate, sulfate removal, $H_2S$ production, effluent TSS, and mass balances of COD, S, and N across the three reactors. Furthermore, the model offers insights into why the withdrawal of sludge from the SANI system is unnecessary, as evidenced by comparisons of predicted and measured effluent TSS and P concentrations.[44]

In BSR, the SRB organisms that rely on external carbon sources, utilize influent COD for biomass growth while concurrently converting sulfate into dissolved $H_2S$. The organic content in the influent becomes carbon-deficient when the COD to Total Organic Carbon (TOC) ratio exceeds 2.67[78]. The experimental synthetic saline wastewater used in this study exhibited a COD-to-TOC ratio ranging between 2.5 and 3, indicating a deficiency

in carbon within the organic compounds entering the SANI system. Consequently, these organics provided more electrons for sulfate reduction than the necessary supply of $HCO_3^-$ for alkalinity increase. In such cases, the $H_2S/HS^-$ system compensates for the deficit in alkalinity.

## The stoichiometry of sulfate reduction in the SRUSB

Under carbon-deficient conditions, the typical chemical process of sulfate reduction utilizing a biodegradable organic compound of $C_xH_yO_zN_a$ to generate biomass with composition $C_kH_lO_mN_n$, incorporating phosphorous yields, has been detailed in the equation below[44]:

$$\begin{aligned} &C_xH_yO_zN_aP_b + \left[(1-E)\frac{\gamma_s}{8}\right]\mathrm{SO_4}^{2-} + [3x - z + 4b - \frac{E_{\gamma_s}}{\gamma_B} \times (3k - m + n + 4p) \\ &- 4(1-E)\frac{\gamma_s}{8}]\mathrm{H_2O} \rightarrow [x - a + b + E\frac{\gamma_s}{\gamma_B}(n - k + p) - (1-E)\frac{\gamma_s}{8}]\mathrm{H_2S} + \\ &\left[2(1-E)\frac{\gamma_s}{8} - E\frac{\gamma_s}{\gamma_B}(n - k - p) - (x - a - b)\right]\mathrm{HS^-} + [E\frac{\gamma_S}{\gamma_B}]C_xH_yO_zN_aP_b + \\ &[a - nE\frac{\gamma_S}{\gamma_B}]\mathrm{NH_4}^+ + [x - kE\frac{\gamma_S}{\gamma_B}]\mathrm{HCO_3}^- + [b - pE\frac{\gamma_S}{\gamma_B}]\mathrm{H_2PO_4}^- \end{aligned} \tag{2.3}$$

The $\gamma_S$ and $\gamma_B$ represent the electrons accessible for redox reactions within each mole of the biodegradable organic compound, $C_xH_yO_zN_aP_p$, and per mole of the SRB biomass, $C_kH_lO_mN_nP_p$, respectively[68]:

$$\begin{aligned} \gamma_S &= 4x + y - 2z - 3a + 5b \quad (e^- eq/mol) \\ \gamma_B &= 4k + l - 2m - 3n + 5p \quad (e^- eq/mol) \end{aligned} \tag{2.4}$$

The E represents the amount of COD leaving the SRUSB reactor daily, considering both active and endogenous sludge mass, as a fraction of the biodegradable organics utilized within the reactor daily, maintaining a stable condition. This definition of E is derived from the COD-based anaerobic digestion kinetic model, E is given by[44]:

$$E = \frac{Y_{SRB}}{[1 + b_{SRB}R_s(1 - Y_{SRB})]} \tag{2.5}$$

In the equation, $R_s$ represents the sludge age within the SRUSB reactor in days. $Y_{SRB}$ signifies the yield coefficient denoting the amount of anaerobic biomass produced per unit of degraded COD (mg of COD biomass per mg of degraded COD). Meanwhile, $b_{SRB}$ stands for the rate of endogenous respiration of the anaerobic biomass in units of reciprocal days.

Equation 2.5 assumes negligible production of endogenous residue due to extremely low values for both the endogenous respiration rate $b_{SRB}$ and the unbiodegradable fraction $f_{SRB}$ for SRB, specifically, $b_{SRB}$ being 0.04/day and $f_{SRB}$ being 0.08 in the completed study.

The concentration of COD per mole and the molar weight $M_w$ of the influent organic substrate, $C_xH_yO_zN_aP_b$, are provided as part of the context:

$$COD = 8[y + 2(2x - z) - 3a + 5b] \quad (g.COD/mol) \tag{2.6}$$

$$M_w = 12x + y + 16z + 14a + 31b \quad (g.drymass/mol) \tag{2.7}$$

## Mixed weak acid/base chemistry

The SRUSB's pH is forecasted by employing mixed weak acid/base chemistry, incorporating the complete array of biological sulfate reduction byproducts obtained from the earlier stoichiometric computations. Due to the influent's carbon deficiency, it inadequately provides $HCO_3$ necessary for the alkalinity rise through sulfate reduction. Consequently, the sulfide system compensates for the deficit in alkalinity through the production of $(HS^-)$. This mechanism, governed by the $H_2S/HS^-$ system with a $pK_S$ value around 7, ultimately determines the pH in the following manner:

$$\mathrm{H_2S} \rightarrow \mathrm{H^+ + HS^-} \tag{2.8}$$

$$K_S = \frac{[\mathrm{HS^-}][\mathrm{H^+}]}{[\mathrm{H_2S}]} \tag{2.9}$$

$$[\mathrm{H^+}] = \frac{[\mathrm{K_S}][\mathrm{H_2S}]}{[\mathrm{HS^-}]} \tag{2.10}$$

$$\text{pH} = -\log\left(\frac{K_S[\text{H}_2\text{S}]}{[\text{HS}^-]}\right) = \text{p}K_S - \log\left(\frac{[\text{H}_2\text{S}]}{[\text{HS}^-]}\right) \tag{2.11}$$

$K_S$ stands for the equilibrium constant of the $H_2S/HS^-$ system, and its logarithm, $pK_S$, equals 7.05.

## The stoichiometry of autotrophic denitrification in the anoxic filter

In the laboratory-scale SANI system, the effluents from the SRUSB reactor and the anoxic filter were blended via recirculation between the nitrifying filter and the anoxic filter. This combination contains adequate $S^{2-}$ and $NO_3{}^-$ for autotrophic denitrification within the anoxic filter. Despite only 13% of the influent COD reaching the anoxic filter from the SRUSB, the findings indicated that autotrophic denitrification predominantly facilitates $NO_3{}^-$ removal in this process. Consequently, $H_2S$ serves as the electron donor for denitrification, shaping the stoichiometry of autotrophic denitrification in the process as shown below:

$$\begin{aligned}&\frac{\text{kE}}{\gamma_B}\text{HCO}_3{}^- + \frac{\text{nE}}{\gamma_B}\text{NH}_4{}^+ + \frac{\text{pE}}{\gamma_B}\text{H}_2\text{PO}_4{}^- + \frac{2}{10}(\text{1-E})\text{NO}_3{}^- + \frac{2}{10}(\text{1-E})\text{NO}_3{}^- + \frac{1}{8}\text{H}_2\text{S} + \\ &[\frac{4}{8} - \frac{6}{10}(\text{1-E}) - \frac{\text{E}}{\gamma_B}(3\,\text{k-m}_4{}^+\text{p})]\text{H}_2\text{O} \rightarrow \frac{\text{E}}{\gamma_B}\text{C}_x\text{H}_y\text{O}_z\text{N}_a\text{P}_b + \frac{1}{8}\text{SO}_4{}^{2-} + \frac{1}{10}(\text{1-E})\text{N}_2 + \\ &[\frac{2}{8} - \frac{2}{10}(\text{1-E}) - \frac{\text{E}}{\gamma_B}(\text{k-n}^+\text{p})]\text{H}^+\end{aligned} \tag{2.12}$$

The quantity of available electrons $\gamma_B$ for redox reactions per mole in autotrophic denitrifying biomass, $C_xH_yO_zN_aP_b$, is represented by e. It signifies the mass of COD leaving the anoxic filter as autotrophic denitrification biomass and intrinsic sludge daily, relative to the mass of $NO_3{}^-$ reduced in the anoxic filter each day at a constant rate. This is mathematically expressed as:

$$E = \frac{Y_A D}{(1 + b_{AD} R_s)} \tag{2.13}$$

Where $R_s$ denotes the sludge age in the anoxic filter (in days), $Y_{AD}$ represents the yield coefficient of autotrophic denitrifying microorganisms (measured in mg COD biomass/mg$NO_3$–N

reduced), and $b_{AD}$ signifies the endogenous respiration rate of autotrophic denitrifying microorganisms (in 1/day).

## The stoichiometry of nitrification in the aerobic filter

The stoichiometry of the nitrification process within the aerobic filter is characterized as:

$$\frac{14nE}{8\gamma_B}\mathrm{CO_2} + \mathrm{NH_4}^+ + 14\left[\frac{1}{7} - \frac{E}{8\gamma_B}\left(\frac{m}{2} - \frac{9n}{4} - \frac{5p}{4} - \frac{l}{4}\right)\right]\mathrm{O_2} + \frac{14pE}{8\gamma_B}\mathrm{H_2PO_4}^- \rightarrow \left[\frac{1}{14} + \frac{E}{8\gamma_B}\left(\frac{3p}{2} - \frac{l}{2} + \frac{n}{2}\right)\right]\mathrm{H_2O} + 14\left(\frac{1}{14} - \frac{14nE}{8\gamma_B}\right)\mathrm{NO_3}^- + 14\left[\frac{1}{7} - \frac{nE}{8\gamma_B}(P+n)\right]\mathrm{H}^+ + \frac{14nE}{8\gamma_B}C_xH_yO_zN_aP_b \tag{2.14}$$

Whereby $\gamma_B$ represents the number of electrons per mole present in autotrophic nitrifier biomass denoted as $C_xH_yO_zN_aP_b$. Meanwhile, stands for the daily amount of COD leaving the aerobic filter, encompassing autotrophic nitrification biomass and endogenous sludge. This quantity is a fraction of the daily ($NH_4^+$) oxidized, maintaining equilibrium. Specifically, E" is derived from the -based kinetic equation:

$$E = \frac{Y_A N}{(1 + b_{AN} R_s)} \tag{2.15}$$

where $R_S$ signifies the sludge age within the aerobic filter (measured in days). $Y_{AN}$ represents the yield coefficient of autotrophic nitrification biomass, measured in milligrams of COD produced per milligram of N consumed, while $b_{AN}$ denotes the endogenous respiration rate of autotrophic nitrification biomass (expressed in units of inverse days).

The model's projections aligned closely with actual measurements across various parameters like COD, $NO_3^-$, $SO_4^{2-}$ removal, $S^{2-}$ production, effluent TSS, and the overall balances of COD, S, and N across the three reactors. By comparing predictions to actual effluent TSS and P concentrations, the model clarified why sludge extraction from the SANI system is unnecessary. The steady-state model's TSS forecast was based on the assumption

that the biomass in each reactor's effluent equates to the new biomass generated within that specific reactor. The minimal variance between measured and predicted effluent TSS, validated this assumption, albeit the slightly elevated TSS measurements stemmed from the model's oversight of inorganic matter in the effluent. Yet, the overall growth of biomass within the SANI system gets nearly balanced out in the effluent, obviating the need for sludge withdrawal for a period of 500 days.

The effluent maintains very low suspended solids due to the process's low net yield, preventing sludge accumulation. This was corroborated by TP balance assessments across the reactors, where TP content measurements aligned at 99%. The influent's P content adequately supports biomass growth at an average COD of 245 mg/L, resulting in minimal P intake for biomass growth per day during steady-state conditions. Essentially, the daily new biomass production in each reactor nearly equals the cumulative biomass loss from endogenous decay and effluent wash-out. Additionally, the model established in this study accurately predicts the fraction of COD converted to sludge mass, further affirming the minimal sludge production in the SANI system. A pilot-scale SANI plant treating saline sewage at 10 m3/day was scaled up from the lab-scale system treating synthetic saline sewage to further investigate the results obtained from the developed model.

### 2.3.3 A Pilot Trial of the SANI Model

The laboratory-scale experiment described in section 2.3.1 verified the absence of excessive sludge generation when treating artificial saline sewage.[45] This trial indicated no buildup of sludge, S, or P[78]. Although real saline sewage contains a portion of non-biodegradable substances, the behaviour and sludge formation of the SANI process when supplied with genuine saline sewage were uncertain before this investigation. Additionally, it was expected that no methane gas ($CH_4$) would be produced from the SRUSB due to the dominance of SRB over methanogens in saline sewage treatment.[46] Consequently, a pilot trial of the SANI using de-gritted saline sewage was executed in Hong Kong to as-

sess its performance over a 225-day period.[46] The trial focused on monitoring the SANI's efficacy in removing COD, S, and N while analyzing sludge production and the presence of methanogens to validate the assumptions.

The SANI pilot facility was established at the Tung Chung Sewage Pump Station (TCSPS) in Hong Kong (refer to Figure 2.5).

Figure 2.5 The SANI pilot facility was established at the Tung Chung Sewage Pump Station (TCSPS) in Hong Kong.[46]

It primarily comprised the SRUSB, anoxic, and aerobic bioreactors and operated consistently for about 225 days as illustrated below with a conceptual schematic diagram. The facility received a continuous inflow of 10 $m^3/d$ of de-gritted saline sewage, sourced mainly from the Hong Kong International Airport (HKIA) and the Tung Chung district. Throughout the trial, 24-hour composite samples of the influent and effluent from all plant reactors were collected.

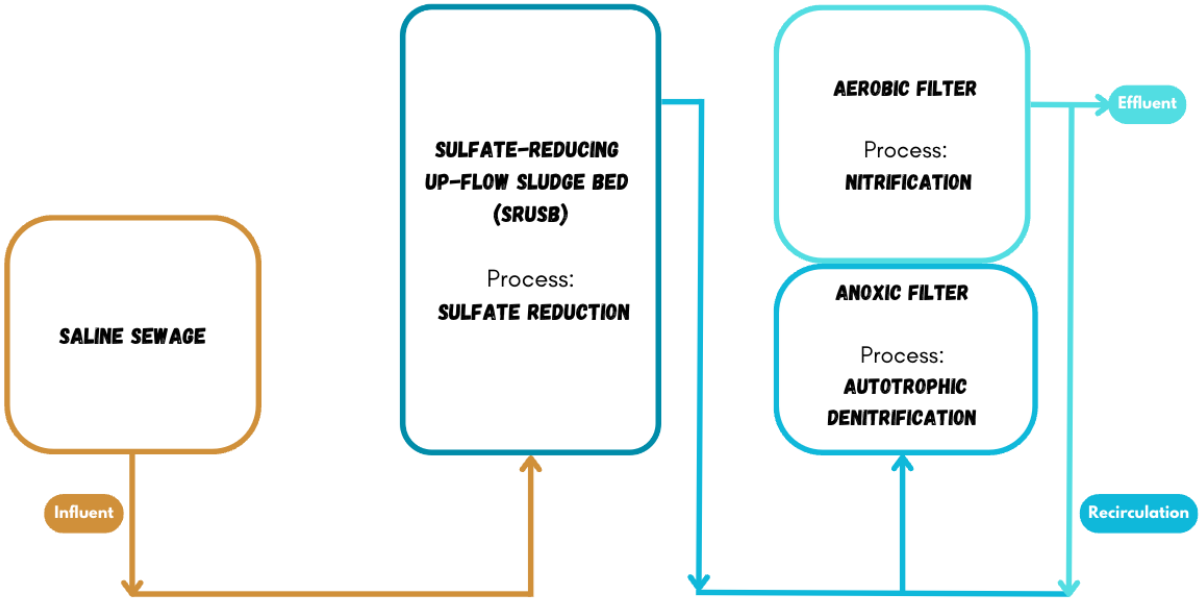


Figure 2.6 A conceptual schematic diagram of the SANI pilot plant that was established at the Tung Chung Sewage Pump Station (TCSPS) in Hong Kong.[46]

The SRUSB, anoxic, and aerobic bioreactors were seeded with anaerobic and activated sludge, respectively, obtained from the Sha Tin sewage Treatment Works. This treatment facility removes COD and TN from saline sewage through a nitrification/denitrification process. The primary operational parameters of the plant are summarized in Table 2.2 below.

Table 2.2 The primary operational parameters of the SANI Pilot plant at the TCSPS in Hong Kong (influent flow rate Q=10 $m^3$/d).[46]

| Reactor | HRT(hr) | SRT(d) | Influent Flow Rate | Recirculation | Temperature(25°C) |
|---|---|---|---|---|---|
| SRUSB | 16 | 90 | Q | - | 25 |
| Anoxic | 5 | 110 | 3.5Q | 2.5Q | 25 |
| Aerobic | 5 | 42 | 3.5Q | - | 25 |

The SRUSB functioned as the primary reactor within the SANI plant. Through the preliminary trial of the SANI process, utilizing $10m^3/d$ of saline sewage, the system achieved average removal efficiencies of $87\%$ for COD, $87\%$ for TSS, and $57\%$ for TN.[46] Notably, no

intentional withdrawal of sludge occurred throughout the 225-day operation of the plant, attributable to an exceptionally low observed sludge yield (0.02 kgVSS/kgCOD removed) from the SRUSB reactor. The examination of Deoxyribonucleic Acid (DNA) extraction and Principal Component Analysis (PCA) amplification results confirmed the absence of methanogens in the SRUSB.

Comparative analysis indicated that the SANI process leads to a remarkable reduction in sludge production by 90%, along with a 35% decrease in energy consumption and a 36% reduction in Greenhouse Gas (GHG) emissions when contrasted with the Conventional Biological Nutrient Removal (CBNR) process.[46] A reliable steady-state model was formulated using data from the pilot plant, effectively predicting the results of the pilot-scale trial. This model provided valuable insights into the factors influencing various bioprocesses and elucidated the underlying reasons for the minimal sludge production observed during the pilot plant demonstration.[43]

Table 2.3 Characteristics of the influent and effluent for each reactor in the lab scale SANI system vs the model.

| **Parameter** | **SRUSB** | **Anoxic filter** | **Aerobic filter** |
|---|---|---|---|
| Sludge age or sludge retention time Rs (days) | 100 | 100 | 100 |
| Sludge COD produced/COD utilized, E | 0.02 | 0.04 | 0.05 |
| Influent flow rate, $Q_{in}$ (L/day) | 16.7 | 32.4 | 32.4 |
| Influent total COD (mg COD/L) | 245 ± 5.4 | 26.3 ± 2.4 | 12.5 ± 1.5 |
| Non-biodegradable particulate COD/influent total COD, $f_{up}$ | 0.004 | 0.4 | 0.4 |
| Effluent total COD (mg COD/L) | 38.2 ± 2.2 | 10.2 ± 1.5 | 7.1 ± 1.1 |
| Overall COD removed | 147 ± 4.3 | 97.1 | 134 ± 6.6 |
| Influent $SO_4$ (mg S/L) | 86 ± 4.5 | 123 ± 7.2 | 134 ± 6.6 |
| Effluent $SO_4$ (mg S/L) | 134 ± 6.6 | 134 ± 6.6 | 138 ± 4.9 |
| Influent $H_2S$ (mg S/L) | – | 13.88 ± 0.6 | 0.4 ± 0.1 |
| Effluent $H_2S$ (mg S/L) | 44.2 ± 1.9 | 0.4 ± 0.1 | 0.03 ± 0.01 |
| Overall S recovery (%) | 94 | – | – |
| Influent alkalinity (mg/L as $CaCO_3$) | 101.4 ± 9.8 | 206.3 ± 7.2 | 205.5 ± 3.8 |
| Effluent alkalinity (mg/L as $CaCO_3$) | 588.5 ± 9.5 | 205.5 ± 7.1 | 162.7 ± 3.5 |
| Influent TN (mg/L) | 36.1 ± 1.1 | 16.6 ± 0.9 | 10.9 ± 0.5 |
| Effluent TN (mg/L) | 34.5 ± 0.9 | 10.9 ± 0.5 | 9.7 ± 0.6 |
| Overall TN removal (%) | 74 | – | – |

### 2.3.4 The Steady State Model Based on the Pilot-Plant

This section provides an extensive examination of a research study designed to expand upon the steady-state SANI system model introduced in section 2.3.2[44]. The objective was to conduct a comprehensive assessment of the SANI pilot plant, which operated with $10m3/d$ of authentic screened saline sewage over a period of 225 days in Hong Kong, as detailed in the preceding chapter[46]. The primary objectives of this investigation included the calibration of the hydrolysis model, determination of the influent Unbiodegradable Particulate Organics (UPO) fraction through anaerobic hydrolysis batch testing utilizing real saline sewage, and the measurement of volumetric and media surface-specific denitrification and nitrification rates. Subsequently, the model predictions were compared against experimental data obtained during the steady-state operation of the SANI pilot plant. By

characterizing sewage organic matter and fine-tuning the model with relevant parameters, it was successfully calibrated to a pilot plant for the SANI process. The resulting model accurately predicted the outcomes of the pilot-scale trial, shedding light on the factors influencing different bioprocesses and the minimal sludge production observed in the SANI process.

After fine-tuning the steady-state lab model to create the pilot-scale simulation model, the simplified stoichiometries, with the main reactants and products, of the SANI pilot system were represented as follows, Biological sulfate reduction in the SRUSB[46,43]:

$$100gCOD + 150.2g{SO_4}^{2-} + 43.7g{H_2O} \rightarrow 53.2g{H_2S} + 1.9gSludge + 190.0g{HCO_3}^{-} \quad (2.16)$$

Autotrophic denitrification in the anoxic bioreactor[43]:

$$100g{NO_3}^{-} + 5.9g{HCO_3}^{-} + 35.92g{H_2S} \rightarrow 22.58g{N_2} + 101.42g{SO_4}^{2-} + 2.15gSludge \quad (2.17)$$

Nitrification in the aerobic bioreactor[43]:

$$100g{NH_4}^{+} + 7.33g{HCO_2} + 346.67g{O_2} \rightarrow 5.22gSludge + 344.44g{NO_3}^{-} + 11.11g{H}^{+} + 98g{H_2O} \quad (2.18)$$

As per the above equations, the determined sludge yield coefficients for the SANI pilot plant were remarkably low, specifically at 0.02 kg VSS/kg COD removed, 0.10 kg VSS, and 0.07 kg VSS for the SRUSB, anoxic, and aerobic bioreactors, respectively.[43] This solidified the confirmation of the SANI system's exceptionally low sludge production when compared to conventional activated sludge systems. These coefficients provided explicit insight into the causes and conditions contributing to the minimized sludge generation observed in the SANI pilot plant during real saline sewage treatment.

In general, the steady-state model predictions aligned well with the actual data from

the three bioreactors as shown by the results listed in Table 2.4. In the case of the SRUSB, both COD and sulfate removals slightly exceeded the measured data due to the assumption of complete mixing in the reactor. However, it's important to note that there is approximately 5% hydraulic short-circuiting flow (bypass flow) and 35% dead space in the SRUSB of the SANI pilot plant.[46] These factors were suggested to contribute to the observed lower effluent COD compared to the measured data.[43]

Table 2.4 Characteristics of the influent and effluent for each reactor in the SANI pilot plant.[46]

| Parameters | SRUSB | | BAR1 | BAR1 Effluent | BAR2 | Calculated |
|---|---|---|---|---|---|---|
| | Influent | Effluent | Influent | BAR2 Influent | Effluent | Concentration |
| VSS (mg/L) | 186 ± 55.3 | 52.1 ± 22.3 | 23.5 ± 7.1 | 12.5 ± 4.3 | 9.0 ± 2.4 | 21.3 |
| Unfiltered COD (mgCOD/L) | 431 ± 132.6 | 98.8 ± 60.9 | 65.9 ± 17.4 | 55.0 ± 18.7 | 53.9 ± 10.8 | 66.7 |
| Filtered COD (mgCOD/L)b | 157.9 ± 86.2 | 39.7 ± 5.6 | 30.9 ± 10.3 | 30.2 ± 11.6 | 30.7 ± 9.2 | 33.3 |
| $SO_4^{2-}$ (mgS/L) | 195.7 ± 18.0 | 65.4 ± 15.2 | 142.3 ± 25.7 | 169.4 ± 34.3 | 172.3 ± 34.4 | 141.7 |
| $H_2S$ (mgS/L) | 4.0 ± 4.7 | 124.1 ± 14.4 | 31.3 ± 4.8 | 3.0 ± 1.2 | 0 | 35.5 |
| Unfiltered TKN (mgN/L) | 87.5 ± 8.5 | 85.3 ± 8.6 | 39.2 ± 4.4 | 35.7 ± 5.6 | 23.4 ± 5.5 | 41.1 |
| Filtered TKN (mgN/L) | 70.5 ± 5.7 | 70.9 ± 5.6 | 36.5 ± 4.4 | 35.3 ± 3.8 | 23.2 ± 4.3 | 36.8 |
| FSA (mgN/L) | 44.8 ± 6.6 | 45.4 ± 6.0 | 16.9 ± 4.5 | 16.4 ± 2.7 | 3.4 ± 2.4 | 15.4 |
| $NO_3^-$ (mgN/L) | 0 | 0 | 13.5 ± 1.8 | 2.2 ± 2.4 | 16.8 ± 3.2 | 12.0 |
| Unfiltered TP (mgP/L) | 7.8±1.2 | 7.6±1.0 | 5.9±0.7 | 5.7±0.5 | 5.6 ± 0.6 | 6.2 |
| Filtered TP (mgP/L) | 5.8±0.8 | 5.7±0.6 | 5.8±0.7 | 5.6±0.8 | 5.6 ± 0.6 | 5.6 |
| OP (mgP/L) | 5.3±0.7 | 5.2±0.8 | 5.3±0.7 | 5.3±0.5 | 5.3±0.5 | 5.3 |
| Total Alkalinity ($mgCaCO_3/L$) | 223±100.5 | 736.9±170.1 | 281.4±75.2 | 247.7±70.5 | 120.5 ± 62.4 | 296.6 |
| $H_2CO_3$ Alkalinity ($mgCaCO_3/L$) | 219.0±104.3 | 576.7±174.0 | 252.8±75.1 | 245.7±71.6 | 120.5 ± 62.4 | 250.8 |
| $H_2S$ Alkalinity ($mgCaCO_3/L$) | 4.6±1.0 | 160.2±11.2 | 28.6±4.6 | 2.0±0.2 | 0 | 45.8 |

The measured effluent $H_2S$ was lower than predicted, and this was attributed to two main factors: a) the actual COD removal being lower than predicted, and b) a small amount of $H_2S$ undergoing oxidation to elemental S.[43] Evidence of this oxidation was found in the form of white elemental S on the internal wall of the effluent pipe of the SRUSB. This analysis also elucidated the COD mass balance of 81% for the SRUSB. In the anoxic reactor, while the predicted $H_2S$ removal matched the measured data, the $NO_3^-$ removed through autotrophic denitrification, utilizing $H_2S$ as the electron donor, fell short of the measured values. This discrepancy indicated that not all the $H_2S$ removed in the anoxic reactor was utilized by autotrophic denitrification. In other words, a portion of the $H_2S$ underwent oxidation due to dissolved O introduced by the recirculation flow from the

aerobic reactor to the anoxic reactor.[43]

To show the enhancement of the pilot-scale steady-state model for the SANI pilot system, the model was compared with the performance of the lab-scale steady-state model. The latter was also implemented for the SANI pilot plant using identical inputs, encompassing influent characteristics, flow rates, organics and biomass compositions, HRT, and solids retention time (SRT), among others, mirroring the conditions of the pilot-scale steady-state model.

Given that approximately 217.5 mg COD/L of Biodegradable Particulate Organics (BPO) in the influent needed hydrolysis before utilization, and the lab-scale steady-state model lacked anaerobic hydrolysis kinetics, it yielded significantly lower values for COD removal, sulfate reduction, and total alkalinity variation compared to the pilot-scale steady-state model.[43] This resulted in a notable deviation between experimentally measured values and the predictions from the lab-scale steady-state model.

Furthermore, in contrast to the pilot-scale steady-state model, the lab-scale model failed to anticipate variations in sulfate and $H_2S$ concentrations in the aerobic reactor.[43] Consequently, the alkalinity consumption stemming from the oxidation of $H_2S$ and $HS^-$ to $SO_2$ by Dissolved Oxygen (DO) was not accounted for in the lab-scale model. Hence, it became imperative to develop a pilot-scale steady-state model and characterize the influent organics and biomass compositions specifically tailored for the SANI pilot system treating real saline wastewater.

### 2.3.5 Large Scale Demonstration

A successful operation of a $10m^3/d$ SANI pilot plant, spanning over 200 days at the Tung Chung sewage pumping station[43], effectively treated saline sewage and remarkably reduced biological sludge production by up to 90%. However, the extended HRT of 34 hours proved impractical for full-scale application, signalling the necessity for further SANI process optimization.

To delve deeper into the practical application of the process, an extensive large-scale trial took place at the Sha Tin Sewage Treatment Works (STSTW) in Hong Kong.[79] This section outlines the design, and operating conditions, and evaluates the performance of the large-scale plant concerning organic and N removal via the S cycle, as well as organic C and N conversions. The sludge reduction efficiency of the SANI process is scrutinized by comparing measured data with those from the conventional activated sludge (CAS) process. Additionally, distinctions between large-scale SANI, pilot-scale SANI, and the CAS process are explored and discussed.

The SANI demonstration plant, situated within two vacant rectangular primary sedimentation tanks at the STSTW as depicted in Figure 2.7, was established with the purpose of treating 800 to 1000 $m^3$/d or the equivalent of 2500 to 3000 Population Equivalents (PE) of domestic saline sewage. The influent for the demo plant consisted of saline sewage that underwent on-site screening through 6 mm coarse screen bars and grit removal chambers.

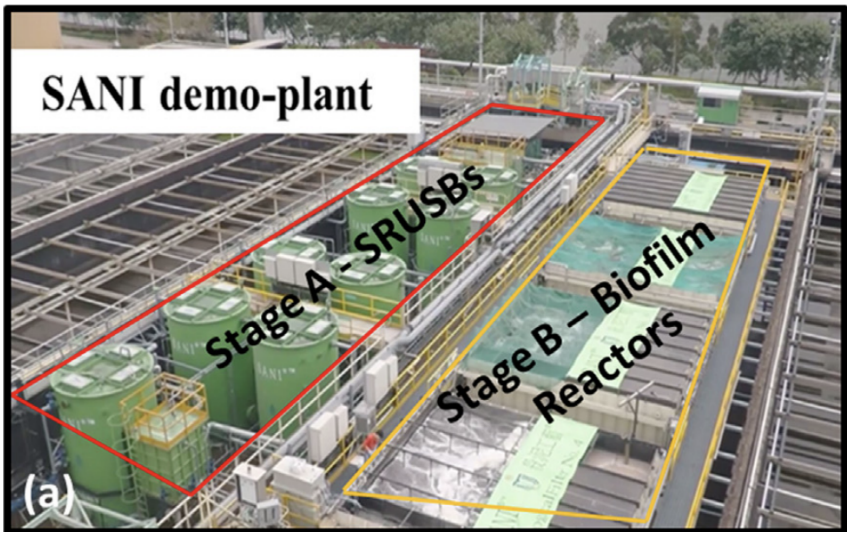


Figure 2.7 The SANI demonstration plant.[79]

Throughout the operational period spanning 250 days, the sewage temperature and pH exhibited variations within the ranges of 20°C to 30°C and 7.0 to 8.0, respectively. Concurrently, the conductivity ranged from 14,000 to 24,000 ms/cm. The primary objective

of the demo plant was to meet the discharge standards established for existing sewage treatment works.

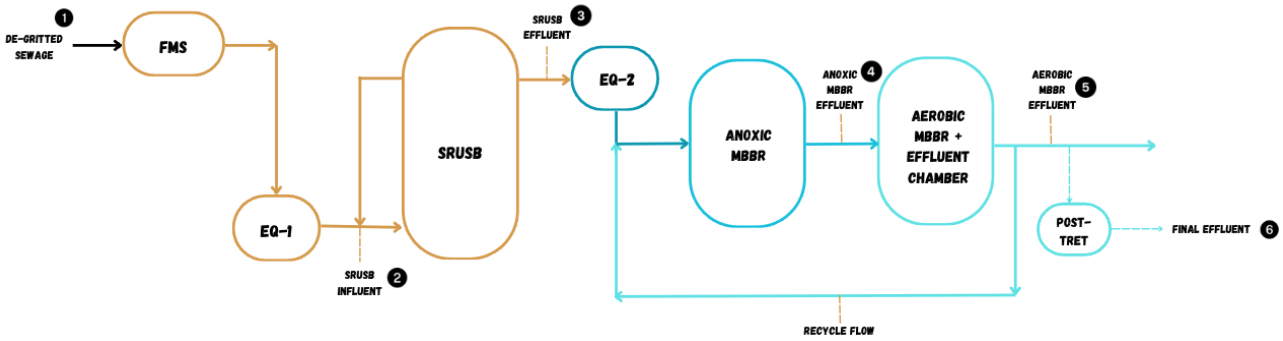


Figure 2.8 The process flow diagram of the SANI-MBBR (EQ = feed tank; SRUSB = sulfate reduction upflow sludge bed; MBBR = moving bed biofilm reactor; SANI = sulfate reduction autotrophic denitrification nitrification integrated).[79]

The process flowchart of the demo plant, illustrated in Figure 2.8, comprised the following stages: i) pre-treatment using Fine Mesh Sieves (FMS), ii) Stage A treatment involving reactors for organic removal through biological sulfate reduction (SRUSB), iii) Stage B treatment employing a MBBR for N removal through aerobic autotrophic nitrification and anoxic S-oxidizing autotrophic denitrification, and iv) post-treatment utilizing a dedicated reactor.

The Hydraulic Retention Time and the rates of loading and conversion were regarded as the pivotal factors influencing the design and functioning of full-scale plants. In this investigation, the HRT of the SRUSB reactor, specifically in Stage A of the process, demonstrated a notable achievement. The HRT was effectively reduced by almost 70%, decreasing from 16 hours in the Tung Chung pilot plant SRUSB reactor[43] to 4.8 hours in the demo plant SRUSB reactor.

Table 2.5 Quality of the influent and effluent during stable operation (Phases II and III).

| Parameter (unit) | Degritted sewage (FMS influent) | SRUSB influent (FMS effluent) | SRUSB effluent | Anoxic MBBR effluent | Aerobic MBBR effluent | Post-treatment effluent |
|---|---|---|---|---|---|---|
| TSS (mg/L) | 302 ± 43 | 192 ± 47 | 59 ± 23 | 72 ± 20 | 68 ± 19 | 15 ± 5 |
| $TCOD_c$ (mg/L) | 486 ± 52 | 352 ± 55 | 95 ± 26 | 118 ± 42 | 112 ± 25 | 62 ± 43 |
| $SCOD_c$ (mg/L) | 156 ± 32 | 133 ± 35 | 55 ± 17 | 49 ± 17 | 45 ± 26 | 43 ± 25 |
| $BOD_5$ (mg/L) | 231 ± 22 | 178 ± 48 | – | – | 31 ± 9 | 5.6 ± 1.8 |
| $SO_4^{2-}$ (mg S/L) | 295 ± 32 | 298 ± 30 | 212 ± 23 | 263 ± 25 | 276 ± 25 | – |
| TDS (mg S/L) | 1.5 ± 1.7 | 2.6 ± 2.5 | 79 ± 5.8 | 5.1 ± 6.4 | <0.1 | – |
| TAN (mg N/L) | 33 ± 4.3 | 37 ± 5.8 | 41 ± 4.5 | 14 ± 5.2 | 1.3 ± 0.9 | 0.43 ± 0.39 |
| $NO_3^-$ (mg N/L) | 1.3 ± 0.8 | 1.2 ± 0.6 | 1.7 ± 1.6 | 1.4 ± 2.0 | 7.9 ± 3.2 | 7.5 ± 1.6 |
| $NO_2^-$ (mg N/L) | <0.05 | <0.05 | <0.05 | <0.05 | 1.3 ± 1.1 | 0.23 ± 0.07 |
| TN (mg N/L) | 53 ± 8.2 | 48 ± 6.7 | 43 ± 4.6 | 19 ± 5.1 | 16 ± 4.5 | 8.4 ± 1.6 |
| TP (mg P/L) | 6.1 ± 1.1 | 5.5 ± 1.2 | 3.7 ± 0.6 | 3.4 ± 0.4 | 3.3 ± 0.4 | 0.9 ± 0.3 |
| $H_2CO_3$ Alk. (mg CaCO3/L) | 180 ± 25 | 217 ± 33 | 400 ± 55 | 208 ± 66 | 113 ± 46 | – |
| Total Alk. (mg CaCO3/L) | 204 ± 30 | 247 ± 42 | 509 ± 53 | 214 ± 69 | 114 ± 45 | – |

Furthermore, significant reductions in HRTs were achieved for the anoxic and aerobic chambers of the SANI pilot plant (Stage B) in this investigation. The Tung Chung pilot plant, utilizing two identical fixed Bed Biological Aerobic/Anoxic Filters (BAF) for nitrification and denitrification, had a combined HRT of 18.8 hours[43]. In contrast, the MBBR reactor of the demo plant achieved a reduced HRT of 6.7 hours, encompassing the anoxic, aerobic, and effluent chambers. This falls within the typical range of 4 to 8 hours for commercial (MBBR) reactors employed in the treatment of domestic sewage[55]. This research demonstrated that the HRT for the entire SANI plant could be established at 12.5 hours, including an additional 1 hour allocated for post-treatment, even under the highest load conditions and at the lowest temperature experienced in the local sewage treatment. This finding indicates the feasibility of implementing a compact SANI-MBBR treatment plant.

Throughout the entire duration of the study, intentional removal of excess sludge from the reactors did not take place, affirming the remarkably low sludge production rate evident in the SANI-MBBR system. The demo plant successfully established a compact and robust S cycle biosystem. In comparison to conventional activated sludge plants in Hong Kong, the demo plant showcased a reduced spatial requirement by 30-40% and generated 60-70% less biological sludge, all while maintaining a commendable effluent quality. The

acquired experience and observations suggest the potential for process enhancements, primarily through optimized process control and reactor configuration, thereby contributing to the enhancement of energy efficiency.

## 2.4 Model Description Of The PWM_SA

The University of Cape Town three-phase plant-wide model, known as PWM_SA, was developed to simulate biological processes and predict material output including COD, C, H, O, N, and P across the unit processes of a WWTP.[35] The model relies on a rigorous material mass balance approach. This model is constructed by integrating the compatible Three-Phase Activated Sludge Model No. 2 (ASM2-3P), which accounts for activated sludge N and P removal, as well as aerobic or anoxic-aerobic digestion, with the Three-Phase Anaerobic Digestion Model (SDM-3P) designed for anaerobic digestion processes.[19] This linkage ensures a cohesive and comprehensive representation of the WWTP, emphasizing accurate tracking and management of materials throughout various stages and processes.[34]

The ASM2-3P model is an extension of the International Water Association (IWA) activated sludge model No.2 proposed by the IWA task Group[31]. The ASM2 developed by the IWA task Group is a widely accepted model extensively employed in the design, operation, and process optimization of nutrient removal Biological Excess Phosphorus Removal (BEPR) systems within activated sludge environments. It serves as a foundational tool for further model development, often utilized as a platform for various applications.[77]

The ASM2-3P incorporates biological growth and death processes for Ordinary Heterotrophic Organisms (OHO), Polyphosphate Accumulating Organisms (PAO), and accumulator of Ammonia Oxidising Organism (ANO) biomass, denoted in the models as OHO, PAO, and ANO, respectively. The model predicts oxygen demand and sludge production while addressing the storage and lysis of polyphosphate (PP) and poly-3-hydroxyalkanoates (PHA) for PAOs, specifically in the context of strictly aerobic P uptake in BEPR systems.

The ASM2 model underwent modification through the inclusion of the Inorganic Set-

tleable Solids (ISS)[21], complemented by an algorithmic mixed weak acid/base chemistry model.[3] This integration, along with a set of universally selected components, was undertaken to ensure seamless compatibility in the development of the plant-wide model. An essential step in achieving this compatibility involved the conversion of the model process stoichiometry from (COD)-based to mass concentration-based.

Furthermore, the kinetic and stoichiometric coefficients associated with the ASM2-3P rates underwent thorough evaluation and transformation to align with the revised components and stoichiometric process coefficients, now expressed in different units. In certain instances, kinetic equations, along with their included parameters, were adjusted to establish consistency with the components of the ASM2-3P model. This meticulous adaptation and alignment were vital to enable a coherent and integrated representation of the plant-wide model.

The SDM-3P model builds upon the two-phase PWM _SA model.[68] The IWA AD model delineates its structure through three overarching biological processes—acidogenesis, acetogenesis, and methanogenesis—in conjunction with an extracellular degradation step and an extracellular hydrolysis step.[2] These processes involve the collaborative efforts of four organism groups: acidogens, acetogens, acetoclastic methanogens, and hydrogenotrophic methanogens. In SDM1, the breakdown of influent organics is specified by the disintegration of substrates into carbohydrates, proteins, and lipids. Subsequently, these components undergo hydrolysis to generate monosaccharides, amino acids, and long-chain fatty acids, respectively.

The UCT SDM-3P model[68] shares similarities with SDM1, as it incorporates reactions facilitated by the same four organism groups. However, it features a singular hydrolysis process acting on a generic organic material representing sewage sludge, denoted as $C_X H_Y O_Z N_A$. This hydrolysis process directly produces an idealized carbohydrate, namely 'glucose,' while maintaining COD, C, N, H, and O mass balances, and concurrently generating $NH_3$ while consuming $H_2CO_3$. The subsequent processes following hydrolysis, char-

acterized by their significantly faster rates, are handled stoichiometrically to yield end products in the digester, such as biomass, $CH_4, CO_2,$ and water.

In short, the SDM-3P model is an extension of the PWM _SA model[68], seamlessly integrating it into a three-phase mixed weak acid/base chemical and physical processes model encompassing the inorganic C, $NH_4^+$, $CH_3COO^-$, $CH_3CH_2COO^-$, and $PO_4^{3-}$ systems. Key enhancements include the incorporation of additional soluble and BPO components, representing materials amalgamated from diverse sources within the WWTP for introduction into the anaerobic digester. The model now accounts for the digestion of waste-activated sludge derived from BEPR systems. Additionally, it introduces an ionic speciation routine and interphase transfer processes to model "instantaneous" aqueous phase equilibrium reactions and ion pairing, along with considering active gas exchange and multiple mineral precipitation phenomena.

The ionic speciation routine in the PWM_SA model, presents a comprehensive algebraic approach specifically designed to simulate the rapid equilibrium reactions of ionic dissociation and ion pairing.[3] This unique feature allows for the independent modelling of these swift processes separate from the slower biological and physical processes. Notably, this approach is versatile and can be applied to various combinations of mixed weak acid/base systems. Given the relatively sluggish nature of weak acid/base chemistry processes associated with precipitation and gas exchange, they are integrated with the slower bioprocesses, which are characterized and modelled through kinetic equations.[3] The algebraic-based ionic equilibrium model seamlessly integrates with models that incorporate kinetics for biologically mediated unit processes within WWTPs, provided there is a clear understanding of the interactions between these processes and weak acid/base species.[26]

The input of aqueous ionic species into the model is determined by utilizing measured influent parameters such as conductivity, temperature, pH, OP, Free and Saline Ammonia (FSA), $NO_3-$,$SO_{42}-$,$H_2CO_3$ alkalinity, and VFAs. The quantification of these variables, including a 5-point titration of Moosbrugger (1992) for measuring $H_2CO_3$ al-

kalinity and Volatile Fatty acids (VFA), facilitates comprehensive speciation of OP, FSA, VFA, inorganic carbon, and water within weak acid/base systems.[49] This thorough characterization, including ion-pairing considerations, is implemented during the influent characterization process. Notably, the ions from the five weak acid/base systems, along with $NO_3^-$ and $SO_{42}^-$, do not individually contribute sufficient ionic strength to match the measured conductivity. Consequently, sodium chloride is hypothetically introduced into the model influent characterization pre-processor, adjusting the conductivity to align with the measured values. This addition of sodium chloride ensures the requisite ionic strength, enabling accurate adjustments of dissociation and stability constants, and solubility products, and establishing the initial charge concentration aligned with the measured conductivity. The species and ions determined through the above-mentioned process constitute the overall charge input to the model. Once this influent charge is established, the model systematically accommodates any alterations in charge, whether gained or lost, attributed to bioprocesses, physical and chemical reactions, including mineral precipitation or ion pairing, ultimately predicting the output charge and pH. The resulting charge, coupled with the final concentrations of weak acid/base species, is then converted back to proton balance alkalinity parameters through a post-processing effluent transformer. This transformation is essential for facilitating a comparison between predicted and measured parameters, especially considering that measured results are derived from the proton balance approach. Therefore, the characterization of both influent and effluent is achieved through conductivity and proton balance parameters to facilitate measurement, while the model is fundamentally rooted in charge accounting to enable simulation. Transformation calculations seamlessly link these two approaches.

### 2.4.1 Biological reactions in the UCT SDM3P

The structural framework of the PWM_SA model, as outlined in the previous chapter, encompasses three primary biological processes—acidogenesis, acetogenesis, and methano-

genesis—alongside extracellular degradation and hydrolysis steps, as depicted in Figure 3.1 below. In the SANI process reactions, $SO_4^{2-}$ serves as the electron acceptor, leading to the formation of $H_2S$ and incorporating the additional reactions of acetotrophic sulfidogenesis and hydrogenotrophic methanogenesis. These integrated processes govern the activities of five distinct organism groups: acidogens, acetogens, acetoclastic methanogens, sulphidogens, and hydrogenotrophic methanogens.

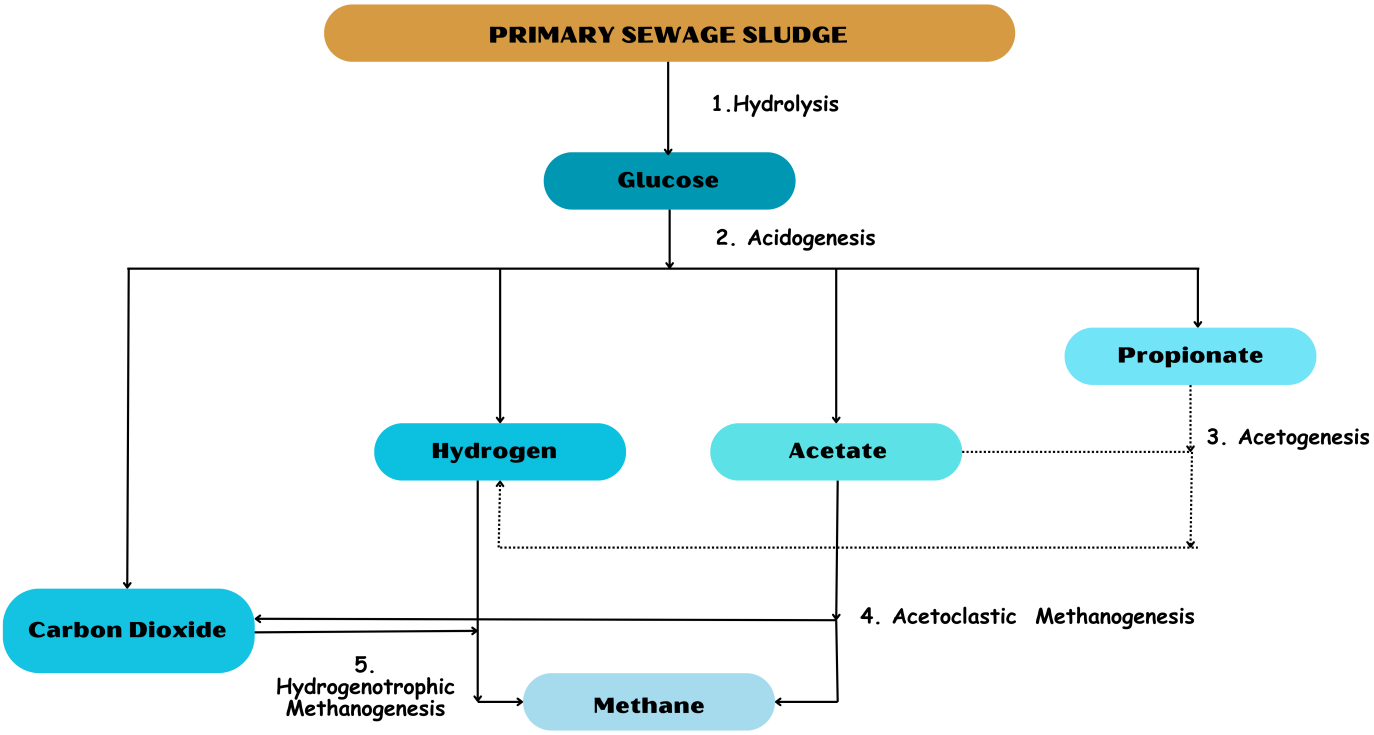


Figure 2.9 Diagram illustrating the schematic representation of the anaerobic digestion processes according to the UCTSDM1).[68]

## Hydrolysis

Anaerobic hydrolysis is a solubilization process where biodegradable particulate organics are broken down and converted into Fermentable Biodegradable Soluble Organics (FBSO) by extracellular hydrolytic enzymes produced by acidogenic microorganisms.[7] As the slowest and rate-limiting step in anaerobic sulfate reduction, anaerobic hydrolysis significantly impacts the HRT of SRUSB systems, with no biomass growth occurring during this phase.

The stoichiometry for anaerobic hydrolysis is represented by Equation 3.4.[46]

$$\mathrm{C}_x\mathrm{H}_y\mathrm{O}_z\mathrm{N}_a + \frac{1}{2}\left(\frac{1}{2}y - z - \frac{3}{2}a\right)\mathrm{H}_2\mathrm{CO}_3 \rightarrow \frac{1}{6}\left(x + \frac{1}{4}y - \frac{1}{2}z - \frac{3}{4}a\right)\mathrm{C}_6\mathrm{H}_{12}\mathrm{O}_6 + \left(\frac{1}{2}y - x - \frac{3}{2}a\right)\mathrm{H}_2\mathrm{O} + \mathrm{aNH}_3 \tag{2.19}$$

where:

$\mathrm{C}_x\mathrm{H}_y\mathrm{O}_z\mathrm{N}_a$ is BPO from the system influent $= XS\,(\mathrm{mol/m^3})$;

$\mathrm{H}_2\mathrm{CO}_3$ is $\mathrm{H}_2\mathrm{O} + \mathrm{CO}_2 = \mathrm{S}_{\mathrm{HCO3}}\,(\mathrm{mol/m^3})$;

$\mathrm{C}_6\mathrm{H}_{12}\mathrm{O}_6$ is FBSO COD $= SF\,(\mathrm{mol/m^3})$;

$\mathrm{NH}_3$ is ammonia released from the anaerobic hydrolysis of BPO $= SNH4\,(\mathrm{mol/m^3})$.

The predominant approach for modelling the rate of hydrolysis of particulate organic material has conventionally employed first-order kinetics. Numerous researchers, have adopted straightforward first-order equations.[27,16] These equations are solely dependent on the concentration of the biodegradable substrate, expressed as COD:

$$\mathrm{r}_{\mathrm{HYD}} = \mathrm{k}_h[\mathrm{S}_{\mathrm{bp}}] \tag{2.20}$$

where:

$r_{HYD}$ is the hydrolysis rate $(\mathrm{mol}\ S_{bp}/L \cdot d)$;

$k_h$ is the first-order hydrolysis kinetic rate constant $(/d)$;

$[S_{bp}]$ is the biodegradable particulate organics concentration $(\mathrm{mol/L})$.

The utilization of first-order kinetics in modelling the hydrolysis process has demonstrated that the resulting first-order rate constant ($K_H$) values are situation-specific. These values exhibit variations dependent on factors such as sludge age or, equivalently, hydraulic re-

tention time.[5,31,32,69] Given the objective of developing a kinetic model applicable across a range of sludge ages, researchers have explored alternative, more general approaches.[69]

Recognizing that the rate of hydrolysis is influenced by multiple factors, including temperature, pH, acidogen organism concentration, type, particle size, and concentration of organics, attention has been directed toward incorporating these variables into the kinetic model. Among these factors, acidogen organism concentration intuitively plays a pivotal role in regulating the hydrolysis rate and thus should find inclusion in the kinetic rate expression. In addressing this, acidogen active biomass was directly incorporated into the first-order kinetics[23]:

$$\mathrm{r_{HYD}} = \mathrm{k_H[S_{bp}][Z_{AD}]} \tag{2.21}$$

where:

$k_H$ is the first-order hydrolysis kinetic rate constant (/d);

$[Z_{AD}]$ is the acidogen active biomass concentration (mol/L).

Monod kinetics also find widespread application in the modelling of biological wastewater treatment procedures. The rate expression is illustrated as[32,53,13]:

$$\mathrm{r_{HYD}} = \frac{\mu_{\mathrm{max,HYD}}[\mathrm{S_{bp}}]}{\mathrm{K_{SM,HYD}} + [\mathrm{S_{bp}}]}[\mathrm{Z_{AD}}] \tag{2.22}$$

Where:

$\mu_{max,HYD}$ is the maximum specific hydrolysis rate constant (mol $S_{bp}/(molZ_{AD} \cdot d)$);

$K_{SM,HYD}$ is the Monod half saturation constant for hydrolysis (mol $S_{bp}/L$).

To model the hydrolysis of particulate slowly biodegradable COD in activated sludge systems, planar surface-mediated reaction kinetics, also known as Contois kinetics, was ap-

plied.[40,13] With a single set of constant values, these kinetics yielded reasonable predictions across a broad range of activated sludge system conditions, including variations in sludge age. Recognizing the similarities between hydrolysis processes in activated sludge and anaerobic digestion, both operating on the same organic components present in raw sewage, this approach was also explored for the anaerobic digestion model:

$$\mathrm{r_{HYD}} = \frac{\mathrm{k_{max,HYD}} \frac{[\mathrm{S_{bp}}]}{[\mathrm{Z_{AD}}]}}{\mathrm{K_{SS,HYD}} + \frac{[\mathrm{S_{bp}}]}{[\mathrm{Z_{AD}}]}} [\mathrm{Z_{AD}}] \tag{2.23}$$

where:

$k_{\text{max,HYD}}$ Maximum specific hydrolysis rate constant (mol $S_{bp}/(molZ_{AD} \cdot d)$);

$K_{\text{SS,HYD}}$ Half saturation constant for hydrolysis (mol $S_{bp}/L$).

Regardless of the chosen hydrolysis formulation, the hydrolysis process under consideration does not facilitate the growth of acidogen biomass. Instead, 1 gCOD of sewage sludge transforms into 1 gCOD of glucose intermediate. The growth of acidogens ensues from the acidogenic conversion of the glucose intermediate into Short-Chain Fatty Acids (SCFA) and H. This conversion, occurring immediately relative to the hydrolysis rate, leads to zero accumulation of glucose within the anaerobic digestion system.

## Acidogenesis

Post-hydrolysis, the relatively simple and soluble compounds, namely amino acids, sugars, and fatty acids, undergo subsequent processes. During fermentation, these compounds are subjected to acidogenesis, resulting in the production of SCFAs, alcohols, $CO_2$, H, and $NH_4^+$. This bioprocess can be quantitatively represented by the following stoichiometric

equation:[46]

$$\left(\frac{1}{Y_{AD}}\right)\mathrm{C_6H_{12}O_6} + (n)\mathrm{NH_3} + \left[\frac{4+(m-\frac{5}{3}k)Y_{AD}}{Y_{AD}}\right]\mathrm{H_2O} \rightarrow \mathrm{C_kH_lO_mN_n} + \left[\frac{2(1-\frac{1}{6}kY_{AD})}{Y_{AD}}\right]\mathrm{HCO_3^-} + \left[\frac{2(1-\frac{1}{6}kY_{AD})}{Y_{AD}}\right]\mathrm{H^+} + \left[\frac{4+(m-\frac{1}{2}l+\frac{3}{2}n+\frac{2}{3}k)Y_{AD}}{Y_{AD}}\right]\mathrm{H_2} + \left[\frac{2(1-\frac{1}{6}kY_{AD})}{Y_{AD}}\right]\mathrm{C_2H_4O_2} \tag{2.24}$$

where:

$\mathrm{C_6H_{12}O_6}$ is FBSO COD $= S_F\,(\mathrm{mol/m^3})$;

$\mathrm{C_kH_lO_mN_n}$ is the elemental composition of the acidogenic microorganisms $= Z_{AD}\,(\mathrm{mol/m^3})$;

$\mathrm{C_2H_4O_2}$ is VFA in the form of acetate $= S_{VFA}\,(\mathrm{mol/m^3})$;

$Y_{AD}$ is the yield coefficient of the acidogenic microorganisms (mol/mol).

Acidogenesis involves the utilization of the model intermediate glucose by acidogenic organisms, resulting in the production of propionic acid ($CH_3CH_2COOH$), acetic acid ($CH_3COOH$), H, $CO_2$, and protons.[35] Specifically, when operating under conditions characterized by low H partial pressure, the acidogenic reaction yields only ($CH_3COOH$), H, and $CO_2$. The formulation of this process is expressed in terms of the growth rate of acidogens $(r_{ZAD})$, modelled using a Monod equation, as outlined below[27,54]:

$$\mathrm{r_{Z_{AD}}} = \frac{\mu_{\mathrm{max,AD}}[S_{\mathrm{bpf}}]}{K_{\mathrm{S,AD}} + [S_{\mathrm{bpf}}]}\left(1 - \frac{[\mathrm{H_2}]}{k_{\mathrm{H2}} + [\mathrm{H_2}]}\right)[Z_{\mathrm{AD}}] \tag{2.25}$$

where:

$\mu_{\text{max,AD}}$ Maximum specific growth rate constant for the acidogens (/d);

$K_{S,AD}$ Half saturation concentration for acidogens (mol/L);

$[S_{bsf}]$ Biodegradable soluble (glucose) substrate concentration (mol/L);

$[\mathrm{H_2}]$ Hydrogen concentration (mol/L);

$K_{\mathrm{H_2}}$ Hydrogen inhibition constant for high $p_{\mathrm{H_2}}$ (mol/L).

The second component within the parentheses in the above equation is referred to as a non-competitive inhibition function, it addresses the decline in reaction rate occurring with elevated $pH_2$ levels. At heightened $pH_2$ levels, alongside $CHC_3OOH$, H, and $CO_2$, $CH_3CH_3COOH$ is also generated. This process involves the production of $CH_3CH_3COOH$ under high $pH_2$ conditions. The growth rate of acidogens during ($CH_3CH_2COOH$) production at elevated $pH_2$ levels is determined by the identical Monod kinetic equation used for low $pH_2$ conditions:

$$\mathrm{r_{Z_{AD}}} = \frac{\mu_{\text{max,AD}}[S_{\text{bpf}}]}{K_{\text{S,AD}} + [S_{\text{bpf}}]} \left( \frac{[\mathrm{H_2}]}{k_{\text{H2}} + [\mathrm{H_2}]} \right) [Z_{\text{AD}}] \tag{2.26}$$

To regulate the activity of this process in correspondence with $pH_2$ levels, the non-competitive inhibition function enclosed within the parentheses orchestrates the activation of the process in high $pH_2$ environments while deactivating it in low $pH_2$ environments. This control mechanism is governed by the switching constant $k_{\text{H2}}$. Furthermore, to ensure consistent glucose ($S_{bsf}$) utilization rates across varying $pH_2$ conditions, including the intermediate range, the rate of acetate production as shown above undergoes adjustment. Specifically, this adjustment involves subtracting the value of the inhibition function from 1 in Equation 3.12.

## Acetogenesis

During acetogenesis, propionic acid generated under elevated $pH_2$ conditions undergoes degradation when $pH_2$ levels decrease, catalyzed by acetogenic microorganisms, resulting in the production of acetate.[48] This degradation rate is characterized in relation to the growth rate of acetogenic organisms, modelled using a Monod equation to represent the specific growth rate:[48]

$$\mathrm{r}_{\mathrm{Z_{AC}}} = \frac{\mu_{\mathrm{max,AC}}[HPr]}{K_{\mathrm{S,AC}} + [HPr]} \left(1 - \frac{[\mathrm{H_2}]}{k_{\mathrm{H2}} + [\mathrm{H_2}]}\right) [Z_{\mathrm{AC}}] \tag{2.27}$$

where:

$\mu_{\mathrm{max,AC}}$ Maximum specific growth rate constant for the acetogens (/d);

$K_{S,AC}$ Half saturation concentration for acetogens (mol/L);

$[HPr]$ Undissociated propionic acid concentration (mol/L);

$[Z_{\mathrm{AC}}]$ Acetogenic organism concentration (mol/L).

In the modelling of weak acid/base chemistry, it becomes necessary to account for both the undissociated and dissociated forms of propionic acid as compounds, aligning with empirical observations. Equation 3.12 expresses the specific growth rate as a Monod function in terms of the undissociated propionic acid species, rather than the more prevalent dissociated species. This choice ensures consistency with experimental findings.[48]

The inclusion of the same non-competitive inhibition function within the parentheses of Equation 3.10 and Equation 3.11 is warranted by the sensitivity of the acetogenesis process to $pH_2$ levels, wherein its activity diminishes with increasing $pH_2$.[20] Consequently, as $pH_2$ rises, not only do acidogens initiate propionic acid production, but also the rate of propionic acid utilization by acetogens decreases. This dual effect leads to a gradual

accumulation of propionic acid as $pH_2$ increases, contributing to a decline in pH when the growth rate of hydrogen-consuming hydrogenotrophic methanogens decreases for various reasons mentioned in the next chapter.

## Acetoclastic Methanogenesis

Acetoclastic methanogenesis, also known as acetate cleavage, is the biochemical process responsible for converting ($CH_3COOH$) into $CH_4$ and $CO_2$, facilitating the growth of acetoclastic methanogens.[43] The rate of this reaction is described using a Monod equation as well, specifically focusing on the growth rate of acetoclastic methanogens. The equation is formulated as follows:[48]

$$\mathrm{r}_{\mathrm{Z_{AM}}} = \frac{\mu_{\mathrm{max,AM}}[HAc]}{K_{\mathrm{S,AM}} + [HAc]}[Z_{\mathrm{AM}}] \tag{2.28}$$

where:

$\mu_{\mathrm{max,AM}}$ Maximum specific growth rate constant for the acetoclastic methanogens (/d);

$K_{S,AM}$ Half saturation concentration for acetoclastic methanogens (mol/L);

$[HAc]$ Undissociated ($CH_3COOH$) concentration (mol/L);

$[Z_{\mathrm{AM}}]$ Acetoclastic methanogen organism concentration (mol/L).

Regarding acetogens, the rate at which acetoclastic methanogens grow is dependent on the concentration of undissociated ($CH_3COOH$) species. Additionally, in the stoichiometry of the process, the uptake of ($CH_3COOH$) occurs through its undissociated species, while the production of $CO_2$ is facilitated through $H_2CO_3$.

## Hydrogenotrophic Methanogenesis

Hydrogenotrophic methanogenic organisms employ $H_2$ and $CO_2$ to produce $CH_4$ and water.[44] This process is characterized by the growth rate of hydrogenotrophic methanogens,

which is mathematically described using the Monod equation.[48]

$$r_{Z_{AM}} = \frac{\mu_{max,HM}[H_2]}{K_{S,HM}{}^{+}[H_2]}[Z_{HM}] \tag{2.29}$$

where:

$\mu_{max,HM}$ Maximum specific growth rate constant for the hydrogenotrophic methanogens (/d);

$K_{S,HM}$ Half saturation concentration for hydrogenotrophic methanogens (mol/L);

$[H_2]$ Molecular hydrogen concentration (mol/L);

$[Z_{HM}]$ Hydrogenotrophic methanogens organism concentration (mol/L).

Consistent with other processes, the uptake of $CO_2$ for hydrogenotrophic methanogenesis occurs through the bicarbonate $HCO_3{}^{-}$ species.[46]

### 2.4.2 Biological reactions in the ASM2-3P

This section explores the intricate bioprocesses mediated by OHOs, ANOs, and PAOs within the ASM2-3P model. These organism groups form the cornerstone of the ASM2-3P model, each playing a vital role in the removal of contaminants from wastewater.

OHOs, by efficiently degrading organic matter, facilitate the conversion of biodegradable compounds into biomass. The ANOs, on the other hand, contribute to N removal through the conversion of $NH_4{}^{+}$ to $NO_2{}^{-}$ and $NO_3{}^{-}$ via nitrification processes.[73] Concurrently, PAOs aid in P removal by actively uptaking and storing P within the biological reactor.[19]

The synergistic interactions among these organism groups underpin the efficacy of ASM2-3P in wastewater treatment, enabling the removal of organic C, N, and P contaminants. Through a sophisticated network of biochemical reactions and metabolic pathways, OHOs, ANOs, and PAOs collectively enhance the efficiency and performance of the acti-

vated sludge system.[22] A comprehensive understanding of these bioprocesses is paramount for optimizing wastewater treatment procedures and fostering sustainable environmental management practices.

## Nitrification

Nitrification stands as a biological mechanism wherein FSA undergoes oxidation into $NO_2^-$ into $NO_3^-$ under the influence of autotrophic nitrifying organisms.[19,20] This intricate process unfolds through two sequential steps: initially, ANOs catalyze the conversion of FSA to $NO_2^-$, a process represented by equation 3.17 below.[19,21] Subsequently, nitrite-oxidizing organisms proceed to further transform $NO_2^-$ into $NO_3^-$, as depicted by Equation 3.18:[20]

$$\mathrm{NH_4^+} + \frac{3}{2}\mathrm{O_2}(ANOs) \rightarrow \mathrm{NO_2^-} + \mathrm{H_2O} + 2\,\mathrm{H^+} \tag{2.30}$$

$$\mathrm{NO_2^-} + \frac{1}{2}\mathrm{O_2}(NNOs) \rightarrow \mathrm{NO_3^-} \tag{2.31}$$

The stoichiometry of nitrification is represented as:[42]

$$\begin{aligned}&\frac{14nE}{8\gamma_B}\mathrm{CO_2} + \mathrm{NH_4^+} + 14\left[\frac{1}{7} - \frac{E}{8\gamma_B}\left(\frac{m}{2} - \frac{9n}{4} - \frac{5p}{4} - \frac{l}{4}\right)\right]\mathrm{O_2} + \frac{14pE}{8\gamma_B''}\mathrm{H_2PO_4^-} \rightarrow \\ &\left[\frac{1}{14} + \frac{E}{8\gamma_B}\left(\frac{3p}{2} - \frac{l}{2} + \frac{n}{2}\right)\right]\mathrm{H_2O} + 14\left(\frac{1}{14} - \frac{14nE}{8\gamma_B}\right)\mathrm{NO_3^-} + 14\left[\frac{1}{7} - \frac{nE}{8\gamma_B}(P+n)\right]\mathrm{H^+} \\ &+ \frac{14nE}{8\gamma_B}C_xH_yO_zN_aP_b\end{aligned} \tag{2.32}$$

where

$\gamma_B$ electron donating capacity per mole of autotrophic nitrifier biomass,$C_xH_yO_zN_aP_b$

$E$ is the flux of COD exiting the aerobic filter which consists of autotrophic nitrification biomass and endogenous sludge. This is expressed as a fraction of the $NH_4^+$ oxidation flux

at steady state, derived from the nitrogen-based kinetic equation of:

$$E = \frac{Y_A N}{(1 + b_{AN} R_s)} \tag{2.33}$$

where $R_S$ signifies the sludge age within the aerobic filter (measured in days). The $Y_{AN}$ represents the yield coefficient of autotrophic nitrification biomass, measured in milligrams of COD produced per milligram of N consumed, while $b_{AN}$ denotes the endogenous respiration rate of autotrophic nitrification biomass (expressed in units of inverse days).

The growth process in the steady-state nitrification model relies on two key assumptions. Firstly, autotrophic nitrifying organisms utilize both $NH_4^+$ and $NO_2^-$ to fulfil their energy requirements, while also utilizing a portion of the ammonia for synthesizing N cell mass.[74] This suggests that nitrifying organisms function as catalysts for nitrification, where the synthesis of N is disregarded due to the minor fraction (1%) of $NH_4^+$ being nitrified to $NO_3^-$ by these organisms. Secondly, it is posited that ANOs directly convert $NH_4^+$ into $NO_3^-$. This assertion holds true because the rate of $NH_4^+$ conversion to $NO_2^-$ by ANOs is slower compared to the rate of $NO_2^-$ conversion to $NO_3^-$ by nitrite-oxidizing organisms. Therefore, any available $NO_2^-$ will promptly undergo direct conversion to $NO_3^-$ in the absence of compounds inhibiting nitrite-oxidizing organisms at the treatment facility. Consequently, only the kinetics of ANOs are factored into the steady-state model. In essence, these two assumptions indicate that the rate of $NH_4^+$ conversion equals the rate of $NO_3^-$ formation as indicated below:[19]

$$\frac{dN_a}{dt} = \frac{dN_t}{dt} = \frac{1}{Y_A} \frac{\mu_{aMt} N_a}{K_{nT} + N_A} X_{BA} \tag{2.34}$$

where:

$N_n$ $NO_3^-$ concentration (mgNO3-N/l),

$\mu_{aMt}$ maximum specific growth rate (mgANOVSS/mgANOVSSS/d),

$N_a$ ammonia concentration (mgN/l),

$K_{nT}$ half saturation constant,

$Y_A$ yield coefficient of the nitrifiers (mgVSS/mgN),

$X_{BA}$ ANO concentration (mgANOVSS/l).

The endogenous respiration process of ANOs is depicted similarly to that of the OHO).[19] Nonetheless, there's a notable distinction in the endogenous respiration rates: OHOs exhibit a significantly higher rate ($b_H$ = 0.24/ d) compared to ANOs ($b_H$ = 0.04/ d).

$$O_n = 4.57\frac{dN_a}{dt} = 4.57\frac{dN_n}{dt} \tag{2.35}$$

where:

$dN_a$ $NH_4^+$ utilisation rate (mgN/l),

$dN_n$ $NO_3^-$ utilisation rate (mgNO3-N/l),

$O_n$ Nitrification oxygen utilisation rate (mgO2/l.d),

## Heterotrophic Denitrification

Heterotrophic denitrification, the conversion of excess $NO_3^-$ into $N_2$ facilitated by Heterotrophic Denitrifiers (HDN), follows nitrification in wastewater treatment systems.[19] The HDNs use FBSO COD ($C_6H_{12}O_6$) as electron and carbon sources to convert $NO_3^-$ into $N_2$. This pro-

cess is illustrated in the following stoichiometric equation:[42]

$$\left(\frac{1}{Y_{HDN}}\right)\mathrm{C_6H_{12}O_6} + (n^{'})\mathrm{NH_4}^{+} + \left[\frac{\frac{25}{6} + \frac{1}{3}(-2k^{'} + m^{'} + \frac{3}{2}n^{'} - \frac{1}{2}l^{'})Y_{HDN}}{Y_{HDN}}\right]\mathrm{NO_3}^{-} +$$
$$\left[\frac{-5 + (k^{'} - n^{'}).Y_{HDN}}{Y_{HDN}}\right]\mathrm{H}^{+} + \left[\frac{-\frac{1}{2} + \frac{1}{2}(-2k^{'} + l^{'} - 3n^{'})Y_{HDN}}{Y_{HDN}}\right]\mathrm{H_2O}$$
$$\rightarrow \mathrm{C_{k^{'}}H_{l^{'}}O_{m^{'}}N_{n^{'}}} + \frac{1}{2}\left[\frac{\frac{25}{6} + \frac{1}{3}(-2k^{'} + m^{'} + \frac{3}{2}n^{'} - \frac{1}{2}l^{'})Y_{HDN}}{Y_{HDN}}\right]\mathrm{N_2} + \left[\frac{6 - k^{'}.Y_{HDN}}{Y_{HDN}}\right]\mathrm{HCO_3}^{-} \tag{2.36}$$

where:

$\mathrm{C_6H_{12}O_6}$ FBSO COD $= S_F$ (mol/m$^3$);

$\mathrm{C_{k^{'}}H_{l^{'}}O_{m^{'}}N_{n^{'}}}$ is the elemental composition of the heterotrophic denitrifiers$(HDN) = Z_{HDN}$(mol/m$^3$);

$Y_{HDN}$ is the yield coefficient of the HDNs (mol/mol).

To optimize this process, it is advised to include an unaerated compartment in aerobic systems designed for nitrification.[19] This allows the aerobically generated $NO_3^-$ to undergo denitrification, thereby reducing its concentration in the effluent. Consequently, denitrification leads to decreased $NO_3^-$ levels in the effluent, benefiting the recovery of alkalinity and reducing oxygen demand.[19]

Designing for denitrification involves determining the substrate concentration required to denitrify the produced $NO_3^-$, considering the anoxic biomass fraction and the rate of $NO_3^-$ flux into the anoxic zone.[75] Substrates for denitrification include influent Readily Biodegradable COD (RBCOD), Slowly Biodegradable COD (SBCOD), and SBCOD generated by biomass through endogenous respiration. The denitrification model is developed based on the kinetics of $NO_3^-$ conversion to $N_2$ using the available substrate.[19]

The steady-state denitrification model was formulated based on empirical observations regarding the influence of organic composition on the denitrification process. It was noted

that RBCOD degrades more rapidly than SBCOD due to its smaller particle size and thus two anoxic reactors are normally used, primary and secondary reactors.[19] In the primary anoxic reactor, denitrification occurs in two distinct phases: an initial rapid phase primarily driven by the utilization of both influent RBCOD and SBCOD, followed by a slower phase predominantly relying on influent SBCOD. Meanwhile, in the secondary anoxic reactor, the denitrification rate is predominantly influenced by the utilization of SBCOD derived from biomass decay. This phase is comparably slower than the second phase in the primary anoxic reactor due to the inherently slower rate of endogenous respiration.[19]

## Biological Excess Phosphorus Removal

Biological excess P removal involves the uptake and release of P facilitated by PAOs.[19] To optimize BEPR, several strategies are employed, including the establishment of an anaerobic zone conducive to the proliferation of PAOs while preventing the reintroduction of $O_2$ and $NO_3^-$ into this zone.[66] Within the anaerobic zone, OHOs coexist with PAOs and ferment incoming readily RBCOD into VFAs. The PAOs subsequently assimilate VFAs, converting them into a high-energy organic compound internally stored as PHA. The energy for PHA formation is derived from the breakdown of internally stored PP within PAOs, leading to the release of orthophosphates and metals into the bulk solution.[20]

In the subsequent aerobic or anoxic zones, PAOs utilize the internally stored PHA for cellular growth and energy production, including the uptake of P from the bulk solution to form PP.[22] The net P removal is calculated as the difference between P uptake in the aerobic/anoxic zones and P release in the anaerobic zone. The biological excess P removal model is based on the principles of substrate allocation between PAOs and OHOs for their respective growth.[19] Once the fraction of influent biodegradable COD allocated to each organism is determined, their biomass can be quantified. By accounting for the P content within each biomass, the overall P removal comprises the sum of P removal achieved by each organism and the P removed through the accumulation of inorganic matter in the

influent.[17]

## Biomass Growth and Death

The biological behaviour of organisms is characterized by two fundamental processes: growth and endogenous respiration.[19] Ordinary heterotrophic organisms utilize biodegradable organic matter to proliferate their cell mass. A portion of these biodegradable organics is allocated to cell mass generation, while the remaining fraction is directed towards energy production, crucial for sustaining anabolic and other cellular activities. *Monod (1949)*[48] investigated the growth dynamics of organisms in conditions where the substrate is limited but nutrients such as N, P, and O are abundant. The growth rate of organisms can be mathematically described using the Monod kinetics[48]:

$$\mu = \frac{\mu_m . S_b}{K_s + S_b} \tag{2.37}$$

$\mu$ Specific growth rate of organisms (g/g.d),

$\mu_m$ Maximum specific growth rate (/d),

$K_S$ Substrate half maximum saturation coefficient (mgCOD/l),

$S_b$ Concentration of biodegradable organic material (mgCOD/l).

Biomass decay is represented in the model based on the concept of endogenous respiration. In the steady-state activated sludge model, endogenous respiration involves the degradation of a portion of the active biomass, estimated to be around 24%.[19] Upon biomass decay, a segment of the resulting dead biomass, approximately 80%, is considered biodegradable and undergoes catabolic breakdown to generate energy, a process that consumes O. Meanwhile, the remaining fraction, constituting 20%, comprises non-biodegradable material

termed as the endogenous residue. This residue accumulates within the reactor as part of the VSS and is ultimately removed alongside the waste sludge, effectively remaining within the system for the duration of the sludge age.[19,20]

The prediction of the endogenous residue concentration in the reactor is determined using[19]:

$$X_E = f_{CV} f b_H X_H \tag{2.38}$$

Additionally, the O consumed during endogenous respiration, known as the carbonaceous oxygen utilization rate (Oc), is computed utilizing Equation:[20]

$$Oc = f_{CV}(1 - f) b_H X_H \tag{2.39}$$

of the steady-state activated sludge model.[33]

### 2.4.3 Components

An initial stride in developing the PWM_SA involved choosing a comprehensive set of components that would be applicable across all unit processes within the plant. The existing model consists of twenty particulate components as shown in Table 2.6, primarily encompassing precipitates generated during anaerobic digestion, sewage particulate organics, and biomass. Storage products like polyphosphate and poly-hydroxy-alkanoates are treated as distinct components within this category, originating from activated sludge and anaerobic digestion units. The principal gases released during transformation reactions in municipal waste treatment are also integrated. The remaining components, totalling thirteen, are all soluble. They include three dissolved sewage organics, thirteen dissolved ionic components, three dissolved gases (O, H, and N), and water.

The model necessitates the establishment of rigorous material mass balances for the targeted transformation processes. To ensure precision, the elemental formulations of each component are incorporated. Most components, such as dissolved ionic components,

gases, and precipitates, possess distinctive chemical formulations, facilitating direct calculations of their molar and material masses (COD, C, H, O, N, and P). However, for organic components—specifically the seven organism groups and sewage components like FBSO, Unbiodegradable Soluble Organics (USO), BPO, UPO —parameterized compositions in the general form ($C_XH_YO_ZN_AB$) were assigned, allowing their compositions to be entered as model inputs. Consequently, the elemental molar ratios (X, Y, Z, A, and B values) in their formulation were encoded as model parameters to accommodate the variability in sewage characteristics. All organism groups, whether aerobic or anaerobic, share the same elemental formulation of $\mathrm{C_{X_o}H_{Y_o}O_{Z_o}N_{A_o}P_{B_o}}$, with each organism component serving as a representative "surrogate" performing a specific function of interest, aligning with the conventional practice in wastewater treatment plant modelling.[31] Additionally, PP ( $Mg_dK_eCa_fPO_3$) and PHA ($C_4H_6O_2$), typically stored within P accumulating organisms (PAOs), are included as separate components in the model to avoid complexities associated with extending the PAO biomass formula and merging stoichiometric coefficients in transformations.

All components are input in mass concentrations, measured in milligrams per litre. However, provisions were additionally made to parameterize component descriptions in terms of their COD and molar concentrations, serving a pivotal role in formulating stoichiometric coefficients and variables within the model. Expressing certain components in molar concentrations, such as [$H_2CO_3$], becomes necessary for modelling the ($CO_2$) partial pressure in the weak acid/base chemistry section of the model.[9]

Table 2.6 The Universally Selected Model Components. [28,19]

| | Component Name | Empirical formula | Notation |
|---|---|---|---|
| Total Dissolved Ionic Concentrations | Water | $H_2O$ | $H_2O$ |
| | Hydrogen ion | $H^+$ | S_H |
| | Sodium | $Na^+$ | S_Na |
| | Potassium | $K^+$ | S_K |
| | Calcium | $Ca^{2+}$ | S_Ca |
| | Magnesium | $Mg^{2+}$ | S_Mg |
| | Ammonium | $NH_4{}^+$ | S_$NH_4$ |
| | Chloride | $Cl^-$ | S_Cl |
| | Acetate | $CH_3COO^-$ | S_Ac |
| | Propionate | $CH_3CH_2COO^-$ | S_Pr |
| | Carbonate | $CO_3{}^{2-}$ | S_$CO_3$ |
| | Sulphate | $SO_4{}^{2-}$ | S_$SO_4$ |
| | Phosphate | $PO_4{}^{3-}$ | S_$PO_4$ |
| | Nitrate | $NO_3{}^-$ | S_$NO_3$ |
| Soluble Organics | Dissolved hydrogen | $H_2$ | S_$H_2$ |
| | Dissolved oxygen | $O_2$ | S_$O_2$ |
| | Unbiodegradable Soluble Organics | $CH_{Yu}O_{Zu}N_{Au}P_{Bu}$ | S_U |
| | Fermentable Biodegradable Soluble Organics | $CH_{Yf}O_{Zf}N_{Af}P_{Bf}$ | S_F |
| | Glucose | $C_6H_{12}O_6$ | S_Glu |
| Particulates | Unbiodegradable particulate organics | $CH_{Yup}O_{Zup}N_{Aup}P_{Bup}$ | X_U_Inf |
| | Biodegradable particulate organics | $CH_{Ybp}O_{Zbp}N_{Abp}P_{Bbp}$ | X_B_Org |
| | Primary sludge biodegradable particulate organics | $CH_{Ybps}O_{Zbps}N_{Abps}P_{Bbps}$ | X_B_Inf |
| | Polyphosphate | $K_{kp}Mg_{mp}CacpPO_3$ | X_PAO_PP |
| | Poly-hydroxy-alkanoate | $C_4H_6O_2$ | X_PAO_Stor |
| | Struvite | $MgNH_4PO_4 \cdot 6\,H_2O$ | X_Str_$NH_4$ |
| | Calcium Phosphate | $Ca_3(PO_4)_2$ | X_ACP |
| | K-struvite | $MgKPO_4 \cdot 6\,H_2O$ | X_Str_K |
| | Calcite | $CaCO_3$ | X_Cal |
| | Magnesite | $MgCO_3$ | X_Mag |
| | Newberyite | $MgHPO_4$ | X_Newb |
| | Influent inorganic settleable solids | | X_ISS |
| Microorganism Biomass | Ordinary heterotrophic organisms | $CH_{Yo}O_{Zo}N_{Ao}P_{Bo}$ | X_OHO |
| | Phosphate accumulating organisms | $CH_{Yo}O_{Zo}N_{Ao}P_{Bo}$ | X_PAO |
| | Autotrophic nitrifying organisms | $CH_{Yo}O_{Zo}N_{Ao}P_{Bo}$ | X_ANO |
| | Acidogens | $CH_{Yo}O_{Zo}N_{Ao}P_{Bo}$ | X_ZAD |
| | Acetogens | $CH_{Yo}O_{Zo}N_{Ao}P_{Bo}$ | X_ZAC |
| | Acetoclastic Methanogens | $CH_{Yo}O_{Zo}N_{Ao}P_{Bo}$ | X_ZAM |
| | Hydrogenotrophic methanogens | $CH_{Yo}O_{Zo}N_{Ao}P_{Bo}$ | X_ZHM |
| | Endogenous residue | $CH_{ye}O_{ze}N_{ae}P_{be}$ | X_U_Org |
| Gases | Carbon dioxide | $CO_2$ | G_$CO_2$ |
| | Methane | $CH_4$ | G_$CH_4$ |

### 2.4.4 Parameters and Variables

Parameters in the model are constants derived from experimental measurements, calibration with a model, or existing literature. They encompass values such as kinetic rate constants, temperature, elemental stoichiometric compositions, and yield coefficients. These parameters remain constant throughout a simulation but can be adjusted via the user interface between simulation runs if necessary. Variables in the model are entities or species that undergo changes at each time step throughout the simulation. The parameters and variables that are used in the PWM_SA are explicitly outlined in the Gujer matrix attached as supplementary Data. The Gujer matrix serves as a standardized and structured method for presenting bioprocess stoichiometry within WRRF models.[3] It provides a clear and concise overview of the bioprocesses and their associated components. The Gujer matrix is explicitly defined and categorized in the methodology chapter.

### 2.4.5 Ionic Species Selected for the Model

The ionic speciation routine within the PWM_SA employs a comprehensive algebraic method to separate the modelling of rapid ionic dissociation and ion pairing equilibrium reactions from slower biological and physical processes. This approach applies to a variety of mixed weak acid/base systems. Since the weak acid/base chemistry processes involved in precipitation and gas exchange are relatively slow, they are modelled alongside the slow bioprocesses using kinetic equations.[3] This algebraic-based ionic equilibrium model can be seamlessly integrated with kinetic models for biologically mediated unit processes occurring in WWTPs, provided the interactions between these processes and weak acid/base species are understood.

The concentrations of ionic species from various weak acid/base sub-systems, which are simultaneously present in solution and influence pH, are determined by sets of aqueous phase equilibrium dissociation and mass balance equations (refer to Table 2.7 below for an example).

Table 2.7 Example for equilibrium and mass balance equations for ionic speciation. [3]

| Weak Acid Sub-System | Aqueous Phase Equilibrium Equations | Mass Balance Equation |
|---|---|---|
| Ammonia | $[NH_3] = \frac{K_{NH_4} \cdot [NH_4^+]}{(H^+)}$ <br> $[NH_4SO_4^-] = \frac{[SO_4^{2-}] \cdot [NH_4^+]}{K_{NH_4SO_4}}$ | $N_T = [NH_4^+] + [NH_3] + [NH_4SO_4^-]$ |

**Note:** Where $(H^+)$ is the H ion activity, [X] the molar concentrations of species X and $K'_X$ is the thermodynamic equilibrium constant for species X, adjusted for Debye Hückel effects to account for the activity of ions in low salinity water. [70]

Given that total concentrations are crucial for material balance calculations, Brouckaert (2010) included the total species components as shown in Table 2.8 to represent the comprehensive concentrations of the different weak acid/base systems. For instance, the $CO_3$ component encompasses $CO_3^{2-}$, $HCO_3^-$, $H_2CO_3$, and various other aqueous ion pair (excluding precipitates) carbonate complexes in the solution, such as $MgCO_3$ and $CaHCO_3^+$. The potential ion pairs are listed in Table 2.8.

Table 2.8 Ionic Species Selected for the Three Phase Modelling

| | | | | | |
|---|---|---|---|---|---|
| 1 | $H^+$ | Hydrogen ion | 23 | $NH_4SO_4^-$ | Ammonium sulphate |
| 2 | $Na^+$ | Sodium | 24 | $MgPO_4^-$ | Magnesium phosphate |
| 3 | $K^+$ | Potassium | 25 | $CaCH_3COO^+$ | Calcium acetate |
| 4 | $Ca^{2+}$ | Calcium | 26 | $CaCH_3CH_2COO^+$ | Calcium propionate |
| 5 | $Mg^{2+}$ | Magnesium | 27 | $CaHCO_3^+$ | Calcium bi-carbonate |
| 6 | $NH_4^+$ | Ammonium | 28 | $NaSO_4^-$ | Sodium sulphate |
| 7 | $Cl^-$ | Chloride | 29 | $MgHPO_4$ | Magnesium hydrogen phosphate |
| 8 | $CH_3COO^-$ | Acetate | 30 | $CH_3COONa$ | Sodium Acetate |
| 9 | $CH_3CH_2COO^-$ | Propionate | 31 | $H_2CO_3$ | Di-hydrogen carbonate |
| 10 | $CO_3^{2-}$ | Carbonate | 32 | $MgSO_4$ | Magnesium sulphate |
| 11 | $SO_4^{2-}$ | Sulphate | 33 | $HPO_4^{2-}$ | Hydrogen phosphate |
| 12 | $PO_4^{3-}$ | Phosphate | 34 | $NH_3$ | Ammonia |
| 13 | $NO_3^-$ | Nitrate | 35 | $MgCO_3$ | Magnesium carbonate |
| 14 | $OH^-$ | Hydroxide ion | 36 | $ACPO_4^-$ | Calcium Phosphate |
| 15 | $CH_3COOH$ | Acetic acid | 37 | $MgHCO_3^+$ | Magnesium hydrogen carbonate |
| 16 | $CH_3CH_2COOH$ | Propionic acid | 38 | $CaHPO_4^-$ | Calcium hydrogen phosphate |
| 17 | $HCO_3^-$ | Bi-carbonate | 39 | $NaCO_3^-$ | Sodium carbonate |
| 18 | $CaSO_4$ | Calcium sulphate | 40 | $MgH_2PO_4^+$ | Magnesium di-hydrogen phosphate |
| 19 | $H_2PO_4^-$ | Di-hydrogen phosphate | 41 | $NaHCO_3$ | Sodium hydrogen carbonate |
| 20 | $MgCH_3COO^+$ | Magnesium acetate | 42 | $NaHPO_4^-$ | Sodium hydrogen phosphate |
| 21 | $MgCH_3CH_2COO^+$ | Magnesium propionate | 43 | $CaOH^+$ | Calcium hydroxide |
| 22 | $CaCO_3$ | Calcium carbonate | 44 | $MgOH^+$ | Magnesium hydroxide |

The reviewed literature provides critical insights into wastewater treatment technologies, particularly the innovative SANI system. This system has shown significant potential in addressing water stress in regions like Hong Kong, where salinity in wastewater poses unique challenges. [46] The adaptation of the SANI system within the South African context

offers a promising avenue for addressing freshwater scarcity, with key differences such as population density, operator skills, and user acceptability requiring careful consideration.

In water-stressed regions like South Africa, the relevance of the SANI system lies in its ability to reduce sludge production, optimize nutrient removal, and achieve energy-efficient wastewater treatment. These attributes directly address pressing challenges in resource-constrained environments. Furthermore, the application of modelling frameworks, such as the PWM _SA model, facilitates a quantitative evaluation of the feasibility of integrating SANI infrastructure. This highlights the importance of calibrated and validated models to simulate real-world system performance accurately.[42]

Modelling plays a critical role in assessing the feasibility and effectiveness of implementing the SANI system in regions like South Africa. The extension of the PWM _SA model to incorporate SANI-specific bioprocesses demonstrates the potential for adapting established frameworks to local conditions. Verification of these models is paramount to ensure scientific accuracy, internal consistency, and realistic predictions relative to real-world measurements.[42] The steady-state and kinetic models developed for the SANI system provide a foundation for evaluating its performance under varying conditions, enabling optimization for regional applications.

Current research addresses gaps in model representation to ensure accurate simulations of the SANI system. This includes incorporating region-specific influent characteristics, refining stoichiometric and kinetic parameters, and validating models with empirical data from pilot studies in South Africa.

In conclusion, the SANI system represents a transformative approach to saline sewage treatment. Its adaptation and implementation in South Africa could address critical water management challenges, provided that regional differences are carefully considered and addressed through robust modelling and pilot-scale validation.

# Chapter 3: Methodology

This section outlines the approach used to extend and verify the PWM_SA model by incorporating sulfate reduction and autotrophic denitrification processes present in the SANI system. The model simulates key processes within the SRUSB, anoxic, and aerobic reactors, using the Gujer matrix framework to represent the biochemical reactions. After verification through the mass balance, the model was integrated into the WEST software, and verified by running simulations using the SANI pilot plant experimental influent data and plant conditions. A final mass balance check was performed post-simulation to check and verify the model's internal consistency.

## 3.1 Inclusion of a steady state model for anaerobic Biological Sulphate Reduction (BSR)

The steady-state model for BSR was developed using primary sewage sludge as the carbon source and electron donor. This model is analogous to the Sötemann (2005b) model for methanogenic anaerobic digestion systems. In the effort to apply the PWM_SA model to BSR systems, the model was extended to incorporate BSR processes in WEST.[76] The BSR reactions were coded using the same methodology as the methanogenic equations.[26,47] The derivation and coding of the sulfidogenic reactions also prompted further verification of the existing PWM_SA model.

Similar to the methanogenic reactions, where stoichiometry was derived on a mole basis, a similar approach was applied to the sulfidogenic system, with stoichiometric derivations based on identified reaction pathways.[69,56,38] This extension introduced three growth equations and three decay equations for the reactions shown in Figure 3.1, under the assumption that butyrate and higher VFAs are not present in this system. For the SANI process reactions, $SO_4^{2-}$ serves as the electron acceptor, resulting in the formation of $H_2S$.

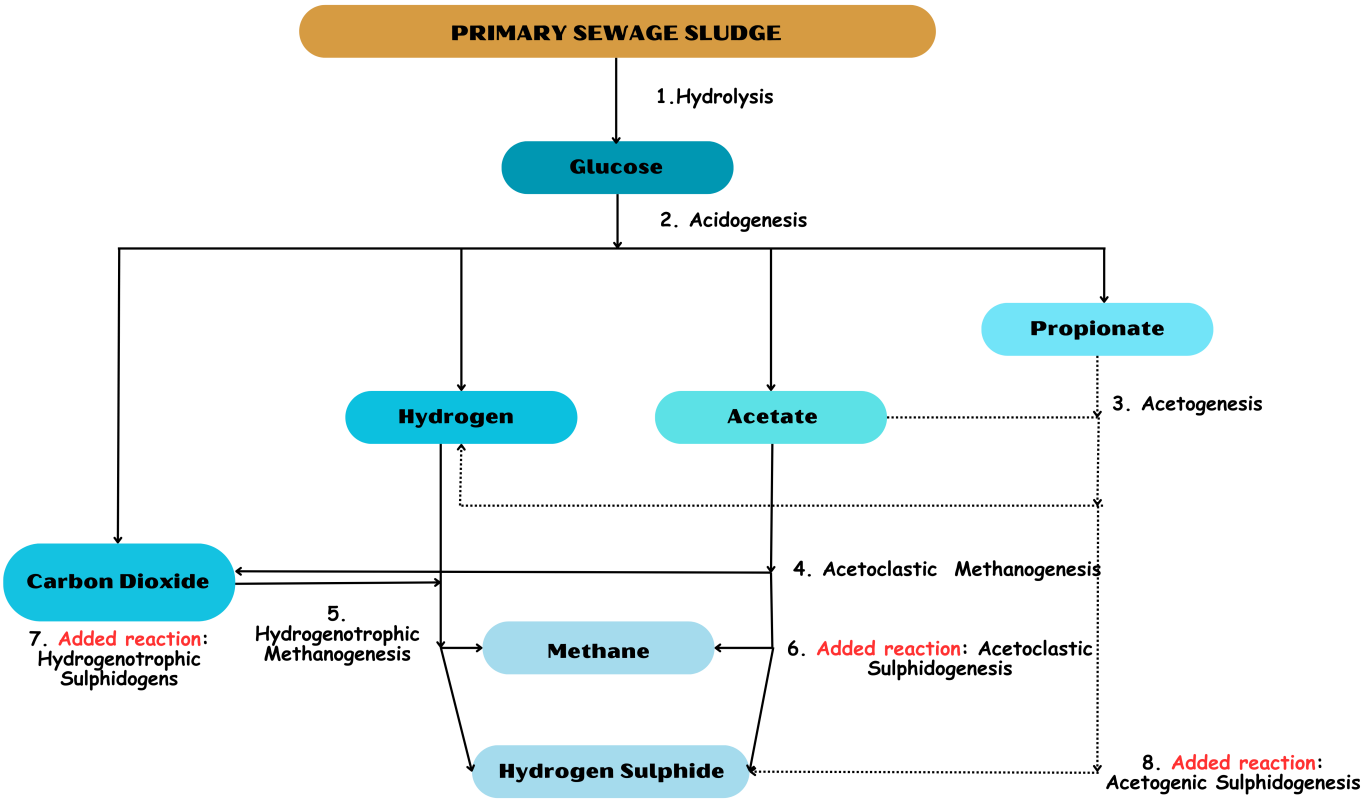


Figure 3.1 Diagram illustrating the schematic representation of the anaerobic digestion processes according to the UCTSDM1 including BSR.[68,56]

In the extended PWM_SA model for BSR anaerobic digestion, $H_2S$ is represented in its partially dissociated form, $HS^-$. The speciation routine allocates $HS^-$ to either $H_2S$ or $HS^-$ based on the pH. This distinction is crucial because the undissociated form (i.e. $H_2S$) is toxic to methanogenic, sulfidogenic, and acetogenic bacteria[36].

Currently, the BSR reactions within WEST are not coded to interact with methanogenic reactions due to insufficient data. However, literature indicates that sulfidogenic organisms generally outcompete methanogens for available substrates and this depends on reactor conditions, the concentration of $SO_4^{2-}$ in the mixed liquor also needs calibration for a more refined model.[17] A simple switching parameter allows users to select either sulfidogenesis or methanogenesis. Since methanogenic reactions are deactivated during BSR, the impact of undissociated $H_2S$ on acetogenic and methanogenic organisms is not considered at this stage. However, their toxicity is accounted for in the sulfate-reducing processes. A linear

inhibition term was used to represent this, as shown in Equation 3.1 below, but it was found to be unstable when $H_2S$ concentrations exceed the inhibition constant (KI).

$$\mathrm{I_{H_2S}}=1-\frac{\mathrm{H_2S}}{\mathrm{K_I}} \tag{3.1}$$

The model stability was improved by matching the $50\%$ inhibition point to an exponential function. This adjustment prevents the inhibition term from reaching zero, which generally enhances the stability of the model. The KI value, which represents the inhibition constant, varies among different organism groups. For acetogenic sulfidogens, particularly propionate-degraders, the KI value is 0.185 gS/l.[38]

$$\mathrm{I}=\mathrm{e}^{-\left(\frac{[\mathrm{H_2S}]}{0.600556\mathrm{K_I}}\right)^2} \tag{3.2}$$

Furthermore, a $SO_4^{2-}$ switching function is included to manage conditions when $SO_4^{2-}$ concentrations are low. This function deactivates the BSR processes if there is insufficient $SO_4^{2-}$ to sustain them.[38] The constant (KN) values, which vary among different organism groups, were taken directly from Kalyuzhnyi (1998) as shown below.

$$\mathrm{sulphate\,switching\,term}=\frac{[\mathrm{SO_4{}^{2-}}]}{\mathrm{K_N}+[\mathrm{SO_4{}^{2-}}]} \tag{3.3}$$

### 3.1.1 Added Biological Reactions

This sections of this section introduce the additional biological reactions incorporated into the PWM_SA model, focusing on sulfidogenic and denitrifying processes. It specifically covers acetotrophic and hydrogenotrophic sulfidogenesis, where microorganisms utilize acetate ($C_2H_3O_2^-$) and H to produce $H_2S$, and autotrophic denitrification, where $NO_3^-$ is reduced to $N_2$ using $H_2S$ as the electron donor. Additionally, it explains the growth and decay processes of various microbial groups, detailing the stoichiometric equations that

represent their interactions and contributions to biomass production and S reduction.

## Biological Sulfate Reduction (BSR)

The added sulfidogenic bioprocesses include Hydrogenotrophic Sulfidogens (HS) and AS, which are distinguished based on the substrates they utilize: ($C_2H_3O_2^-$) and H, respectively.[43] Acetotrophic sulfidogenesis is mediated by AS organisms that convert VFAs into $H_2S/HS^-$ and $HCO_3^-$. On the other hand, hydrogenotrophic sulfidogenesis involves HS organisms that utilize hydrogen gas ($H_2$) to produce $H_2S/HS^-$.[35,37,42]

### Acetotrophic sulfidogenesis

In acetotrophic sulfidogenesis, ($C_2H_3O_2^-$) acts as a crucial substrate, supplying electrons necessary for both the anabolic and catabolic processes carried out by acetotrophic sulfidogenic organisms.[43] This utilization of ($C_2H_3O_2^-$) results in the production of two key substances: $H_2S/HS^-$ and $H_2CO_3$. The anabolic pathway contributes to the generation of $HCO_3^-$, while the catabolic pathway leads to the formation of $H_2S$. Equation 3.4 provides the stoichiometry underlying acetotrophic sulfidogenesis:[42]

$$\begin{aligned}&\left(\frac{1}{Y_{AD}}\right)\mathrm{C_2H_4O_2}+(n)\mathrm{NH_3}+\left[\frac{1+\frac{1}{4}(m-2k-\frac{1}{2}l+\frac{3}{2}n)Y_{AS}}{Y_{AS}}\right]\mathrm{SO_4}^{2-}+\\&\left[\frac{-\frac{1}{2}+\frac{3}{2}\left(\frac{1}{6}k+\frac{1}{4}m-\frac{1}{8}l+\frac{3}{8}n\right)Y_{AS}}{Y_{AS}}\right]\mathrm{H^+}\rightarrow\mathrm{C}_k\mathrm{H}_l\mathrm{O}_m\mathrm{N}_n+\left[\frac{2-kY_{AS}}{Y_{AS}}\right]\mathrm{HCO_3}^-\\&\left[\frac{\frac{1}{2}+\frac{1}{8}(m-2k-\frac{1}{2}l+\frac{3}{2}n)Y_{AS}}{Y_{AS}}\right]\mathrm{H_2S}+\left[\frac{\frac{1}{2}+\frac{1}{8}(m-2k-\frac{1}{2}l+\frac{3}{2}n)Y_{AS}}{Y_{AS}}\right]\mathrm{HS^-}+\\&\left[\frac{(k-\frac{1}{2}l+\frac{3}{2}n)Y_{AS}}{Y_{AS}}\right]\mathrm{H_2O}\end{aligned}\tag{3.4}$$

where:

$C_2H_4O_2$ VFA in the form of acetate $= S_{VFA}$ (mol/m$^3$);

$C_kH_lO_mN_n$ is the elemental composition of the AS($AS$) $= Z_{AS}$(mol/m$^3$);

$Y_{AS}$ is the yield coefficient of the As (mol/mol).

**Hydrogenotrophic sulfidogenesis**

Hydrogen, an intermediary product generated during biological acidogenesis, serves as a readily available resource for HS to produce biomass and $H_2S/HS^-$. Additionally, the alkalinity derived from carbonic acid $H_2CO_3$ is utilized for microbial growth during anabolic processes, while alkalinity from $H_2S/HS^-$ is generated during catabolic activities. This process is represented by the stoichiometric equation below:[46,42]

$$\left(\frac{1}{Y_{HS}}\right)\mathrm{H_2} + \left[\frac{\frac{1}{4} - \frac{1}{4}(2k - m - \frac{3}{2}n + \frac{1}{2}l)Y_{HS}}{Y_{HS}}\right]\mathrm{SO_4}^{2-} + (n)\mathrm{NH_3}$$
$$+ \left[\frac{\frac{1}{8} + \frac{1}{8}(2k + 3m + \frac{9}{2}n + \frac{3}{2}l)Y_{HS}}{Y_{HS}}\right]\mathrm{H^+} \rightarrow \mathrm{C_kH_lO_mN_n} + \left[\frac{\frac{1}{8} - \frac{1}{8}(2k - m - \frac{3}{2}n + \frac{1}{2}l)Y_{HS}}{Y_{HS}}\right]\mathrm{H_2S}$$
$$\left[\frac{\frac{1}{8} - \frac{1}{8}(2k - m - \frac{3}{2}n + \frac{1}{2}l)Y_{HS}}{Y_{HS}}\right]\mathrm{HS^-} + \left[\frac{1 + (k + \frac{3}{2}n - \frac{1}{2}l)Y_{HS}}{Y_{HS}}\right]\mathrm{H_2O} \tag{3.5}$$

where:

$C_kH_lO_mN_n$ is the elemental composition of the HS($HS$) $= Z_{HS}$(mol/m$^3$);

$Y_{HS}$ is the yield coefficient of the HS (mol/mol).

## Autotrophic Denitrification

Autotrophic denitrification is facilitated by Autotrophic Denitrifiers (ADN) using dissolved $H_2S/HS^-$ as the electron donor.[26] This process reduces $NO_3^-$ to $N_2$ through catabolism,

while anabolism generates biomass and consumes $H_2CO_3$ alkalinity as the carbon source. The stoichiometry of autotrophic denitrification is shown below:[42]

$$k^{'}\mathrm{HCO_3}^{-} + (n^{'})\mathrm{NH_4}^{+} + \left(\frac{1}{Y_{ADN}}\right)\mathrm{NO_3}^{-} + \left[\frac{\frac{5}{16} + \frac{1}{16}(4k^{'} - 2m^{'} - 3n^{'} + l^{'})Y_{ADN}}{Y_{ADN}}\right]\mathrm{H_2S}$$
$$\left[\frac{\frac{5}{16} + \frac{1}{16}(4k^{'} - 2m^{'} - 3n^{'} + l^{'})Y_{ADN}}{Y_{ADN}}\right]\mathrm{HS}^{-} + \left[\frac{\frac{1}{2} + \frac{1}{2}(-2k^{'} - 3n^{'} + l^{'})Y_{ADN}}{Y_{ADN}}\right]\mathrm{H_2O}$$
$$\rightarrow \mathrm{C_{k'}H_{l'}O_{m'}N_{n'}} + \left[\frac{\frac{5}{8} + \frac{1}{8}(4k^{'} - 2m^{'} - 3n^{'} + l^{'})Y_{ADN}}{Y_{ADN}}\right]{\mathrm{SO_4}}^{2-} + \left(\frac{1}{2Y_{ADN}}\right)\mathrm{N_2}$$
$$\left[\frac{\frac{1}{16} + \frac{1}{16}(-4k^{'} - 6m^{'} + 7n^{'} + 3l^{'})Y_{ADN}}{Y_{ADN}}\right]\mathrm{H}^{+} \tag{3.6}$$

where:

$\mathrm{C_{k'}H_{l'}O_{m'}N_{n'}}$ is the elemental composition of the autotrophic denitrifiers$(ADN) = Z_{ADN}$(mol/m$^3$); $Y_{ADN}$ is the yield coefficient of the ADN (mol/mol).

## Biomass Growth and Death

The death and decay processes for the anaerobic SRB groups (AD, AS, and HS), the anoxic denitrifying microorganisms (ADN and HDN), and the aerobic autotrophic nitrifiers (AN) were deemed to be identical.[46] During endogenous decay, the biomass degrades and releases its BPO into the bulk liquid, contributing to the pool of biodegradable organics with the same elemental composition as that in the system influent. Given the low yield and endogenous mass loss rates of all biomass in the SANI system, the generation of unbiodegradable endogenous residue is considered negligible.[43]

To account for the various biomass and BPO compositions, a generalized stoichiometric equation for endogenous decay was developed. This equation applies to biomass with the composition $\mathrm{C_kH_lO_mN_n}$ and influent BPO composition $\mathrm{C_xH_yO_zN_a}$. The generalized

stoichiometry for the endogenous decay of all organism groups (AD, AS, HS, ADN, HDN, and AN) can be expressed by Equations. (3.7)-(3.9 ) below:[46]

For the SRB groups (AD, AS, HS), the stoichiometric equation can be expressed as follows:

$$\begin{aligned}&\mathrm{C}_k\mathrm{H}_l\mathrm{O}_m\mathrm{N}_n + \left[\frac{k(3y-2z-9a)+l(z-3x)+m(2x+3a-y)+n(9x-3z)}{\gamma_S}\right]\mathrm{H_2O}\\&\rightarrow \frac{\gamma_B}{\gamma_S}\mathrm{C}_x\mathrm{H}_y\mathrm{O}_z\mathrm{N}_a + \left[\frac{k(y-2z-3a)+x(2m+3n-l)}{\gamma_S}\right]\mathrm{H_2CO_3}+\\&\left[\frac{n(4x+y-2z)+a(2m-4k-l)}{\gamma_S}\right]\mathrm{NH_3}\end{aligned} \tag{3.7}$$

Where:

$\mathrm{C}_k\mathrm{H}_l\mathrm{O}_m\mathrm{N}_n$ = elemental composition of the SRB groups$(Z_{AD}, Z_{AS}, Z_{HS})$;

$\mathrm{C}_x\mathrm{H}_y\mathrm{O}_z\mathrm{N}_a$ = elemental composition of the BPO;

$\gamma_S$ = electrons available per mole of the BPO , $(\mathrm{C}_x\mathrm{H}_y\mathrm{O}_z\mathrm{N}_a)$

$= 4x + y - 2z - 3a + 5b\,(\mathrm{e^-}\ \text{eq/mol})$;

$\gamma_B$ = electrons available per mole of the SRB biomass $(\mathrm{C}_k\mathrm{H}_l\mathrm{O}_m\mathrm{N}_n)$

$= 4k + l - 2m - 3n + 5p\,(\mathrm{e^-}\ \text{eq/mol})$;

$\mathrm{H_2CO_3} = \mathrm{H_2O} + \mathrm{CO_2}$.

For the anoxic denitrifying microorganisms (ADN, HDN):

$$\begin{aligned}&\mathrm{C_{k'}H_{l'}O_{m'}n_{a'}} + \left[\frac{k'(3y-2z-9a)+l'(z-3x)+m'(2x+3a-y)+n'(9x-3z)}{\gamma_S}\right]\mathrm{H_2O}\\&\rightarrow \frac{\gamma_B'}{\gamma_S}\mathrm{C}_x\mathrm{H}_y\mathrm{O}_z\mathrm{N}_a + \left[\frac{k'(y-2z-3a)+x(2m'+3n'-l')}{\gamma_S}\right]\mathrm{H_2CO_3}+\\&\left[\frac{n'(4x+y-2z)+a(2m'-4k'-l')}{\gamma_S}\right]\mathrm{NH_3}\end{aligned} \tag{3.8}$$

Where:

$\mathrm{C_{k'}H_{l'}O_{m'}n_{a'}}$ = elemental composition of the denitrifying microorganisms$(Z_{ADN}, Z_{HDN})$;

$\mathrm{C}_x\mathrm{H}_y\mathrm{O}_z\mathrm{N}_a$ = elemental composition of the BPO;

$\gamma_S$ = electrons available per mole of the BPO , $(\mathrm{C}_x\mathrm{H}_y\mathrm{O}_z\mathrm{N}_a)$

$= 4x + y - 2z - 3a + 5b\,(\mathrm{e^-}\ \text{eq/mol})$;

$\gamma_B^{'}$ = electrons available per mole of the denitrifying microorganisms $(\mathrm{C}_k\mathrm{H}_l\mathrm{O}_m\mathrm{N}_n)$

$= 4k^{'} + l^{'} - 2m^{'} - 3n^{'} + 5p^{'}\ (\mathrm{e^-}\ \text{eq/mol})$;

$\mathrm{H_2CO_3} = \mathrm{H_2O} + \mathrm{CO_2}$.

For the aerobic ANs:

$$\mathrm{C_{k''}H_{l''}O_{m''}n_{a''}} + \left[\frac{k^{''}(3y - 2z - 9a) + l^{''}(z - 3x) + m^{''}(2x + 3a - y) + n^{''}(9x - 3z)}{\gamma_S}\right]\mathrm{H_2O}$$
$$\rightarrow \frac{\gamma_B^{''}}{\gamma_S}\mathrm{C}_x\mathrm{H}_y\mathrm{O}_z\mathrm{N}_a + \left[\frac{k^{''}(y - 2z - 3a) + x(2m^{''} + 3n^{''} - l^{''})}{\gamma_S}\right]\mathrm{H_2CO_3} +$$
$$\left[\frac{n^{''}(4x + y - 2z) + a(2m^{''} - 4k^{''} - l^{''})}{\gamma_S}\right]\mathrm{NH_3} \tag{3.9}$$

Where:

$\mathrm{C_{k''}H_{l''}O_{m''}n_{a''}}$ = elemental composition of the ANs$(Z_{AN})$;

$\mathrm{C}_x\mathrm{H}_y\mathrm{O}_z\mathrm{N}_a$ = elemental composition of the BPO;

$\gamma_S$ = electrons available per mole of the BPO , $(\mathrm{C}_x\mathrm{H}_y\mathrm{O}_z\mathrm{N}_a)$

$= 4x + y - 2z - 3a + 5b\,(\mathrm{e^-}\ \text{eq/mol})$;

$\gamma_B^{'}$ = electrons available per mole of the denitrifying microorganisms $(\mathrm{C}_k\mathrm{H}_l\mathrm{O}_m\mathrm{N}_n)$

$= 4k^{'} + l^{'} - 2m^{'} - 3n^{'} + 5p^{'}\ (\mathrm{e^-}\ \text{eq/mol})$;

$\mathrm{H_2CO_3} = \mathrm{H_2O} + \mathrm{CO_2}$.

## 3.2 Gujer Matrix Development

The primary objective of this study was to integrate the processes of the SANI system into the PWM_SA model and to verify the model to ensure its ability to accurately replicate the behaviour of the SANI system. To achieve this, a Gujer matrix was developed to incorporate sulfate reduction and autotrophic denitrification processes, along with their associated components, parameters, stoichiometric relationships, and kinetic constants.

A Gujer matrix serves as a systematic framework in wastewater treatment modelling, effectively representing the biological and chemical processes within a system.[27] It is particularly valuable for detailing the stoichiometry of transformations in models such as the Activated Sludge Model (ASM). This matrix offers a clear and concise depiction of how various compounds are consumed and produced across different processes. Typically, bioprocess kinetics are integrated alongside the matrix, facilitating a deeper understanding and analysis of the system.

Gujer matrices enable mass balance verification by summing the products of each component's elemental and charge content with their respective stoichiometric coefficients (as illustrated in the Gujer matrix provided as supplementary Data).[30] This method ensures that all elements within the bioprocesses remain in equilibrium.

### 3.2.1 Gujer Matrix Notation

The use of a standardized notation in the Gujer matrix for wastewater treatment models provides a uniform way to represent various state variables and processes, facilitating the comparison of models and experimental data. By employing a consistent framework, it becomes easier to interpret and share information. Furthermore, this notation method is well accepted by the IWA modelling community and was thus adopted for this study.[9]

In the Gujer matrix notation, the primary symbol represents particle size and must always be provided. This main symbol is in uppercase italics, signifying whether the component is soluble (S), particulate (X), or colloidal (C) as shown in Figure 3.2.

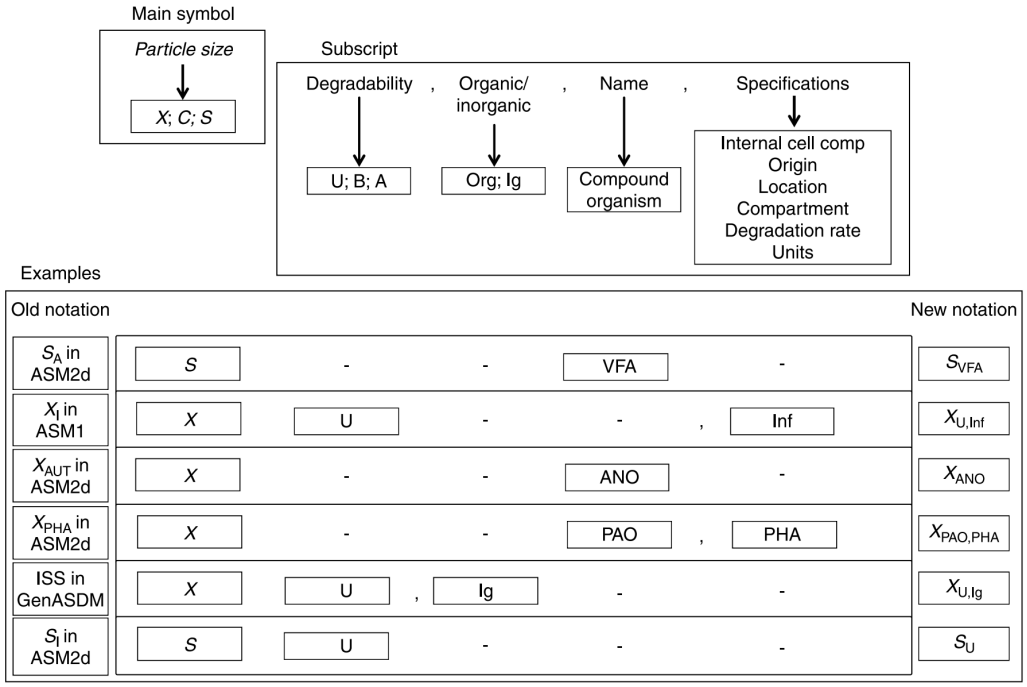


Figure 3.2 Description of the used notation for state variables in the PWM_SA Gujer matrix. [9]

This differentiation helps to classify materials based on how they behave within the treatment system. The subscript can include up to four levels, each offering specific information: degradability, the organic or inorganic nature of the compound, the name of the compound or organism, and any additional specifications needed for further detail. The subscript is presented in uppercase, or a mix of upper and lowercase for clarity, and is not italicized.

Degradability is one of the most critical aspects of WWT models, distinguishing between undegradable (U), biodegradable (B), and abiotically convertible (A) compounds. This classification allows for a better understanding of how different substances are processed or transformed within treatment systems. The notation also includes whether a compound is organic (Org) or inorganic (Ig), which is useful for identifying autotrophic versus heterotrophic metabolism. The third level in the subscript provides the specific name of the compound or organism. For compounds with lengthy chemical formulas, abbreviations or chemical symbols (e.g., $NH_4$, $CH_4$) are used for simplicity.

In cases where additional specifications are necessary, such as indicating the source of a compound (e.g., 'Inf' for influent-derived) or differentiating between compartments (e.g., SCO2, L for liquid phase), the notation can be extended to include this detail. This ensures that models can accurately reflect complex interactions, such as endogenous processes or structural components of biomasses (e.g., $X_{PAO,PHA}$ for PHA storage in PAOs outlined in Figure 3.3).

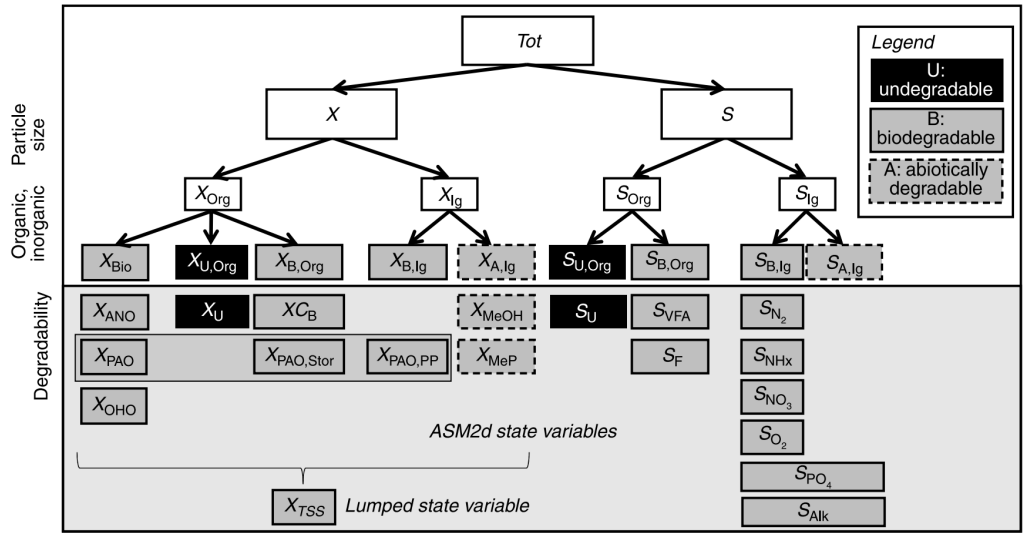


Figure 3.3 The proposed notational framework used in the ASM2d state variables. [9]

The framework also allows for notations that specify ion activity and concentration, with brackets (e.g., $S_{[NH4]}$) used for ion concentration and parentheses (e.g., $S_{(NH4)}$) for ion activity. This level of detail supports the differentiation between total compounds and their ionic forms, ensuring precision in modelling processes like substrate utilization by autotrophic organisms or inhibition mechanisms.

### 3.2.2 Model Extension

The extension of the model involved the incorporation of sulfate reduction and autotrophic denitrification processes, as well as the relevant components, parameters, stoichiometric relationships, and kinetic constants to the already developed PWM_SA Gujer matrix. The first step was to identify the biological processes that are to be added to the PWM_SA. The

below growth and decay processes were incorporated into the UCT ASM2-3P and SDM3P (sub-models of PWM_SA as described in section 2.4) Gujer matrices using the chemical equations described in section 3.1.

Table 3.1 The BSR and AD reactions that were added to the PWM_SA model.[28,19]

| **Model** | **Added reaction** | **Type of reaction** |
|---|---|---|
| ASM2-3P | Autotrophic Denitrification | Anoxic Growth of Autotrophic Denitrifiers |
| | | Lysis of Autotrophic denitrifiers |
| SDM-3P | Biological Sulfate Reduction | Uptake of sugars in SDM |
| | | Death and decay of the sugar degraders in SDM1 |
| | | Uptake of propionate in SDM1 |
| | | Death and decay of the propionate degraders |
| | | Growth of acetogenic SRB biomass |
| | | Death and decay of the acetogenic SRB |
| | | Uptake of acetate in SDM |
| | | Death and decay of the acetate degraders |
| | | Growth of acetoclastic SRB |
| | | Uptake of hydrogen in SDM |
| | | Death and decay of the hydrogen degraders |
| | | Growth of hydrogenotrophic SRB |
| | | Death and decay of the hydrogenotrophic SRB |

The key components involved in sulfate reduction and autotrophic denitrification were then defined and also incorporated into the Gujer matrix in the same format and notation as represented in Table 3.2 below:

Table 3.2 The added model components for SRB (Where X denotes concentration).[28,19]

| | **Component Name** | **Empirical formula** | **Notation** |
|---|---|---|---|
| Added components | Hydrogen sulfide | $HS^-$ | S_HS |
| | Acetoclastic sulfidogens | $C_kH_lO_mN_n$ | X_ACS |
| | Hydrogenotrophic sulfidogens | $C_kH_lO_mN_n$ | X_HS |
| | Autotrophic denitrifying organisms | $C_kH_lO_mN_n$ | X_ADO |
| | Autotrophic denitrifiers | $C_kH_lO_mN_n$ | X_AD |
| | Acetotrophic sulfidogens | $C_kH_lO_mN_n$ | X_AC |

Additionally, kinetic parameters such as maximum growth rates and saturation/inhibition

were determined together with stoichiometric parameters that allowed for the inclusion of S in the elemental composition of the organic components as represented in Table 3.3:

Table 3.3 The added model parameters for sulfate reduction and autotrophic denitrification. [28,19]

| Parameters | | Description | Value |
|---|---|---|---|
| Kinetic parameters | K_S_HS | Saturation/inhibition coeff for growth on S_HS | 4 |
| | mu _ADO | Maximum growth rate | 1 |
| | b _ADO | Decay rate | 0.15 |
| Stoichiometric parameters | Y_ADO | Yield For Autotrophic Biomass | 0.24 |
| | i_S_Org_mol_perC | S/C : organisms | 0.0001 |
| | i_S_SU_mol_perC | S/C: unbiodegradable soluble | 0.00001 |
| | i_S_SF_mol_perC | S/C: fermentable soluble | 0.00001 |
| | i_S_XUInf_mol_perC | S/C: unbiodegradable particulate | 0.00001 |
| | i_S_XUOrg_mol_perC | S/C: endogenous residue | 0.00001 |
| | i_S_XBOrg_mol_perC | S/C: biodegradable particulate | 0.00001 |
| | i_S_XBInf_mol_perC | S/C: PS biodegradable particulate | 0.0001 |

The above step was followed by the addition of the yield coefficients (which represent the efficiency of substrate conversion into biomass) and decay factors (which account for biomass decay) for the new processes. This step ensures that the matrix reflects not only the transformation of components but also the growth and decay of microorganisms. The stoichiometric and kinetic constants for SRB in anaerobic sulfate reduction were derived through model fitting to experimental data from previous studies. These values, presented in Table 3.4, were also incorporated into the PWM_SA Gujer matrix.

Table 3.4 Stoichiometric and kinetic constants used in the PWM_SA. [56,38]

| **Parameters** | $\mu_{max}$ ($d^{-1}$) | $K_S$ ($mol/m^3$) | $K_N$ ($mol/m^3$) | $K_I$ ($mol/m^3$) | **Y** (mol/mol) | **b** ($d^{-1}$) |
|---|---|---|---|---|---|---|
| Acidogens (AD) | 4.000 | 0.780 | N/A | 5.78125 | 0.10740 | 0.0410 |
| Acetotrophic sulfidogens (AS) | 0.612 | 0.370 | 0.200 | 5.12500 | 0.01869 | 0.0275 |
| Hydrogenotrophic sulfidogens (HS) | 2.800 | 0.004 | 0.200 | 17.18750 | 0.00707 | 0.0600 |

The stoichiometric and kinetic constants for ADs and ANs were primarily derived from the ASM3, presented in Table 3.5. [28,27] The kinetic and stoichiometric constants for ADNs are presented below, respectively:

Table 3.5 Stoichiometric and kinetic constants used in the PWM_SA as taken from ASM3.[56]

| **Parameters** | $\mu_{max}$ ($d^{-1}$) | $K_{H2S}$ ($mol/m^3$) | $K_{NH4}$ ($mol/m^3$) | $K_{NO3}$ ($mol/m^3$) | $K_{O2}$ ($mol/m^3$) | Y (mol/mol) | b ($d^{-1}$) |
|---|---|---|---|---|---|---|---|
| Heterotrophic denitrifiers (HDN) | 2.0 | n/a | 0.000714 | 0.0357 | 0.00625 | 0.72838 | 0.10 |
| Autotrophic denitrifiers (ADN) | 1.0b | 0.4938 | 0.000714 | 1.0786 | 0.00625e | 0.08262f | 0.04 |
| Autotrophic nitrifiers (AN) | 1.0 | N/Aa | 0.071430 | n/a | 0.0156 | 0.01541 | 0.01 |

The next step involved defining the stoichiometric relationships between the components involved in the added processes. This included specifying the consumption and production rates of each component facilitated by SRB and ADO. These stoichiometric coefficients are essential for accurately representing the sulfate reduction and autotrophic denitrification processes in the Gujer matrix, ensuring that the model can simulate the transformation and interactions of each component within the extended PWM_SA model accurately. Table 3.6 below presents the stoichiometric coefficient equations for the components of the autotrophic denitrification processes added to the model, the stoichiometric coefficient equations for the components of the added SRB processes are presented in the Gujer matrix attached as supplementary Data.

Table 3.6 The stoichiometric coefficients of the autotrophic denitrification processes components.

| | | |
|---|---|---|
| **Anoxic Growth of Autotrophic Denitrifiers** | | |
| G1-1 | $H_2O$ | $\left(0.8 - \frac{24 \cdot Y\_ADO}{5} + \frac{Y\_ADO}{\text{gam\_o}} \cdot (24 + 32 \cdot i\_P\_Org\_mol\_perC + 32 \cdot i\_S\_Org\_mol\_perC - 8 \cdot i\_O\_Org\_mol\_perC)\right) \cdot MW\_H2O$ |
| G2-1 | S_H | $\left(-0.6 + \frac{8 \cdot Y\_ADO}{5} - \frac{Y\_ADO}{\text{gam\_o}} \cdot (16 + 24 \cdot i\_P\_Org\_mol\_perC + 16 \cdot i\_S\_Org\_mol\_perC - 8 \cdot i\_N\_Org\_mol\_perC)\right) \cdot MW\_S\_H$ |
| G3-1 | S_NHx | $\left(-\frac{8 \cdot Y\_ADO}{\text{gam\_o}} \cdot i\_N\_Org\_mol\_perC\right) \cdot MW\_S\_NH$ |
| G4-1 | S_HS | $-MW\_S\_HS$ |
| G5-1 | S_CO3 | $-\frac{8 \cdot Y\_ADO}{\text{gam\_o}} \cdot MW\_S\_CO3$ |
| G6-1 | S_SO4 | $\left(-\frac{8 \cdot Y\_ADO}{\text{gam\_o}} \cdot i\_S\_Org\_mol\_perC + 1\right) \cdot MW\_S\_SO4$ |
| G7-1 | S_PO4 | $-\frac{8 \cdot Y\_ADO}{\text{gam\_o}} \cdot i\_P\_Org\_mol\_perC \cdot MW\_S\_PO4$ |
| G8-1 | S_NOx | $-\frac{8 \cdot (1 - Y\_ADO)}{5} \cdot MW\_S\_NOx$ |
| G9-1 | S_N2 | $\frac{4 \cdot (1 - Y\_ADO)}{5} \cdot MW\_S\_N2$ |
| G10-1 | X_B_Org | $\frac{8 \cdot Y\_ADO}{\text{gam\_o}} \cdot MW\_X\_ADO$ |
| **Lysis of Autotrophic Denitrifiers** | | |
| D1 | $H_2O$ | $\left(\begin{array}{l} 3 + 4 \cdot i\_P\_Org\_mol\_perC + 4 \cdot i\_S\_Org\_mol\_perC - i\_O\_Org\_mol\_perC - \frac{f\_XU\_Bio\_lysis \cdot \text{gam\_o}}{\text{gam\_e}} \cdot \\ (3 + 4 \cdot i\_P\_XUOrg\_mol\_perC + 4 \cdot i\_S\_XUOrg\_mol\_perC) \end{array}\right)$ |
| D2 | S_H | $\left(\begin{array}{l} 2 + 3 \cdot i\_P\_Org\_mol\_perC + 2 \cdot i\_S\_Org\_mol\_perC - i\_N\_Org\_mol\_perC - \frac{f\_XU\_Bio\_lysis \cdot \text{gam\_o}}{\text{gam\_e}} \\ \cdot (2 + 3 \cdot i\_P\_XUOrg\_mol\_perC + 2 \cdot i\_S\_XUOrg\_mol\_perC) \end{array}\right)$ |
| D3 | S_NHx | $\left(i\_N\_Org\_mol\_perC - \frac{f\_XU\_Bio\_lysis \cdot \text{gam\_o} \cdot i\_N\_XUOrg\_mol\_perC}{\text{gam\_e}} - \frac{(1 - f\_XU\_Bio\_lysis) \cdot \text{gam\_o} \cdot i\_N\_XBInf\_mol\_perC}{\text{gam\_bps}}\right)$ |
| D4 | S_CO3 | $\left(1 - \frac{f\_XU\_Bio\_lysis \cdot \text{gam\_o}}{\text{gam\_e}} - \frac{(1 - f\_XU\_Bio\_lysis) \cdot \text{gam\_o}}{\text{gam\_bps}}\right) \cdot MW\_S\_CO3$ |
| D5 | S_SO4 | $\left(i\_S\_Org\_mol\_perC - \frac{f\_XU\_Bio\_lysis \cdot \text{gam\_o} \cdot i\_S\_XUOrg\_mol\_perC}{\text{gam\_e}} - \frac{(1 - f\_XU\_Bio\_lysis) \cdot \text{gam\_o} \cdot i\_S\_XBInf\_mol\_perC}{\text{gam\_bps}}\right)$ |
| D6 | S_PO4 | $\left(i\_P\_Org\_mol\_perC - \frac{f\_XU\_Bio\_lysis \cdot \text{gam\_o} \cdot i\_P\_XUOrg\_mol\_perC}{\text{gam\_e}} - \frac{(1 - f\_XU\_Bio\_lysis) \cdot \text{gam\_o} \cdot i\_P\_XBInf\_mol\_perC}{\text{gam\_bps}}\right)$ |
| D7 | S_U | $-MW\_X\_ADO$ |
| D8 | S_F | $\left(f\_XU\_Bio\_lysis \cdot \frac{\text{gam\_o}}{\text{gam\_e}}\right) \cdot MW\_X\_U\_Org$ |
| D9 | S_Glu | $(1 - f\_XU\_Bio\_lysis) \cdot \frac{\text{gam\_o}}{\text{gam\_bps}} \cdot MW\_X\_B\_Inf$ |
| D10 | X_ADO | $-MW\_X\_ADO$ |
| D11 | X_U_Org | $\left(f\_XU\_Bio\_lysis \cdot \frac{\text{gam\_o}}{\text{gam\_e}}\right) \cdot MW\_X\_U\_Org$ |
| D12 | X_B_Inf | $(1 - f\_XU\_Bio\_lysis) \cdot \frac{\text{gam\_o}}{\text{gam\_bps}} \cdot MW\_X\_B\_Inf$ |

Once the relevant components, parameters, stoichiometric relationships, and kinetic constants for sulfate reduction and autotrophic denitrification were added to the Gujer matrix, the biological processes were then added to the matrix with the processes listed as rows and the components as columns in the format shown in Table below (the G and D symbols represent the stoichiometric equations listed in Table 3.6 above).

Table 3.7 The extended SDM3P section of the stoichiometric matrix for the PWM_SA model.

| **SDM3P section of the Stoichiometric matrix for the PWM_SA model** | | | | | | | | | | | | |
|---|---|---|---|---|---|---|---|---|---|---|---|---|
| **State** | | **Soluble components** | | | | | | | | | | |
| **Expressed as** | | **g/m$^3$** | | | | | | | | | | |
| | **Components** | $H_2O$ | $S_H$ | $S_{NHx}$ | $S_{HS}$ | $S_{VFA}$ | $S_{Pr}$ | $S_{CO3}$ | $S_{SO4}$ | $S_{PO4}$ | $S_{NOx}$ | $S_{N2}$ |
| 1 | Anoxic Growth of Autotrophic Denitrifiers | $G_1-1$ | $G_1-2$ | $G_1-3$ | 0 | $G_1-4$ | $G_1-5$ | $G_1-6$ | $G_1-7$ | $G_1-8$ | $G_1-9$ | $G_1-10$ |
| 2 | Lysis of Autotrophic Denitrifiers | $D_1$ | $D_2$ | $D_3$ | $D_4$ | $D_5$ | $D_6$ | $D_7$ | $D_8$ | $D_9$ | | |

NB: This table shows only the soluble components; the particulate components are given in the Gujer matrix attached as supplementary Data.

Each cell in the matrix contains a stoichiometric coefficient that represents the amount of a component consumed or produced during each process. Positive values in the matrix indicate the production of a component, while negative values denote its consumption as shown in Tables 3.8 and 3.9.

Table 3.8 The extended SDM3P section of the stoichiometric matrix for the PWM_SA model.

| **SDM3P section of the stoichiometric matrix for the PWM_SA model** | | | | | | | | | | | | |
|---|---|---|---|---|---|---|---|---|---|---|---|---|
| **State** | | **Soluble components** | | | | | | | | | | |
| **Expressed as** | | **g/m$^3$** | | | | | | | | | | |
| | **Components** | $H_2O$ | $S_H$ | $S_{NHx}$ | $S_{HS}$ | $S_{VFA}$ | $S_{Pr}$ | $S_{CO3}$ | $S_{SO4}$ | $S_{PO4}$ | $S_{NOx}$ | $S_{N2}$ |
| 1 | Anoxic Growth of Autotrophic Denitrifiers | 14.99 | -1.1 | -1.34 | 0 | -33.08 | -27.70 | 96.06 | -0.79 | -75.39 | 17.03 | 10.38 |
| 2 | Lysis of Autotrophic Denitrifiers | 0.0 | 0.0 | 0.0 | 0.0 | -2.79 | 0.0 | 0.92 | -1 | 0 | 0 | 0.08 |

Table 3.9 The extended ASM2-3P section of the stoichiometric matrix for the PWM_SA model.

| ASM2-3P section of the stoichiometric matrix for the PWM_SA model | | | | | | | | | | | |
|---|---|---|---|---|---|---|---|---|---|---|---|
| State | | Expressed as | | | | | | | | | |
| Processes | | $g/m^3$ | | | | | | | | | |
| | | $H_2O$ | $S_H$ | $S_{NHx}$ | $S_{HS}$ | $S_{VFA}$ | $S_{Pr}$ | $S_{CO3}$ | $S_{SO4}$ | $S_{PO4}$ | $S_{H2}$ |
| 1 | Uptake of sugars in SDM | −11.3 | 3.8 | −1.7 | | 53.1 | 65.8 | 56.6 | 0.0 | −1.0 | 1.8 |
| 2 | Death and decay of the sugar degraders in SDM1 | 0.0 | 0.0 | 0.0 | | | | 0.0 | 0.0 | 0.0 | |
| 3 | Uptake of propionate in SDM1 | −51.7 | 1.9 | −0.3 | | 57.4 | −73.1 | 57.9 | 0.0 | −0.2 | 5.9 |
| 4 | Death and decay of the propionate degraders | 0.0 | 0.0 | 0.0 | | | | 0.0 | 0.0 | 0.0 | |
| 5 | Growth of acetogenic SRB biomass | 0.9 | 1.2 | −0.4 | 23.8 | 56.7 | −73.1 | 57.4 | −69.2 | −0.2 | 0.0 |
| 6 | Death and decay of the acetogenic SRB | 0.0 | 0.0 | 0.0 | | | | 0.0 | 0.0 | 0.0 | |
| 7 | Uptake of acetate in SDM | −16.3 | 0.9 | −0.3 | | −59.0 | | 57.4 | 0.0 | −0.2 | |
| 8 | Death and decay of the acetate degraders | 0.0 | 0.0 | 0.0 | | | | 0.0 | 0.0 | 0.0 | |
| 9 | Growth of acetoclastic SRB | 0.8 | 1.9 | −0.3 | 31.5 | −59.0 | | 114.8 | −91.6 | −0.2 | |
| 10 | Uptake of hydrogen in SDM | 14.0 | −0.5 | −0.1 | | | | −15.8 | 0.0 | 0.0 | −2.0 |
| 11 | Death and decay of the hydrogen degraders | 0.0 | 0.0 | 0.0 | | | | 0.0 | 0.0 | 0.0 | |
| 12 | Growth of hydrogenotrophic SRB | 18.3 | −0.3 | −0.1 | 7.7 | | | −2.0 | −22.3 | −0.1 | −2.0 |
| 13 | Death and decay of the hydrogenotrophic SRB | 0.0 | 0.0 | 0.0 | | | | 0.0 | 0.0 | 0.0 | |

### 3.2.3 Mass Balance Verification

To ensure that the model maintained mass conservation for each component, a mass balance check was performed on the Gujer matrix.[30] This process involved comparing the total amounts of each component entering and leaving the system and verifying that the quantities generated and consumed were consistent with the stoichiometric coefficients provided in the matrix. The verification of the Gujer matrix for mass balance was achieved by summing the product of each component's chemical elements (CHONPS) and its chemical content with the stoichiometric coefficients across each row of the matrix as outlined in Figure 3.4 below.

| Composition Matrix - Balance Check | | | | | | | | | |
|---|---|---|---|---|---|---|---|---|---|
| | COD | C | H | O | N | P | S | Charge | Mass |
| H2O | 0.0 | 0.0 | 0.1 | 0.9 | 0.0 | 0.0 | 0.0 | 0.0 | 0.0 |
| S_H | 0.0 | 0.0 | 1.0 | 0.0 | 0.0 | 0.0 | 0.0 | 1.0 | 0.0 |
| S_NHx | 0.0 | 0.0 | 0.2 | 0.0 | 0.8 | 0.0 | 0.0 | 0.1 | 0.0 |
| S_HS | 1.9 | 0.0 | 0.0 | 0.0 | 0.0 | 0.0 | 1.0 | 0.0 | 0.0 |
| S_VFA | 1.1 | 0.4 | 0.1 | 0.5 | 0.0 | 0.0 | 0.0 | 0.0 | 0.0 |
| S_Pr | 1.5 | 0.5 | 0.1 | 0.4 | 0.0 | 0.0 | 0.0 | 0.0 | 0.0 |
| S_CO3 | 0.0 | 0.2 | 0.0 | 0.8 | 0.0 | 0.0 | 0.0 | 0.0 | 0.0 |
| S_SO4 | 0.0 | 0.0 | 0.0 | 0.7 | 0.0 | 0.0 | 0.3 | 0.0 | 0.0 |
| S_PO4 | 0.0 | 0.0 | 0.0 | 0.7 | 0.0 | 0.3 | 0.0 | 0.0 | 0.0 |
| S_H2 | 7.9 | 0.0 | 1.0 | 0.0 | 0.0 | 0.0 | 0.0 | 0.0 | 0.0 |
| S_Glu | 1.1 | 0.4 | 0.1 | 0.5 | 0.0 | 0.0 | 0.0 | 0.0 | 0.0 |

| Processes | | Components | | | | | | | | | | | | COD | C | H | O | N | P | S | Charge | Mass |
|---|---|---|---|---|---|---|---|---|---|---|---|---|---|---|---|---|---|---|---|---|---|---|
| | | H2O | S_H | S_NHx | S_HS | S_VFA | S_Pr | S_CO3 | S_SO4 | S_PO4 | S_H2 | S_Glu | | | | | | | | | | |
| 1 | Uptake of sugars in ADM | -11.3 | 3.8 | -1.7 | | 53.1 | 65.8 | 56.6 | 0.0 | -1.0 | 1.8 | -180.2 | | 0.0 | 0.0 | 0.0 | 0.0 | 0.0 | 0.0 | 0.0 | 0.0 | 0.0 |
| 2 | Death and decay of the sugar degraders in ADM1 | 0.0 | 0.0 | 0.0 | | | | 0.0 | 0.0 | 0.0 | | | | 0.0 | 0.0 | 0.0 | 0.0 | 0.0 | 0.0 | 0.0 | 0.0 | 0.0 |
| 3 | Uptake of propionate in ADM1 | -51.7 | 1.9 | -0.3 | | 57.4 | -73.1 | 57.9 | 0.0 | -0.2 | 5.9 | | | 0.0 | 0.0 | 0.0 | 0.0 | 0.0 | 0.0 | 0.0 | 0.0 | 0.0 |
| 4 | Death and decay of the propionate degraders | 0.0 | 0.0 | 0.0 | | | | 0.0 | 0.0 | 0.0 | | | | 0.0 | 0.0 | 0.0 | 0.0 | 0.0 | 0.0 | 0.0 | 0.0 | 0.0 |
| 5 | Growth of acetogenic SRB biomass | 0.9 | 1.2 | -0.4 | 23.8 | 56.7 | -73.1 | 57.4 | -69.2 | -0.2 | 0.0 | | | 0.0 | 0.0 | 0.0 | 0.0 | 0.0 | 0.0 | 0.0 | 0.0 | 0.0 |
| 6 | Death and decay of the acetogenic SRB | 0.0 | 0.0 | 0.0 | | | | 0.0 | 0.0 | 0.0 | | | | 0.0 | 0.0 | 0.0 | 0.0 | 0.0 | 0.0 | 0.0 | 0.0 | 0.0 |
| 7 | Uptake of acetate in ADM | -16.3 | 0.9 | -0.3 | | -59.0 | | 57.4 | 0.0 | -0.2 | | | | 0.0 | 0.0 | 0.0 | 0.0 | 0.0 | 0.0 | 0.0 | 0.0 | 0.0 |
| 8 | Death and decay of the acetate degraders | 0.0 | 0.0 | 0.0 | | | | 0.0 | 0.0 | 0.0 | | | | 0.0 | 0.0 | 0.0 | 0.0 | 0.0 | 0.0 | 0.0 | 0.0 | 0.0 |
| 9 | Growth of acetoclastic SRB | 0.8 | 1.9 | -0.3 | 31.5 | -59.0 | | 114.8 | -91.6 | -0.2 | | | | 0.0 | 0.0 | 0.0 | 0.0 | 0.0 | 0.0 | 0.0 | 0.0 | 0.0 |
| 10 | Uptake of hydrogen in ADM | 14.0 | -0.5 | -0.1 | | | | -15.8 | 0.0 | 0.0 | -2.0 | | | 0.0 | 0.0 | 0.0 | 0.0 | 0.0 | 0.0 | 0.0 | 0.0 | 0.0 |
| 11 | Death and decay of the hydrogen degraders | 0.0 | 0.0 | 0.0 | | | | 0.0 | 0.0 | 0.0 | | | | 0.0 | 0.0 | 0.0 | 0.0 | 0.0 | 0.0 | 0.0 | 0.0 | 0.0 |
| 12 | Growth of hydrogenotrophic SRB | 18.3 | -0.3 | -0.1 | 7.7 | | | -2.0 | -22.3 | -0.1 | -2.0 | | | 0.0 | 0.0 | 0.0 | 0.0 | 0.0 | 0.0 | 0.0 | 0.0 | 0.0 |
| 13 | Death and decay of the hydrogenotrophic SRB | 0.0 | 0.0 | 0.0 | | | | 0.0 | 0.0 | 0.0 | | | | 0.0 | 0.0 | 0.0 | 0.0 | 0.0 | 0.0 | 0.0 | 0.0 | 0.0 |
| | | | | | | | | | | | | | Total | **0.0** | **0.0** | **0.0** | **0.0** | **0.0** | **0.0** | **0.0** | **0.0** | **0.0** |

Figure 3.4 Mass balance verification.[30]

The procedure entailed calculating the total contribution of each component to the overall mass balance for each process. This was done by multiplying the stoichiometric coefficients of each component by its chemical content and then summing these products across all components involved in each particular process. The resulting matrix should contain only zeros to show complete mass balance. By performing these calculations, the model was verified to accurately reflect the conservation of mass for each chemical element in the added bioprocesses. This approach ensured that all elements were balanced and that the Gujer matrix effectively represented the mass dynamics within the system.

## 3.3 Outline of SANI Pilot System

The PWM_SA model was further verified using experimental data from the SANI saline sewage treatment system at the Hong Kong pilot plant. Therefore, a detailed analysis of the SANI plant's operating conditions, influent characteristics, and experimental mass balances was necessary to support the calibration process.

Figure 3.5 presents a schematic diagram of the SANI pilot plant, which includes an SRUSB for sulfate reduction, an anoxic (BAR1) for autotrophic denitrification, and an aerobic bioreactor (BAR2) for nitrification.

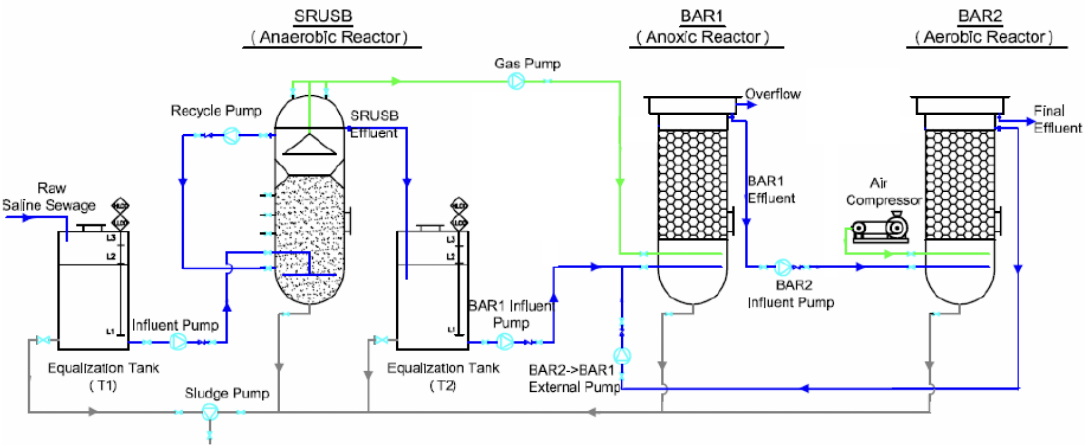


Figure 3.5 Extensive schematic diagram of the SANI pilot plant at the TCSPS.[46]

The SRUSB had a diameter of 1.6 m, a height of 4.2 m, and an effective liquid volume of 6.8 $m^3$. It comprised a sludge-holding zone, a reaction zone, and a liquid-solids separation zone, and was entirely sealed. The anoxic and aerobic reactors (BAR1 and BAR2) were identical, each with a diameter of 1.6 m, a height of 4.4 m, and an effective liquid volume of 3.9 $m^3$. Both reactors were filled with plastic media providing a specific surface area of 115 $m^2$ per $m^3$ of reactor volume and had a porosity of 91%. To regulate the plant's flow, a 700L influent flow regulating tank (T1) and a 700L mid-flow regulating tank (T2) were installed, each equipped with a mixer under sealed conditions. Additionally, a strainer with 6 mm spacing, cleaned daily, was installed before the plant.[46]

The SRUSB, BAR1, and BAR2 were seeded and inoculated with anaerobically digested sludge (MLSS = 8000 mg/L) and recycle-activated sludge (MLSS = 4000 mg/L) sourced from a local secondary saline sewage treatment plant. During the inoculation period, the system was continuously fed with screened saline sewage, gradually increasing the influent flow rate from 2 to 10 $m^3$/d. After approximately one month, the plant stabilized, achieving effluent quality with TSS below 15 mg/L and unfiltered COD below 55 mg/L.

The pilot plant was subsequently operated for 225 days, maintaining an average sewage temperature of 25°C. Table 3.10 details the primary operating conditions of the SANI pilot plant during the steady-state period. A simplified outline of the SANI Pilot system was recreated within WEST's experimental environment, maintaining the same primary operation conditions as the SANI pilot plant.

Table 3.10 The primary operating conditions of the SANI pilot plant during the steady-state period. [46,42]

| Reactors | NHRT (h) | AHRT (h) | SRT (d) | Influent Flow Rate | Recirculation BAR2 $\rightarrow$ BAR1 | Average Temperature°C |
|---|---|---|---|---|---|---|
| SRUSB | $186 \pm 55.3$ | $52.1 \pm 22.3$ | $23.5 \pm 7.1$ | $12.5 \pm 4.3$ | $9.0 \pm 2.4$ | 21.3 |
| BAR1 | $431 \pm 132.6$ | $98.8 \pm 60.9$ | $65.9 \pm 17.4$ | $55.0 \pm 18.7$ | $53.9 \pm 10.8$ | 66.7 |
| BAR2 | $157.9 \pm 86.2$ | $39.7 \pm 5.6$ | $30.9 \pm 10.3$ | $30.2 \pm 11.6$ | $30.7 \pm 9.2$ | 33.3 |

### 3.3.1 Influent Characterization

Understanding the elemental compositions of influent BO and biomass in SRUSB, anoxic, and aerobic, is crucial for formulating stoichiometric equations in wastewater treatment models. These compositions are often determined using established equations. For 1 gram of VSS, the elemental composition represented as $\mathrm{C}_x\mathrm{H}_y\mathrm{O}_z\mathrm{N}_a\mathrm{P}_b$ can be derived from specific mass ratios for C, H, O, N, and P.

These mass ratios—denoted as $f_{cv}$, $f_c$, $f_h$, $f_o$, $f_n$, and $f_p$—represent the ratios of COD, TOC, H, O, organic N (OrgN), and organic P (OrgP) to VSS or the mass of filtered organics. For PO, $f_{cv}$, $f_c$, $f_n$, and $f_p$ can be determined through standard tests measuring COD, TOC, total Kjeldahl nitrogen (TKN) minus FSA, TP, OP, and VSS as listed in Table 3.11. The mass ratios $f_h$ and $f_o$ do not need to be measured directly, as they can be calculated using the COD/VSS ratio and the mass balance equation:

$$f_c + f_h + f_o + f_n + f_p = 1 \tag{3.10}$$

This allows the elemental composition for 1 gram of VSS to be determined by:

$$x = \frac{f_c}{12}, \quad y = \frac{f_h}{1}, \quad z = \frac{f_o}{16}, \quad a = \frac{f_n}{14}, \quad b = \frac{f_p}{31} \tag{3.11}$$

The composition can then be normalized with respect to C (e.g., $\mathrm{C} = 1$).

| Organics | Acetate | FBSO | USO | BPO | UPO | Biomass | ER |
|---|---|---|---|---|---|---|---|
| COD | 1.07 | 1.10 | 1.42 | 1.47 | 1.48 | 1.48 | 1.48 |
| C | 0.40 | 0.49 | 0.53 | 0.55 | 0.54 | 0.52 | 0.52 |
| H | 0.07 | 0.04 | 0.06 | 0.05 | 0.07 | 0.07 | 0.07 |
| O | 0.53 | 0.45 | 0.31 | 0.33 | 0.15 | 0.29 | 0.29 |
| N | 0.00 | 0.03 | 0.09 | 0.06 | 0.22 | 0.10 | 0.10 |
| P | 0.00 | 0.00 | 0.01 | 0.01 | 0.02 | 0.03 | 0.03 |
| x | 3.50 | 7.58 | 5.58 | 6.33 | 4.62 | 4.45 | 4.46 |
| y | 7.00 | 7.00 | 7.00 | 7.00 | 7.00 | 7.00 | 7.00 |
| z | 3.50 | 5.21 | 2.45 | 2.82 | 0.96 | 1.90 | 1.90 |
| a | 0.00 | 0.40 | 0.79 | 0.57 | 1.63 | 0.74 | 0.74 |
| b | 0.00 | 0.01 | 0.06 | 0.03 | 0.08 | 0.08 | 0.08 |

Table 3.11 Mass ratios of the influent wastewater compositions(UPO, BPO, USO).

The concentrations of other components, such as USO, are determined through filtered COD tests, and differences in COD, TOC, OrgN, and OrgP are used to calculate the compositions for FBSO and USO, this data was obtained from the SANI pilot plant influent parameters listed below in Table 3.12.[46]

Table 3.12 Influent characterization of the SANI pilot system.[42]

| **Parameters** | **VFA** | **FSA** | **OP** | **BSO** | **BPO** | **USO** | **UPO** | **Soluble** | **Particulate** | **Total** |
|---|---|---|---|---|---|---|---|---|---|---|
| COD (mg/L) | 34.5 | N/A | N/A | 92.7 | 217.5 | 30.7 | 55.6 | 157.9 | 273.1 | 431 |
| TOC (mg C/L) | 12.9 | N/A | N/A | 40.9 | 82.2 | 11.5 | 20.2 | 65.3 | 102.4 | 167.7 |
| TKN (mg N/L) | N/A | 44.8 | N/A | 2.5 | 8.7 | 23.2 | 8.3 | 70.5 | 17 | 87.5 |
| TP (mg P/L) | N/A | N/A | 5.3 | 0.2 | 1.1 | 0.3 | 0.9 | 5.8 | 2.0 | 7.8 |

The influent parameters listed in Table 3.12 were then used to plot the COD influent characterization block diagram presented in Figure 3.6. Particulate organics are divided into UPO and BPO fractions. The UPO fraction is determined from the overall mass balance

of the system, while the BPO fraction is calculated by subtracting UPO concentrations from the total particulate concentrations.

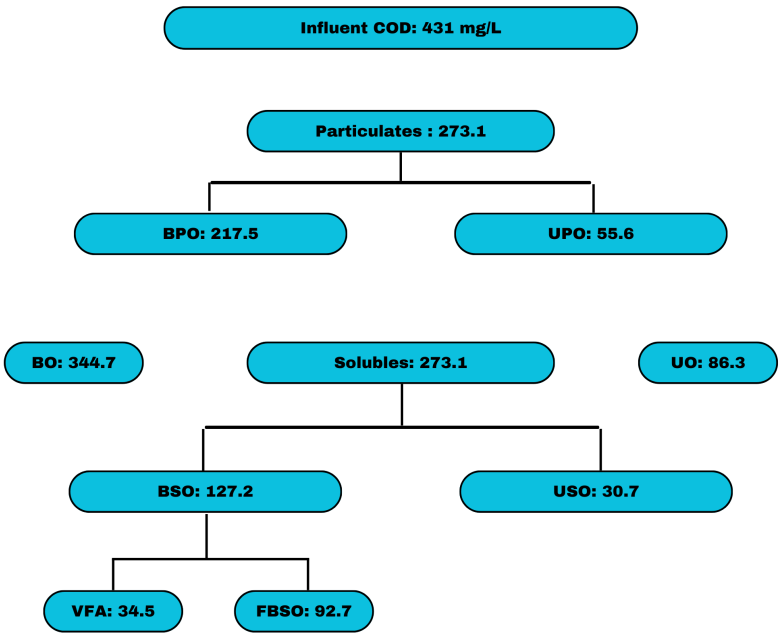


Figure 3.6 Influent wastewater characterization of the SANI Pilot plant.[46]

The elemental compositions of UPO and BPO can then be obtained from mass ratios using equations such as, respectively:

$$C_{1.00}H_{1.57}O_{0.21}N_{0.35}P_{0.02} \tag{3.12}$$

and

$$C_{1.00}H_{1.11}O_{0.45}N_{0.09}P_{0.001} \tag{3.13}$$

This comprehensive approach ensures an accurate representation of organic and inorganic components within wastewater treatment models.

### 3.3.2 Characterization of the Performance of the SANI Pilot Plant

Accurate characterization of the SANI pilot plant's performance was crucial for the calibration process. Throughout the steady-state operation, the influents and effluents of all

bioreactors were systematically analyzed through 24-hour composite sampling. The characteristics of the influent and effluent from each bioreactor in the SANI pilot plant are presented in Table 3.13.

Table 3.13 Characteristics of the influent and effluent for each reactor in the SANI pilot plant.[46]

| Parameters | SRUSB | | BAR1 | BAR1 Effluent | BAR2 | Calculated |
|---|---|---|---|---|---|---|
| | Influent | Effluent | Influent | BAR2 Influent | Effluent | Concentration |
| VSS (mg/L) | 186 ± 55.3 | 52.1 ± 22.3 | 23.5 ± 7.1 | 12.5 ± 4.3 | 9.0 ± 2.4 | 21.3 |
| Unfiltered COD (mgCOD/L) | 431 ± 132.6 | 98.8 ± 60.9 | 65.9 ± 17.4 | 55.0 ± 18.7 | 53.9 ± 10.8 | 66.7 |
| Filtered COD (mgCOD/L)b | 157.9 ± 86.2 | 39.7 ± 5.6 | 30.9 ± 10.3 | 30.2 ± 11.6 | 30.7 ± 9.2 | 33.3 |
| $SO_4^{2-}$ (mgS/L) | 195.7 ± 18.0 | 65.4 ± 15.2 | 142.3 ± 25.7 | 169.4 ± 34.3 | 172.3 ± 34.4 | 141.7 |
| $H_2S$ (mgS/L) | 4.0 ± 4.7 | 124.1 ± 14.4 | 31.3 ± 4.8 | 3.0 ± 1.2 | 0 | 35.5 |
| Unfiltered TKN (mgN/L) | 87.5 ± 8.5 | 85.3 ± 8.6 | 39.2 ± 4.4 | 35.7 ± 5.6 | 23.4 ± 5.5 | 41.1 |
| Filtered TKN (mgN/L) | 70.5 ± 5.7 | 70.9 ± 5.6 | 36.5 ± 4.4 | 35.3 ± 3.8 | 23.2 ± 4.3 | 36.8 |
| FSA (mgN/L) | 44.8 ± 6.6 | 45.4 ± 6.0 | 16.9 ± 4.5 | 16.4 ± 2.7 | 3.4 ± 2.4 | 15.4 |
| $NO_3^-$ (mgN/L) | 0 | 0 | 13.5 ± 1.8 | 2.2 ± 2.4 | 16.8 ± 3.2 | 12.0 |
| Unfiltered TP (mgP/L) | 7.8±1.2 | 7.6±1.0 | 5.9±0.7 | 5.7±0.5 | 5.6 ± 0.6 | 6.2 |
| Filtered TP (mgP/L) | 5.8±0.8 | 5.7±0.6 | 5.8±0.7 | 5.6±0.8 | 5.6 ± 0.6 | 5.6 |
| OP (mgP/L) | 5.3±0.7 | 5.2±0.8 | 5.3±0.7 | 5.3±0.5 | 5.3±0.5 | 5.3 |
| Total Alkalinity ($mgCaCO_3/L$) | 223±100.5 | 736.9±170.1 | 281.4±75.2 | 247.7±70.5 | 120.5 ± 62.4 | 296.6 |
| $H_2CO_3$ Alkalinity ($mgCaCO_3/L$) | 219.0±104.3 | 576.7±174.0 | 252.8±75.1 | 245.7±71.6 | 120.5 ± 62.4 | 250.8 |
| $H_2S$ Alkalinity ($mgCaCO_3/L$) | 4.6±1.0 | 160.2±11.2 | 28.6±4.6 | 2.0±0.2 | 0 | 45.8 |
| COD Mass balance % | 86 | | 90 | | 98 | |
| N Mass balance % | 103 | | 93 | | 106 | |
| S Mass balance % | 95 | | 99 | | 100 | |
| P Mass balance % | 104 | | 97 | | 98 | |

The pilot plant results align well with the theoretical expectations for the biological and chemical processes occurring in the SANI system. The significant reduction in VSS and COD across reactors is consistent with biological degradation and the removal of organic matter. The $SO_4^{2-}$ reduction and $H_2S$ production in the SRUSB reactor confirm effective sulfate reduction and the changes in N species (TKN, FSA, $NO_3^-$) indicate nitrification and denitrification processes, as expected. Overall, the observed results are in line with the anticipated outcomes of the biological and chemical processes at play within the SANI system.

Evaluating the experimental mass balances of the SANI pilot system, as shown in Table 3.13, reveals key insights into the accuracy of the system's performance and the reliabil-

ity of the influent data for modelling purposes. This step was essential for detecting any discrepancies that might result from measurement errors or system inefficiencies, which could compromise the accuracy of the model. Since simulation models are based on the principle of mass conservation, the input data must also produce realistic outcomes. Additionally, proper mass balance evaluation supports the verification of the model, ensuring it accurately reflects real-world processes. Without this, errors in the influent data could propagate throughout the model, leading to faulty predictions of treatment performance. Therefore, verifying mass balance consistency is a critical step in ensuring the influent data's suitability for modelling.

The mass balances for individual reactors demonstrate relatively consistent results, with COD, N, S, and P balances ranging between 86% and 106%, indicating that the majority of these substances are accounted for within each reactor. However, the overall mass balance for the entire system shows some discrepancies, with a 71% COD balance, 97% Nn balance, 86% S balance, and 79% P balance. These deviations suggest potential measurement errors, unaccounted losses, or incomplete reaction pathways. To address this and ensure that the simulation model remains internally consistent and predictive, adjustments to the influent parameters were necessary to achieve complete mass balances. The following table displays the adjusted values obtained from the SANI pilot system, these values were then entered into the model, with consideration for their typical ranges.[4]

Table 3.14 Average influent water qualities used as input to the PWM_SA model.[46]

| Parameters | SRUSB | Anoxic | Aerobic |
|---|---|---|---|
| TSS | 280.19 | 48.57 | 49.27 |
| VSS (mg/L) | 186.19 | 16.80 | 20.59 |
| Unfiltered COD (mgCOD/L) | 439.22 | 72.50 | 78.88 |
| Filtered COD (mgCOD/L) | 157.90 | 46.40 | 46.80 |
| $SO_4^{2-}$ (mgS/L) | 195.70 | 158.70 | 179.22 |
| $H_2S$ (mgS/L) | 4.00 | 41.01 | 20.49 |
| Unfiltered TKN (mgN/L) | 66.13 | 58.04 | 57.52 |
| Filtered TKN (mgN/L) | 49.19 | 54.83 | 54.07 |
| FSA (mgN/L) | 44.80 | 15.30 | 14.69 |
| $NO_3^-$ (mgN/L) | 0.00 | 10.90 | 0.22 |
| Unfiltered TP (mgP/L) | 7.80 | 6.84 | 6.79 |
| Filtered TP (mgP/L) | 5.80 | 6.43 | 6.28 |
| OP (mgP/L) | 5.30 | 6.10 | 5.95 |

With the identified model parameters categorized into influential (those with significant effects) and non-influential (those that can be fixed within a range without affecting model outputs), the final evaluation steps were determined. These steps involve:

- Setting the non-influential parameters to their default values.
- Randomly sampling the influential parameter sets within their specified ranges and conducting simulations to compare predicted model outputs against the experimental data.

In this context, the experimental data stem from the SANI pilot plant system used for model calibration. The calibrated parameters derived from this process remained consistent and were then applied to simulate a full-scale scenario at the SANI pilot plant during the validation phase. Mass balance checks were also conducted on the simulation results to verify the consistency of the system. Detailed explanations accompany these simulations

in the results and discussion chapter, highlighting any observed discrepancies between predicted and actual outputs.

### 3.3.3 Integration of the Model into WEST Software

Once the model was extended to include sulfate reduction and autotrophic denitrification processes—along with the relevant components, parameters, stoichiometric relationships, and kinetic constants—and checked for internal consistency through mass balance checks, it was integrated into the WEST software for simulations.

The WEST simulation, which is a part of the packages in MIKE powered by DHI software,[76] is a versatile and robust tool designed for modelling and simulating water treatment processes. The extended PWM_SA model was then developed within WEST, carefully defining parameters, equations, and interactions to simulate the behaviour of contaminants and other variables throughout the treatment process. This integration involved deriving and coding sulfidogenic reactions, which not only broadened the model's scope but also enhanced verification and refinement within the WEST simulation framework.

# Chapter 4: Results and Discussion

The primary objective of this study was to extend the PWM_SA model by integrating the bio-processes specific to the SANI system, using empirical data from the SANI saline sewage treatment system at the Hong Kong pilot plant. This involved the incorporation of sulfate reduction and autotrophic denitrification processes into the PWM_SA model within the WEST software. The PWM_SA model was checked for internal consistency by ensuring that material (COD, C, H, O N, P, and S) mass and charge balances were met for all processes (see section 3.2.3 which shows how this was done). The final step of model verification involves checking that the simulations resulted in reasonable predictions when compared to the experimental data of the Hong Kong Pilot plant.

In the following sections of this chapter, the results for the SRUSB, anoxic, and aerobic reactors, which were the component units of the SANI system, will be individually analyzed and discussed to evaluate the capability of the mass-balanced model in tracking COD, N, S, and P through the three reactors. Each reactor's performance will be evaluated based on COD removal, $NO_3^-$ and sulfate ($SO_4^{2-}$ reduction, $H_2S$ production, effluent TSS, and the mass balances of COD, N, S and P. The predicted results will also be assessed against the experimental results. However, it is worth noting that a comprehensive calibration against the experimental results was quite challenging due to the following challenges in this process:

- The imperfect experimental mass balances for COD, S, and N, which may have arisen primarily from incomplete sampling, measurement inaccuracies, and potential analytical errors. Moreover, dynamic operating conditions at the pilot scale may have led to unaccounted losses or temporary accumulations of key constituents. To improve future mass balances, increasing sampling frequency, refining measurement protocols, and accounting for all potential inflows and outflows is recommended. This approach will reduce uncertainties and provide more robust data for model calibra-

tion and validation.

- Additionally, it was challenging to calculate the mass balances in the experimental data, because of missing information such as reactor solids concentrations, OUR, and TSS. This lack of data hampered the assessment of organic matter degradation and nutrient removal efficiencies. Important experimental data for parameters like TSS and OUR were missing, which hampered the assessment of organic matter degradation and nutrient removal efficiencies.

- The N-to-COD ratio calculated from experimental data in the SRUSB is unreasonably high compared to literature values.[34,18] This was evidenced by an N-to-COD ratio of approximately 0.7, which exceeds the typical range of 0.06 observed in literature.

## 4.1 SRUSB

The SRUSB results predicted by the extended PWM _SA model compared against the experimentally measured data from the SANI pilot plant are presented in Table 4.1. The SRUSB operates under anaerobic conditions, where SRB drives the key reactions and shows reduced concentrations of COD and $SO_4^{2-}$, with corresponding increases in $H_2S$.

As expected in BSR systems (see section 2.2.1), the effluent demonstrates reduced concentrations of COD and $SO_4^{2-}$, accompanied by an increase in $H_2S$ levels, as illustrated in Figure 4.1. The model predicted results align well with the effluent characteristics expected in BSR systems, showing a COD removal efficiency of 66%, as well as reductions in TSS and VSS concentrations due to the degradation of organic matter, which was used as an electron donor for the growth of SRB.

Table 4.1 Characteristics of the influent and effluent for the SRUSB.

| **Parameters** | **Influent** | **Effluent** | **Removal** |
|---|---|---|---|
| TSS (mg/L) | 280.19 | 128.29 | -151.90 |
| VSS (mg/L) | 186.19 | 42.76 | -143.43 |
| Unfiltered COD (mgCOD/L) | 439.22 | 147.75 | -291.47 |
| Filtered COD (mgCOD/L)b | 157.90 | 81.18 | -76.72 |
| $SO_4^{2-}$ (mgS/L) | 195.70 | 57.59 | -138.11 |
| $H_2S$ (mgS/L) | 4.00 | 142.13 | +138.13 |
| Unfiltered TKN (mgN/L) | 66.13 | 65.02 | -1.11 |
| Filtered TKN (mgN/L) | 49.19 | 56.63 | +7.44 |
| FSA (mgN/L) | 44.80 | 53.40 | +8.60 |
| $NO_3^-$ (mgN/L) | 0.00 | 0.00 | - |
| Unfiltered TP (mgP/L) | 7.80 | 7.63 | -0.17 |
| Filtered TP (mgP/L) | 5.80 | 6.61 | +0.81 |
| OP (mgP/L) | 5.30 | 6.20 | +0.90 |

Additionally, a 71% sulfate removal was achieved, since $SO_4^{2-}$ serves as the electron acceptor in SRB metabolic processes. The reduction of $SO_4^{2-}$ leads to its conversion into $H_2S$, as evidenced by the rise in $H_2S$ levels shown in Figure 4.1.

Nitrogen removal is minimal since the SRUSB reactor primarily facilitates S cycling rather than N removal. However, a decrease in organic N was observed in the effluent with a slight increase in the effluent FSA which may suggest that some bound organic N may have been broken down to form $NH_4^+$. This conversion aligns with typical anaerobic degradation pathways where the organically bound N is released with the breakdown of organics (COD). According to the trend in COD removal noted above, and the determined BPO N/COD ratio of 0.06, it is expected that the N released would increase the quantity of $NH_4^+$ in the AD mixed liquor by 9.68 mgN/L to give an effluent $NH_4^+$ concentration of 53.40 mgN/L. This model's predicted value of the effluent FSA is slightly higher than the measured value of 45.4 mgN/L, this could be because the measured value did not indicate N release with BPO degradation.

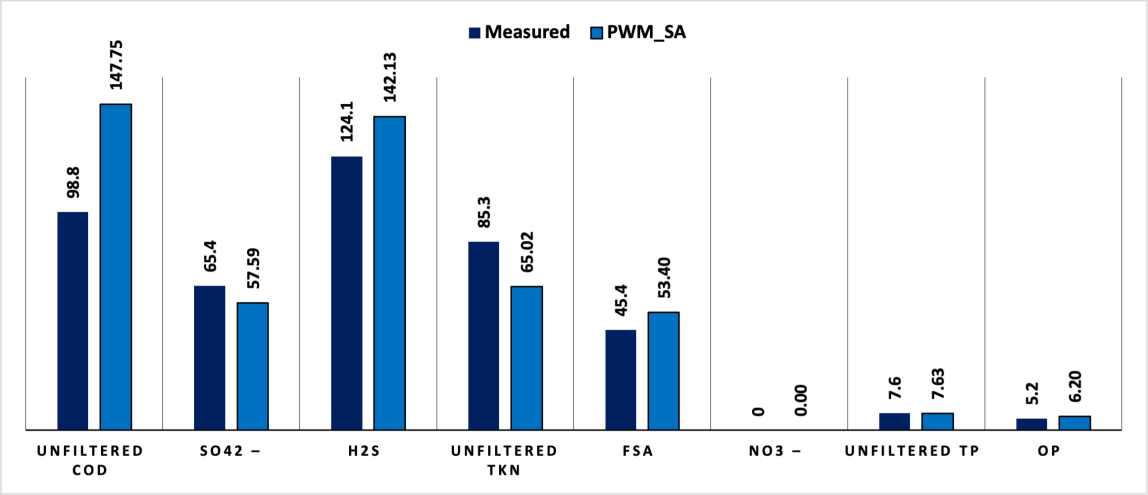


Figure 4.1 Comparative analysis of the SANI pilot plant measured and PWM_SA predicted effluent parameters for the SRUSB reactor.

The P concentration in the effluent remained relatively unchanged from the influent levels, with a small increase in OP which may be attributed to the breakdown of organic P compounds used in biomass and also released as OP.

A comparison of the measured and predicted effluent concentrations for the SRUSB is shown in Table 4.2. The model's predictions generally align with the measured data, though the predicted COD and sulfate removal rates are slightly higher as shown in Figure 4.1. This difference could be due to the assumption that the SRUSB operates as a completely mixed reactor, while in reality, there is approximately 5% hydraulic short-circuiting (bypass flow) and 35% dead space in the reactor at the SANI pilot plant.[46]

Table 4.2 The measured and predicted effluent parameters for the SRUSB.

| Parameters | SRUSB Effluent | |
|---|---|---|
| | SANI Pilot Plant | PWM_SA |
| TSS (mg/L) | - | 128.29 |
| VSS (mg/L) | 52.1 | 42.76 |
| Unfiltered COD (mgCOD/L) | 98.8 | 147.75 |
| Filtered COD (mgCOD/L)b | 39.7 | 81.18 |
| $SO_4^{2-}$ (mgS/L) | 65.4 | 57.59 |
| $H_2S$ (mgS/L) | 124.1 | 142.13 |
| Unfiltered TKN (mgN/L) | 85.3 | 65.02 |
| Filtered TKN (mgN/L) | 70.9 | 56.63 |
| FSA (mgN/L) | 45.4 | 53.40 |
| $NO_3^-$ (mgN/L) | 0 | 0 |
| Unfiltered TP (mgP/L) | 7.60 | 7.63 |
| Filtered TP (mgP/L) | 5.70 | 6.61 |
| OP (mgP/L) | 5.20 | 6.20 |

Additionally, the measured effluent $H_2S$ levels, illustrated in Figure 4.1, are lower than predicted, likely due to lower COD removal than anticipated, and partial oxidation of $H_2S$ to elemental S, as suggested by the white S deposits observed on the internal walls of the SRUSB effluent pipe of the SANI pilot plant.[46]

The predicted effluent TKN values are lower than the measured values due to the influent TKN concentrations in the measured data being unreasonably high. This discrepancy was primarily caused by the N bound in the USO being disproportionately high compared to values commonly observed in the literature. Since the USO component does not participate in any biological processes but simply passes through the system and contributes to the effluent TKN, correcting this N component does not affect the evaluation of the biological process replication in the model.[34,18] To address this issue, the influent TKN values were adjusted to more reasonable levels, resulting in effluent TKN and $NO_3^-$ concentrations that better align with expected outcomes. Further discussion on these adjustments is provided in the following chapters.

### 4.1.1 Mass balances

Figure 4.2 below contains four bar charts that track the concentrations of COD, N, P, and S through the SRUSB reactor and outline the distribution and transformations of each element as it moves through the reactor.

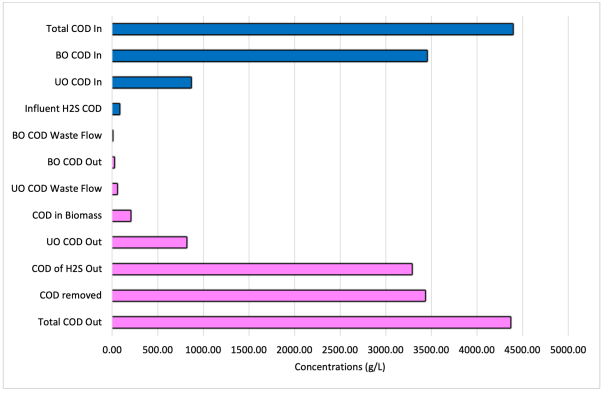


(a) COD tracking

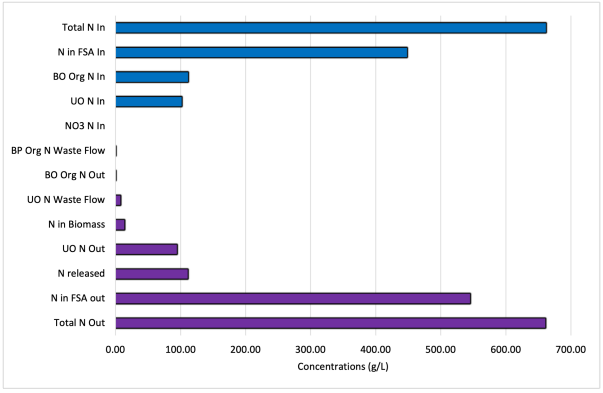


(b) N tracking.

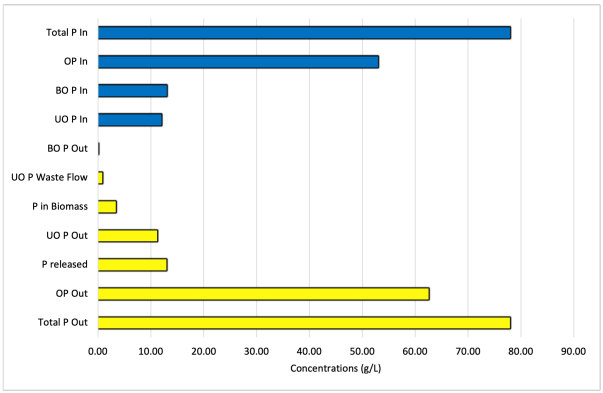


(c) P tracking

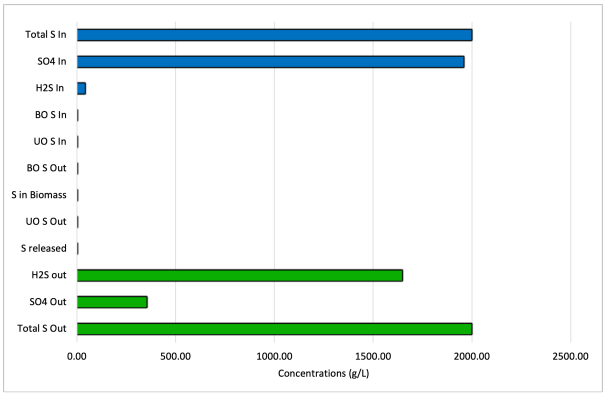


(d) S tracking

Figure 4.2 Comprehensive tracking of COD, N, S, and P through the SRUSB reactor.

The total COD influent is dominated by BO COD, while UO COD and COD from $H_2S$ contribute smaller fractions. As BO COD is consumed, it is primarily transformed into $H_2S$ through sulfate reduction, evidenced by a much higher effluent COD from $H_2S$, with a small portion being assimilated into biomass as shown in Figure 4.2a. The BO COD waste flow and BO COD out remained minimal, indicating high reactor efficiency in removing BO COD. Most of the BO COD was effectively utilized by SRB, contributing significantly to COD removal. The unbiodegradable organic matter remained largely unchanged. The UO

COD out is similar to its influent concentration, confirming that this fraction of COD was not degraded and exited with the effluent.

The transformation of COD into $H_2S$ is significant, with the COD of $H_2S$ out reaching 2837 g/L. This highlights the dominant sulfate reduction pathway, where SRB reduces $SO_4^{2-}$ to $H_2S$ using organic matter as an electron donor. The remaining COD removed (2939 g/L) reflects the overall efficiency of the reactor, which is primarily attributed to sulfate reduction and COD oxidation processes. A COD mass balance of 100% was achieved as presented in Table 4.3, indicating that all influent COD was accounted for either through conversion into $H_2S$, assimilation into biomass, or exiting as UO COD in the effluent or waste flow.

The total N influent is dominated by N in FSA, with additional contributions from BO Org N and UO N as presented in Figure 4.2b. A large portion of the N influent is released as FSA in the effluent. As expected the UO N remained largely unchanged, and the UO N effluent closely matches its influent concentration, confirming that this fraction was not degraded and exited the reactor with the effluent. A small portion of N was assimilated into biomass, further supporting the reactor's ability to process BO N effectively. The N released during the process, combined with N in FSA outflow, contributes to the total N exiting the system. A 100% mass balance was achieved, ensuring that all N inputs were accounted for, either through transformation into biomass, release as FSA, or remaining in the unbiodegradable form.

The total S influent is dominated by $SO_4^{2-}$ with a smaller contribution from $H_2S$ as shown in Figure 4.2d. The $SO_4^{2-}$ was reduced to $H_2S$ as seen by the significant increase in $H_2S$ in the effluent compared to its influent concentration. The S released as $H_2S$ is substantial, highlighting the efficiency of sulfate reduction. The $SO_4^{2-}$ in the effluent is significantly lower than its influent value, indicating that most of the $SO_4^{2-}$ was consumed in the reduction process. A 100% mass balance was achieved, ensuring that all S inputs were accounted for either through conversion to $H_2S$, assimilation into biomass, or re-

maining in the effluent as unconverted S.

The TP influent is dominated by OP and BO P, with additional contributions from UO P as shown in Figure 4.2c. A significant portion of the total P influent is released as OP in the effluent, demonstrating the breakdown of BO P or the release of P bound in BO as OP during hydrolysis of the BO. As expected, UO P remained mostly unchanged indicating that this fraction was not degraded during the process. A portion of the TP is assimilated into biomass, supporting the reactor's efficiency in handling BO P. Phosphorus released during the process, along with OP in the effluent, accounts for the TP exiting the system. A complete mass balance was achieved, ensuring all P inputs were accounted for, whether through use in biomass growth, release as OP, or remaining in the UO form.

Table 4.3 presents the model predicted mass balances alongside the measured data mass balances. It is important to note that the PWM_SA model operates under idealized conditions, where the bioprocesses occur without any unaccounted losses or inefficiencies. Additionally, the model assumes complete mixing within the reactor and ideal flow patterns, which may not accurately reflect the complexities of real-world systems. In contrast, the measured data captures the variability of actual conditions, where operational losses, incomplete reactions, and system inefficiencies are present.

Table 4.3 Comparison of predicted and measured data mass balances of the SRUSB. [46]

| **Parameters** | **Measured** | **PWM_SA** |
|---|---|---|
| COD (gCOD/d) | Influent COD and $H_2S$ = 4390<br>COD accumulation in SRUSB = 323.6<br>COD exiting SRUSB as $H_2S$ = 2482<br>COD exiting SRUSB as unfiltered = 988<br>Total COD exiting SRUSB = 3794 | Influent COD and $H_2S$ = 4392<br>COD in waste flow = 51.50<br>COD exiting SRUSB as $H_2S$ = 2837<br>COD exiting SRUSB as unfiltered = 1321.81<br>Total COD exiting SRUSB = 4379.77 |
| **COD Mass Balance** | **86%** | **100%** |
| Nitrogen (gN/d) | Influent TKN =875<br>Effluent TKN = 853<br>N in UO = 48.4<br>Total effluent TKN =901 | Influent TKN =661.29<br>Effluent TKN = 559<br>N in UO =101.93<br>Total effluent TKN =660.96 |
| **N Mass Balance** | **103%** | **100%** |
| Sulfur (gS/d) | Influent $SO_4$ and $H_2S$ =1997<br>Effluent S = 1895<br>Total effluent S =1895 | Influent $SO_4$ and $H_2S$ =1997<br>Effluent S = 1997<br>Total effluent S =1997 |
| **S Mass Balance** | **95%** | **100%** |
| Phosphorus (gP/d) | Influent P =78<br>Effluent P =81.3<br>P in UO = 5.3<br>Total effluent P =81.3 | Influent P =77.98<br>Effluent P = 77.92<br>P in waste flow =0.06<br>Total effluent P =77.92 |
| **P Mass Balance** | **104%** | **100%** |

The PWM_SA model achieves a 100% COD mass balance, indicating that all COD entering the system is fully accounted for in the effluent, through transformation to $H_2S$, via the waste flow and exiting the reactor as unfiltered COD. In contrast, the measured COD mass balance is only 86%, suggesting potential COD losses within the system. The higher $H_2S$ output predicted by the model (2837 gCOD/d) compared to the measured value (2482 gCOD/d) implies that the model assumes more efficient sulfate reduction processes than were observed experimentally. While the PWM_SA model achieves an S balance at 100%, the measured system shows an S balance of 95%, indicating that some S is unaccounted for, likely retained as elemental S, as discussed in the previous section[46]. This also explains

the lower COD mass balance for the measured data, as less COD is released as $H_2S$.

According to the measured data, the influent TKN was 875 gN/d, and 901 gN/d remained in the effluent. This yielded an N mass balance of 103%, indicating some overestimation of N in the effluent. Moreover, the USO N from measured data was noted to have a significantly higher value than that observed in literature data.[18] In the model, the literature observed value for USO N/mass ratio of 0.09 was adopted and this resulted in a lower influent TKN value of 661.3 gN/d. The calculated N balance for the model was at 100%.

The TP and OP levels in the influent and effluent did not change by much in both cases with the measured P balance slightly exceeding 100%, likely due to analytical errors or external P sources. The PWM_SA model achieved a 100% P balance, indicating accurate prediction.

The model accurately tracks the flow of COD, N, S, and P, ensuring that no losses or unaccounted gains occur within the system. The mass balance for the model reflects internal consistency, confirming that the processes being simulated are correctly represented and follow the principle of mass conservation. This level of accuracy suggests that the model reliably captures the real-world behaviour of the system, reinforcing its credibility for further analysis and predictions.

## 4.2 Anoxic Bioreactor

In the anoxic reactor, the primary process is autotrophic denitrification, where $NO_3^-$ is sequentially reduced through intermediates, such as $NO_2^-$, to produce nitrogen gas ($N_2$). This process is driven by S-oxidizing autotrophic denitrifiers, which utilize $H_2S$, as an electron donor. During denitrification, $H_2S$ is oxidized to $SO_4^{2-}$. Therefore, the expected effluent profile should show an increase in $SO_4^{2-}$ concentrations, a reduction in $H_2S$ levels, and a significant decrease in $NO_3^-$ concentration.

Table 4.4 shows the predicted influent, effluent, and removal concentrations for the

anoxic reactor. The below results demonstrate that the model's behaviour is in line with the theoretical expectations of the anoxic reactor effluent.

Table 4.4 Characteristics of the predicted influent and effluent for the anoxic reactor.

| **Parameters** | **Influent** | **Effluent** | **Removal** |
|---|---|---|---|
| TSS (mg/L) | 48.57 | 49.27 | +0.70 |
| VSS (mg/L) | 16.80 | 20.59 | +3.79 |
| Unfiltered COD (mgCOD/L) | 72.50 | 78.88 | +6.38 |
| Filtered COD (mgCOD/L)b | 46.40 | 46.80 | +0.40 |
| $SO_4^{2-}$ (mgS/L) | 158.70 | 179.22 | +20.52 |
| $H_2S$ (mgS/L) | 41.01 | 20.49 | -20.52 |
| Unfiltered TKN (mgN/L) | 58.04 | 57.52 | -0.52 |
| Filtered TKN (mgN/L) | 54.83 | 54.07 | -0.76 |
| FSA (mgN/L) | 15.30 | 14.69 | -0.61 |
| $NO_3^-$ (mgN/L) | 10.90 | 0.22 | -10.68 |
| Unfiltered TP (mgP/L) | 6.84 | 6.79 | -0.05 |
| Filtered TP (mgP/L) | 6.43 | 6.28 | -0.15 |
| OP (mgP/L) | 6.10 | 5.95 | -0.15 |

The autotrophic denitrifying microorganisms, which utilize $H_2S$ as the electron donor, have a lower biomass yield compared to heterotrophic organisms, which use BO as the electron donor to carry out denitrification in the anoxic zone. According to literature, heterotrophs tend to outcompete autotrophs when the carbon to $NO_3^-$ ratio is high in the anoxic zone, as heterotrophs are faster-growing organisms.[80] However, in this case, the BSR process occurring upstream of the anoxic reactor consumes the sewage BO and generates high concentrations of $H_2S$ (142.13 mgS/L). As a result, autotrophic denitrifiers, despite their lower biomass yields, dominated the reactor, even with a long solids retention time of 110 days.

The predicted VSS and TSS concentrations in the anoxic reactor are 20.59 mg/L and 49.27 mg/L, respectively. Unfortunately, the measured data did not include reactor solids concentrations. Further studies could explore the kinetics of autotrophic and heterotrophic denitrifiers, which work together to remove $NO_3^-$. These studies could also help calibrate

the model to predict anoxic solids concentrations while considering varying carbon and $H_2S$ levels in the anoxic influent.

The increase in $SO_4^{2-}$ concentration (from 158.70 mgS/L to 179.22 mgS/L) as illustrated by Table 4.4 and a corresponding decrease in $H_2S$ concentration (from 41.01 mgS/L to 20.49 mgS/L) align with the S oxidation mechanism involved in autotrophic denitrification, $H_2S$ is oxidized to $SO_4^{2-}$ as S-oxidizing bacteria use it as an electron donor for reducing $NO_3^-$ to $N_2$.

Theoretically, there should be minimal effect on the TKN in the anoxic reactor during autotrophic denitrification because this process primarily targets $NO_3^-$ for reduction, not organic N or $NH_4^+$. The small decreases in unfiltered and filtered TKN (0.52 and 0.76 mgN/L, respectively) along with a reduction in FSA concentration by 0.61 mgN/L indicates that very limited N transformation is occurring. This is in line with the generation of small quantities of biomass in the anoxic zone - hence very low N is used as nutrients for biomass growth.

The $NO_3^-$ concentration decreased significantly from 10.90 mgN/L to 0.22 mgN/L, highlighting the efficiency of the reactor. The $NO_3^-$ was reduced to $N_2$, which is the expected outcome of the denitrification process. There is a minimal reduction in TP, filtered TP, and OP, each decreasing by less than 0.2 mgP/L. This suggests that P removal is not a significant process in the anoxic reactor, which is expected given the low nutrient requirements for the growth of autotrophic denitrifiers in the system. Overall, these results indicate that the model can efficiently predict the functioning of the anoxic reactor.

Table 4.5 presents the measured versus predicted effluent results for the anoxic reactor. The measured unfiltered COD (55 mgCOD/L) is lower than the predicted value (78.88 mgCOD/L). This can be attributed to the overestimation of microbial biomass growth by the model, aligned with the slight increase in the effluent VSS.

Table 4.5 Measured versus predicted effluent results for the anoxic reactor.

| Parameters | SRUSB Effluent | |
|---|---|---|
| | SANI Pilot Plant | PWM_SA |
| TSS (mg/L) | - | 49.27 |
| VSS (mg/L) | 12.5 | 20.59 |
| Unfiltered COD (mgCOD/L) | 55 | 78.88 |
| Filtered COD (mgCOD/L) | 30.2 | 46.80 |
| $SO_4^{2-}$ (mgS/L) | 169.4 | 179.22 |
| $H_2S$ (mgS/L) | 3 | 20.49 |
| Unfiltered TKN (mgN/L) | 35.7 | 57.52 |
| Filtered TKN (mgN/L) | 35.3 | 54.07 |
| FSA (mgN/L) | 16.4 | 14.69 |
| $NO_3^-$ (mgN/L) | 2.2 | 0.22 |
| Unfiltered TP (mgP/L) | 5.7 | 6.79 |
| Filtered TP (mgP/L) | 5.6 | 6.28 |
| OP (mgP/L) | 5.3 | 5.95 |

The model predicts higher unfiltered and filtered TKN values (57.52 mgN/L and 54.07 mgN/L, respectively) compared to the measured values (35.7 mgN/L and 35.3 mgN/L). This is in line with the adjustment of the USO N concentration to lower influent TKN values for the model. However, the predicted FSA (14.69 mgN/L) is close to the measured value (16.4 mgN/L), suggesting reasonable accuracy in predicting the experimental $NH_4^+$ levels. With the inclusion of the USO N value (23.3 mgN/l) that was originally deducted from the experimental influent data for the model, the effluent TKN would also result in a reasonable match.

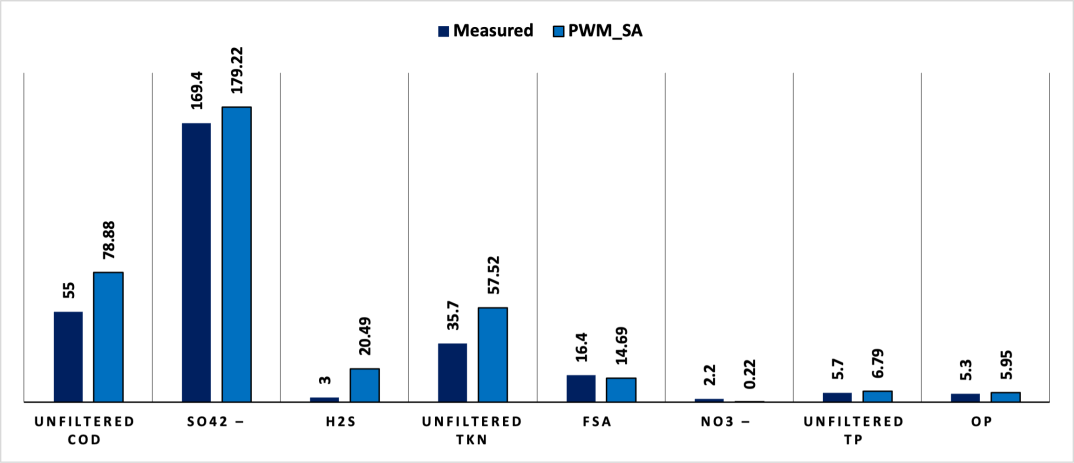


Figure 4.3 Comparative analysis of SANI pilot plant measured and predicted effluent parameters of the anoxic reactor.

The model overpredicts effluent $SO_4^{2-}$ concentrations (179.22 mgS/L predicted vs. 169.4 mgS/L measured) and $H_2S$ concentrations (20.49 mgS/L predicted vs. 3 mgS/L measured) as shown in Figure 4.3. This suggests that in the pilot plant, more $H_2S$ was oxidized to $SO_4^{2-}$ than the model anticipated.

Additionally, the model predicted almost complete $NO_3^-$ removal (0.22 mgN/L), whereas the measured $NO_3^-$ concentration was slightly higher (2.2 mgN/L). Despite this, the predicted amount of $NO_3^-$ denitrified (373 gCOD/d) closely aligns with the measured value (396 gCOD/d). This raises questions about the accuracy of either the measured $NO_3^-$ denitrified or the $H_2S$ oxidized values, or whether there is an additional, unaccounted process in the pilot plant that is consuming more $H_2S$. It suggests a potential issue with the mass balancing of the measured data, making it unclear where the most reliable data points lie. A more detailed mass balance could help identify the most trustworthy aspects of the data and clarify whether the discrepancies are due to measurement inaccuracies or unmodeled processes.

The model predicts slightly higher P concentrations compared to the measured values. The differences are very minimal, with measured TP (5.7 mgP/L) and OP (5.3 mgP/L) slightly lower than the predicted values (6.79 mgP/L for TP and 5.95 mgP/L for OP). These

small discrepancies suggest that P removal processes, such as assimilation by biomass, are reasonably well simulated by the model. Overall the model predictions correlate quite well with the measured data.

### 4.2.1 Mass balances

Figure 4.4 below presents the comprehensive tracking of COD, N, P, and S through the anoxic reactor and outlines the distribution and transformations of each element as it moves through the reactor while Table 4.6 presents the model and measured mass balances.

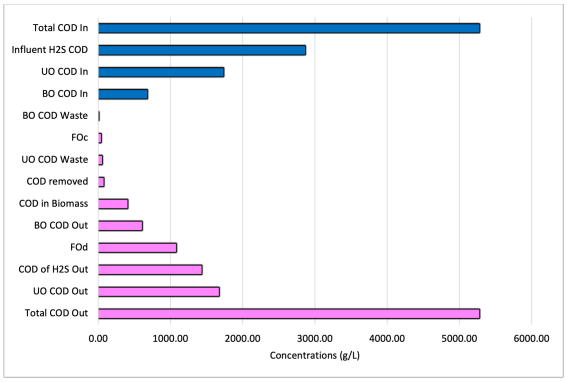


(a) COD tracking

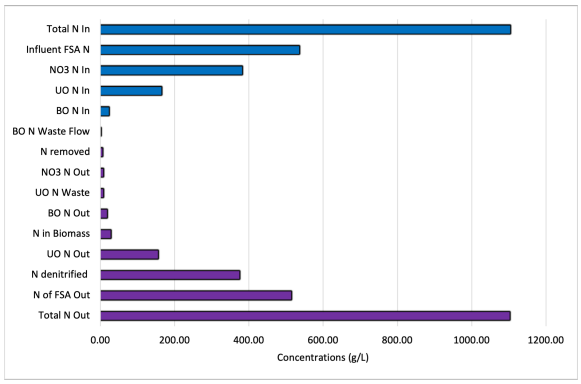


(b) N tracking.

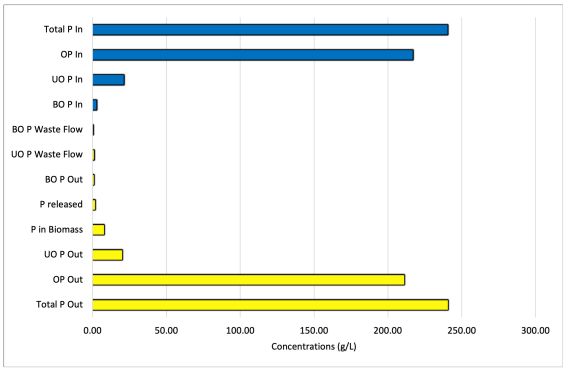


(c) P tracking

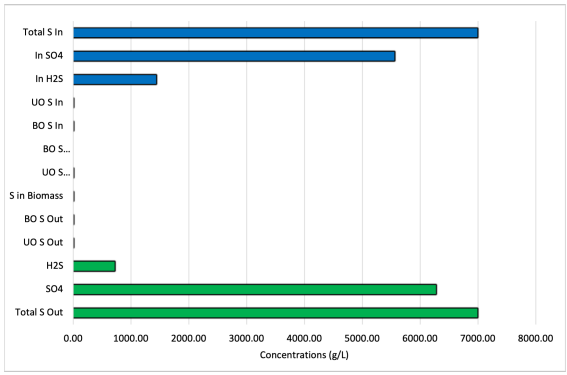


(d) S tracking

Figure 4.4 Comprehensive tracking of COD, N, S, and P through the anoxic reactor.

The total COD influent was predominantly composed of COD from $H_2S$, with additional contributions from UO and BO COD, as illustrated in Figure 4.4a. A large portion of the total COD that entered the reactor exits as COD from $H_2S$ with a substantial reduction

which can be attributed to S-oxidizing autotrophic denitrifiers utilizing $H_2S$ as an electron donor. Biodegradable organic COD was effectively consumed, as reflected by the minimal BO COD concentrations in the effluent, demonstrating efficient microbial degradation. A portion of the COD was incorporated into biomass suggesting the breakdown of BO COD.

The UO COD remained mostly unchanged throughout the system, exiting the reactor with concentrations similar to those in the influent, as expected. A small amount of COD exited as waste flow, contributing to the total COD in the effluent. The system achieved a 100% mass balance as presented in Figure 4.6, ensuring that all COD inputs are accounted for, either through waste flow, assimilation into biomass, exiting as UO or $H_2S$ COD. This highlights the reactor's efficiency in processing and removing BO matter while effectively handling UO fractions.

The total N influent to the anoxic reactor was composed primarily of FSA, $NO_3^-$, UO N, and a smaller portion of BO N. A significant amount of the influent FSA remained unprocessed and exited the system with the effluent as illustrated in Figure 4.4b. The $NO_3^-$ was effectively reduced during autotrophic denitrification, with only a minimal amount detected in the effluent, demonstrating the reactor's ability to convert $NO_3^-$ into $N_2$.

The UO N influent remained largely unchanged confirming that it was not degraded during the denitrification process. The BO N, though present in small amounts, was efficiently consumed within the reactor, with minimal BO N detected in the effluent, suggesting successful microbial breakdown. A small portion of the influent N was used for biomass growth contributing to the overall N removal. A complete N mass balance of 100% confirms that all influents are accounted for in the effluents.

The total S influent was primarily composed of $H_2S$ and $SO_4^{2-}$, with negligible contributions from BO and UO S, as shown in Figure 4.4d. A significant portion of the influent $H_2S$ was oxidized to $SO_4^{2-}$, which aligned with the expected function of S-oxidizing autotrophic denitrifiers in the reactor. This was reflected by the high $SO_4^{2-}$ concentrations in the effluent, while the effluent $H_2S$ levels were considerably lower than in the influent.

Minimal amounts of BO and UO S were present in both the influent and effluent, indicating that these components remained largely unchanged and did not undergo significant transformation in the reactor. The S removal was primarily due to the oxidation of $H_2S$, with only a small fraction being incorporated into biomass. The system achieved a complete mass balance, as all S inputs were accounted for in the effluent, predominantly in the form of $SO_4^{2-}$, with $H_2S$ significantly reduced through autotrophic denitrification.

The TP influent was predominantly composed of OP, with smaller contributions from UO and BO P as presented in Figure 4.4c. The results show that OP, being the largest fraction, exited the reactor almost entirely unchanged, with a substantial portion released as OP in the effluent. The BO P, while present in small amounts at the influent, was nearly completely broken down and removed within the reactor. This is evident from the minimal concentrations of BO P found in both the effluent and waste flows, indicating that the reactor is effectively degrading BO P. Some P was used in biomass growth and a small portion was released during the treatment process, contributing to the overall P outflow with a P mass balance of 100%, ensuring that all P inputs are fully accounted for.

The model effectively predicts the overall mass balance of the reactor, with an achieved COD mass balance of 100%, compared to the measured mass balance of 90%. However, notable differences exist between the measured and predicted total influent COD values. The measured influent COD was 4498 gCOD/d, whereas the model predicted a higher value of 5274 gCOD/d. This deviation is primarily attributed to the adjusted value of $H_2S$ COD in the influent, with the model predicting 2410 gCOD/d compared to the measured value of 2191 gCOD/d or the lower mass balance value of the measured COD. Additionally, the model overpredicted the unfiltered COD in the effluent (2271 gCOD/d) compared to the measured value (1925 gCOD/d). These discrepancies highlight the challenge of calibrating the model without complete kinetic data. Despite this, the model was able to balance COD utilization for denitrification and sulfate reduction, ensuring mass balance consistency.

Table 4.6 Comparison of predicted and measured data mass balances for the anoxic reactor.[46]

| **Parameters** | **Measured** | **PWM_SA** |
|---|---|---|
| COD (gCOD/d) | Influent COD = 2307<br>Influent $H_2S$ COD =2191<br>Total Influent COD = 4498<br>Unfiltered COD out =1925<br>Effluent $H_2S$ COD =210<br>COD equivalent of $NO_3$ denitrification = 1131<br>COD utilized in $SO_4^{-2}$ production = 1897<br>Total COD exiting the reactor = 4032 | Influent COD = 1941<br>Influent $H_2S$ COD = 2410<br>Total Influent COD = 5274<br>Unfiltered COD out = 2271<br>Effluent $H_2S$ COD = 1431<br>COD in biomass = 404<br>FOd (calc. from delta $FN_2$ and $FNO_3$) = 1077<br>Total COD exiting the reactor = 5274 |
| **COD Mass Balance** | **90%** | **100%** |
| Nitrogen (gN/d) | Influent TKN and $NO_3$ =1845<br>Effluent TKN and $NO_3$ = 1327<br>$NO_3$ denitrified = 396<br>Total effluent TKN = 1723 | Influent TKN and $NO_3$ =1104<br>Effluent TKN and $NO_3$ =733<br>$NO_3$ denitrified = 373<br>Total effluent TKN =1102 |
| **N Mass Balance** | **93%** | **100%** |
| Sulfur (gS/d) | Influent $SO_4$ and $H_2S$ = 6076<br>Effluent S = 6034<br>Total effluent S =6034 | Influent $SO_4$ and $H_2S$ =6988<br>Effluent S = 6988<br>Total effluent S = 6988 |
| **S Mass Balance** | **100%** | **100%** |
| Phosphorus (gP/d) | Influent P =206<br>Effluent P =199<br>Total effluent P =199 | Influent P =240<br>Effluent P = 241<br>Total effluent P =241 |
| **P Mass Balance** | **98%** | **100%** |

For N, the model predicted a complete mass balance of 100%, while the measured balance was 93%. The predicted influent TKN and $NO_3$ values were lower (1104 gN/d) than the measured values (1845 gN/d), supporting the adjustments that were made to fit the overall N balance within the model. The effluent TKN and $NO_3$ levels also showed differences, with the model predicting 733 gN/d and the measured value at 1327 gN/d. However, both the predicted and measured values for the amount of $NO_3$ denitrified were similar (373 gN/d predicted vs. 396 gN/d measured), indicating that the model reasonably

predicted the denitrification process, despite the overall N imbalance of the experimental system.

The sulfur mass balance was well predicted by the model, with both the measured and predicted results showing a 100% mass balance. The predicted influent S (6988 gS/d) was slightly higher than the measured value (6076 gS/d). This could be in connection to the $H_2S$ generation in the upstream BSR process. However, both effluent S values were similar, indicating that the model effectively captured the S cycle. This accurate prediction was achieved despite missing SRB kinetic data, suggesting that adjustments to other parameters helped maintain consistency in the S balance.

Finally, the P mass balance was also closely predicted by the model, with the measured value at 98% and the predicted value at 100%.

The model effectively tracks the flow of COD, N, S, and P through the anoxic reactor, ensuring that all material is accounted for with no unexpected losses or gains. The mass balance demonstrates the model's internal consistency, indicating that the simulated processes are well presented.

## 4.3 Aerobic Biorector

The primary process in the aerobic reactor is nitrification, which oxidizes any remaining $NH_4^+$ in the influent from the anoxic reactor. Theoretically, $NH_4^+$ in the effluent should be very low, approaching 0 mgN/L. Most of the $NH_4^+$ is converted into $NO_3^-$ through the action of ammonia-oxidizing bacteria. The effluent results for the aerobic reactor are presented in Table 4.7 along with the influent and removal concentrations.

Table 4.7 Characteristics of the predicted influent and effluent for the aerobic reactor.

| Parameters | Influent | Effluent | Removal |
|---|---|---|---|
| TSS (mg/L) | 49.27 | 16.70 | -32.57 |
| VSS (mg/L) | 20.59 | 6.42 | -14.17 |
| Unfiltered COD (mgCOD/L) | 78.88 | 42.42 | -36.46 |
| Filtered COD (mgCOD/L) | 46.80 | 32.50 | -14.30 |
| $SO_4^{2-}$ (mgS/L) | 179.22 | 199.11 | +19.89 |
| $H_2S$ (mgS/L) | 20.49 | 0.60 | -19.89 |
| Unfiltered TKN (mgN/L) | 57.52 | 55.26 | -2.26 |
| Filtered TKN (mgN/L) | 54.07 | 54.12 | +0.05 |
| FSA (mgN/L) | 14.69 | 0.07 | -14.62 |
| $NO_3^-$ (mgN/L) | 0.22 | 15.25 | +15.03 |
| Unfiltered TP (mgP/L) | 6.79 | 6.52 | -0.27 |
| Filtered TP (mgP/L) | 6.28 | 6.36 | +0.08 |
| OP (mgP/L) | 5.95 | 6.06 | +0.11 |

The TSS and VSS both showed significant reductions, with TSS decreasing from 49.27 mg/L to 16.70 mg/L and VSS dropping from 20.59 mg/L to 6.42 mg/L as shown in Figure 4.5. This was expected because of the lower solids retention time in the aerobic reactor (i.e., SRT of 42) after the anoxic reactor that had a high SRT of 110 days. Also, some of the biomass undergoes endogenous respiration and the solids in the effluent are less than in the reactor due to some solids having been separated through the settling process. These reductions indicate a considerable removal of particulate matter and microbial biomass, which is characteristic of efficient solids separation and microbial degradation in an aerobic environment. The removal of VSS also suggests a decline in active biomass as it is either oxidized or settles out in the system.

The effluent concentrations of N compounds reveal that nitrification was the dominant process in the aerobic reactor. The FSA concentration was 14.69 mgN/L, which dropped drastically to 0.07 mgN/L in the effluent as illustrated in Figure 4.5. This 14.62 mgN/L reduction in $NH_4^+$ demonstrates that the model effectively simulated the reactor conditions, indicating that the reactor environment successfully supported the growth and activity of

ammonia-oxidizing bacteria.

The increase in $NO_3^-$ concentration from 0.22 mgN/L in the influent to 15.25 mgN/L in the effluent further supports the effective completion of the nitrification process. This substantial $NO_3^-$ production suggests that the second stage of nitrification, where $NO_2^-$ is oxidized to $NO_3^-$ by nitrite-oxidizing bacteria, proceeded efficiently.

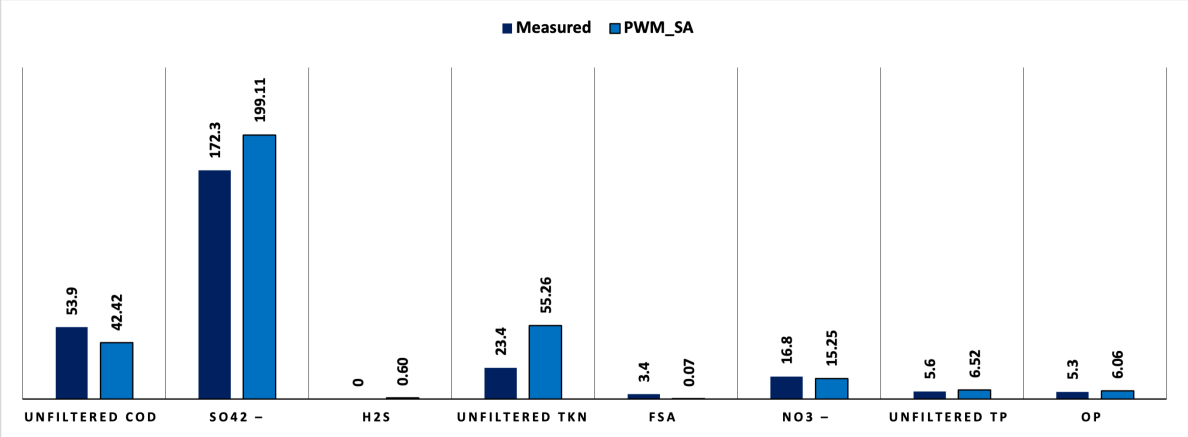


Figure 4.5 Comparative analysis of SANI pilot plant measured and predicted effluent parameters of the aerobic reactor.

On the other hand, TKN remained relatively unchanged, with the influent TKN concentration of 57.52 mgN/L decreasing to 55.26 mgN/L in the effluent. This small change of 2.26 mgN/L implies that the organic N component of TKN was not significantly transformed. While nitrification targets $NH_4^+$, the persistence of organic N suggests that the reactor did not facilitate substantial degradation or transformation of the organic N compounds present in the influent.

The model predicted only minor changes in the concentrations of unfiltered and filtered TP, as well as OP. The influent unfiltered TP concentration of 6.79 mgP/L decreased slightly to 6.52 mgP/L in the effluent, while filtered TP changed marginally from 6.28 mgP/L to 6.36 mgP/L. These results align with the model's expectations, as it does not significantly facilitate P removal.

The stable and slightly increased sulfate levels, from 179.22 mgS/L to 199.11 mgS/L,

indicate that the $H_2S$ is being actively oxidized, likely due to the combined presence of O and the mildly acidic conditions produced by nitrification. This oxidation results in a significant decrease in $H_2S$ concentration, from 20.49 mgS/L to 0.06 mgS/L, as it is consumed in the reaction and converted to $SO_4^{2-}$. This interplay between nitrification and sulfur oxidation highlights the aerobic reactor's effectiveness in removing both $NH_4^+$ and $H_2S$, leading to a more stable effluent with minimized $H_2S$ content, reduced odour, and increased $SO_4^{2-}$ levels.

Table 4.8 presents effluent results for the aerobic reactor from both the SANI pilot plant and the PWM_SA model.

Table 4.8 Measured versus predicted effluent results for the aerobic reactor.

| Parameters | SRUSB Effluent | |
|---|---|---|
| | SANI Pilot Plant | PWM_SA |
| TSS (mg/L) | - | 16.70 |
| VSS (mg/L) | 9 | 6.42 |
| Unfiltered COD (mgCOD/L) | 53.9 | 42.42 |
| Filtered COD (mgCOD/L) | 30.7 | 32.50 |
| $SO_4^{2-}$ (mgS/L) | 172.3 | 199.11 |
| $H_2S$ (mgS/L) | 0 | 0.60 |
| Unfiltered TKN (mgN/L) | 23.4 | 55.26 |
| Filtered TKN (mgN/L) | 23.2 | 54.12 |
| FSA (mgN/L) | 3.4 | 0.07 |
| $NO_3^-$ (mgN/L) | 16.8 | 15.25 |
| Unfiltered TP (mgP/L) | 5.6 | 6.52 |
| Filtered TP (mgP/L) | 5.6 | 6.36 |
| OP (mgP/L) | 5.3 | 6.06 |

The model predictions for unfiltered and filtered COD are relatively close to the measured values. The measured unfiltered COD was 53.9 mgCOD/L, while the model predicted 42.42 mgCOD/L, indicating a slight underestimation of organic matter in the effluent as shown in Figure 4.5. Similarly, the predicted filtered COD was 32.50 mgCOD/L, closely aligning with the measured value of 30.7 mgCOD/L, suggesting that the model rea-

sonably simulates COD removal, though it may slightly underrepresent particulate organic matter persistence in the effluent.

The discrepancies in S and TKN values align with adjustments made to the influent data to ensure that the model remains internally consistent with expected reactor outcomes. The model's prediction of $NO_3^-$ at 15.25 mgN/L closely matches the measured concentration of 16.8 mgN/L as presented in Figure 4.5, indicating that nitrification processes are well represented, despite deviations in other N species.

For P, the model demonstrates a relatively good match with measured values. The predicted unfiltered TP of 6.52 mgP/L and filtered TP of 6.36 mgP/L are slightly higher than the measured 5.6 mgP/L. Similarly, OP is predicted at 6.06 mgP/L compared to the measured 5.3 mgP/L, suggesting that the model simulates P transformations accurately, though it may overpredict P release or underpredict biomass uptake.

### 4.3.1 Mass balances

A comprehensive tracking of COD, N, P, and S through the aerobic reactor, outlining the distribution and transformations of each element as it moves through the reactor, is presented in the graphs in Figure 4.6. Additionally, Table 4.9 provides the model and measured mass balances for the aerobic reactor results.

The total COD influent was primarily driven by the influent $H_2S$ COD, along with contributions from UO and BO COD, as shown in Figure 4.6a. The BO COD was almost entirely consumed, with very minimal BO COD detected in the effluent, indicating efficient microbial oxidation and breakdown. The UO COD remained largely unchanged, and its concentration in the effluent closely matched its influent, confirming that this fraction was not degraded during the process and exited the reactor. A portion of the COD was reduced due to biomass degradation, and the influent $H_2S$ COD exited the reactor with very minimal changes. In this case, the biomass makes up part of the sludge mass (which also includes other particulate organics and inorganics). The biomass itself is made largely of

biodegradable particulate organics but also contains a small portion of nonbiodegradable organics known as endogenous residue. It also has some inorganic dissolved solids that precipitate as inorganic particulates during the drying stage of the ISS tests. The mass balance was successfully achieved, with all COD inputs accounted for through assimilation into biomass or exiting the system either as UO COD or as $H_2S$ COD in the effluent.

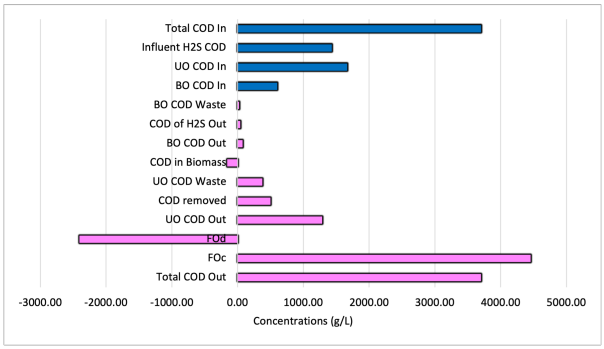


(a) COD tracking

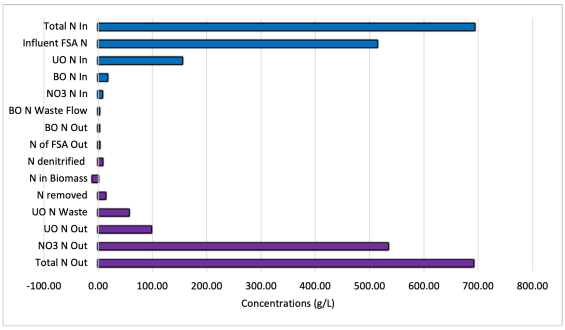


(b) N tracking.

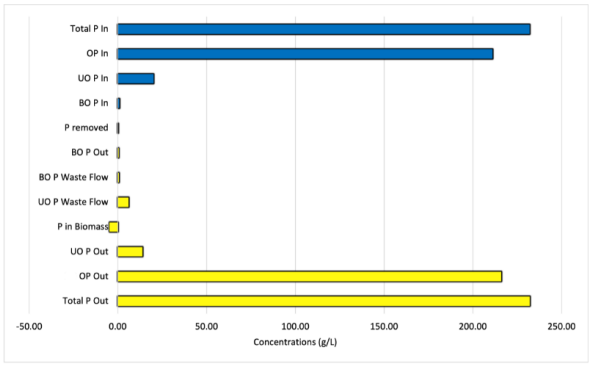


(c) P tracking

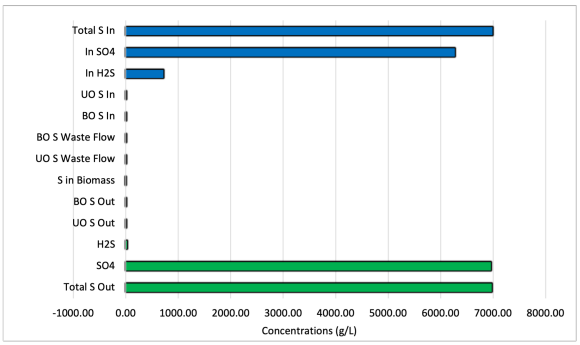


(d) S tracking

Figure 4.6 Comprehensive tracking of COD, N, S, and P through the aerobic reactor.

The total N influent was predominantly comprised of FSA, with additional contributions from UO N and smaller amounts of $NO_3^-$ and BO N, as depicted in Figure 4.6b. The influent FSA was almost completely oxidized to $NO_3^-$ through nitrification, which was evidenced by a large portion of the effluent consisting of $NO_3^-$. The majority of the BO N was consumed, with negligible amounts detected in the effluent, indicating efficient microbial utilization. As expected, the UO N remained largely unchanged, and the UO N in the effluent closely matched the influent concentration, demonstrating that this fraction

was not degraded. A small portion of N was incorporated into biomass, making the final effluent to primarily consist of UO N and $NO_3^-$, with minimal FSA remaining. The system achieved a 100% mass balance, ensuring that all N inputs were accounted for.

In Figure 4.6d, the total influent S primarily consisted of $SO_4^{2-}$ and $H_2S$, along with smaller contributions from UO and BO S. The influent $H_2S$ and $SO_4^{2-}$ remained relatively stable throughout the process, yielding an effluent S composition that primarily included slightly reduced amounts of $SO_4^{2-}$ and $H_2S$, with trace levels of UO S. The total S balance was maintained, with all S inputs accounted for through microbial degradation or remaining untransformed in the effluent.

Similar to the previous two reactors, the influent TP was predominantly composed of OP, with smaller contributions from UO and BO P. The BO P was efficiently consumed by microbial activity, leaving minimal amounts in the effluent. This was evidenced by the negligible concentrations of BO P in the waste flow and effluent. On the other hand, UO P remained mostly unchanged, and its concentration in the effluent closely matched the influent levels, confirming that this fraction was not degraded and exited the system unchanged. The remaining P in the effluent primarily consisted of OP, with smaller amounts of UO P. The TP mass balance was 100%, ensuring that all P inputs were accounted for through various pathways: biomass assimilation, breakdown of BO P, or remaining as UO P in the effluent.

The results presented in Table 4.9 demonstrate that the model maintains a high degree of internal consistency by achieving near-perfect mass balances. However, minor variations exist between the measured and predicted data. The predicted COD mass balance achieves 100%, while the measured COD mass balance of 98% indicates a similarly high level of accuracy with only minor deviations. This suggests that the PWM_SA model effectively captures the major COD transformations within the aerobic reactor. The significant discrepancy between the measured (210 gCOD/d) and predicted (1431 gCOD/d) influent $H_2S$ COD is due to initial adjustments made to maintain internal model consistency,

stemming from missing SRB kinetic parameters and other relevant experimental data.

The model predicts a N mass balance of 99%, closely aligning with the measured 100%. Both the S and P mass balances show perfect consistency between the measured and predicted values (100%), indicating that the model effectively simulates S and P transformations within the reactor.

Table 4.9 Comparison of predicted and measured data mass balances for the aerobic reactor. [46]

| **Parameters** | **Measured** | **PWM_SA** |
|---|---|---|
| COD (gCOD/d) | Influent COD = 1925<br>Influent $H_2S$ COD =210<br>Unfiltered COD out =1886<br>COD utilized in $SO_4$ production= 210 | Influent COD = 2271<br>Influent $H_2S$ COD = 1431<br>Unfiltered COD out =3659<br>COD exiting as $H_2S$ = 42 |
| **COD Mass Balance** | **98%** | **100%** |
| Nitrogen (gN/d) | Influent TKN =1327<br>Effluent TKN = 1407 | Influent TKN =691<br>Effluent TKN = 693 |
| **N Mass Balance** | **100%** | **100%** |
| Sulfur (gS/d) | Influent S = 6034<br>Effluent S = 6031 | Influent S =6975<br>Effluent S = 6987 |
| **S Mass Balance** | **100%** | **100%** |
| Phosphorus (gP/d) | Influent TP =199<br>Effluent TP =196 | Influent TP =237<br>Effluent TP = 237 |
| **S Mass Balance** | **100%** | **100%** |

Despite the discrepancies between the measured and predicted effluent data, the PWM _SA model remains internally consistent, achieving mass balance closures for COD, N, S, and P. This consistency enables effective nutrient tracking through the aerobic reactor, indicating that the model is a reliable tool for simulating key processes within the SANI system.

## 4.4 Overall presentation of results

The previous results chapters provided a detailed analysis of the individual reactors, focusing on the internal consistency of the model, mass balances, and a comparison with the

measured mass balances of the SANI system. The results showed that the model remained internally consistent across all three reactors, with near-perfect mass balances achieved for each. Table 4.10 presents the overall influent and effluent data for the system, encompassing all three reactors—SRUSB, anoxic, and aerobic.

Table 4.10 Influent versus effluent parameter concentrations for the PWM_SA.

| Parameters | SRUSB | | Anoxic | | Aerobic | |
|---|---|---|---|---|---|---|
| | Influent | Effluent | Influent | Effluent | Influent | Effluent |
| TSS (mg/L) | 280.19 | 128.29 | 48.57 | 49.27 | 49.27 | 16.70 |
| VSS (mg/L) | 186.19 | 42.76 | 16.80 | 21.17 | 20.59 | 6.42 |
| Unfiltered COD (mgCOD/L) | 439.22 | 147.75 | 72.50 | 65.94 | 78.88 | 42.42 |
| Filtered COD (mgCOD/L) | 157.90 | 81.18 | 46.40 | 32.82 | 46.80 | 32.50 |
| $SO_4^{2-}$ (mgS/L) | 195.70 | 57.59 | 158.70 | 107.65 | 179.22 | 199.11 |
| $H_2S$ (mgS/L) | 4.00 | 142.13 | 41.01 | 92.06 | 20.49 | 0.60 |
| Unfiltered TKN (mgN/L) | 66.13 | 65.02 | 58.04 | 58.66 | 57.52 | 55.26 |
| Filtered TKN (mgN/L) | 49.19 | 56.63 | 54.83 | 55.17 | 54.07 | 54.12 |
| FSA (mgN/L) | 44.80 | 53.40 | 15.30 | 14.64 | 14.69 | 0.07 |
| $NO_3^-$ (mgN/L) | 0.00 | 0.00 | 10.90 | 0.12 | 0.22 | 15.25 |
| Unfiltered TP (mgP/L) | 7.80 | 7.63 | 6.84 | 6.85 | 6.79 | 6.52 |
| Filtered TP (mgP/L) | 5.80 | 6.61 | 6.43 | 6.34 | 6.28 | 6.36 |
| OP (mgP/L) | 5.30 | 6.20 | 6.10 | 6.03 | 5.95 | 6.06 |

The processes in each reactor were analyzed individually. In the SRUSB reactor, sulfate reduction was the primary process, where $SO_4^{2-}$ was successfully reduced to $H_2S$, as reflected by the significant decrease in $SO_4^{2-}$ concentrations and a corresponding increase in $H_2S$ as shown in Figure 4.7.

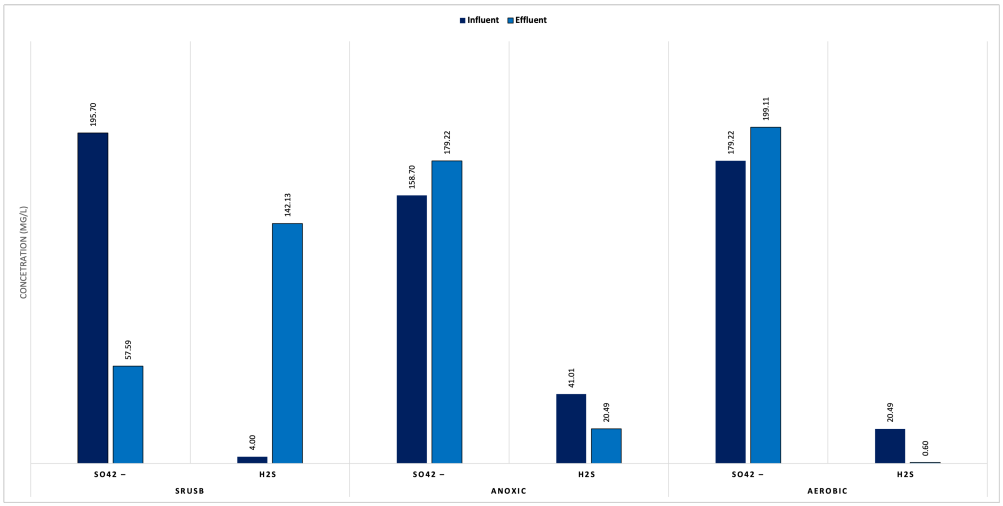


Figure 4.7 Sulfur distribution across the three reactors of the PWM_SA: Influent and Effluent $SO_4^{2-}$ and $H_2S$ Concentrations.

In the anoxic reactor, autotrophic denitrification occurred, reducing $NO_3^-$ to $N_2$ using $H_2S$ as an electron donor as illustrated in Figure 4.8. Finally, in the aerobic reactor, nitrification was dominant, effectively converting $NH_4^+$ to $NO_3^-$. These results confirm the model's accuracy in capturing the key biological processes within each reactor.

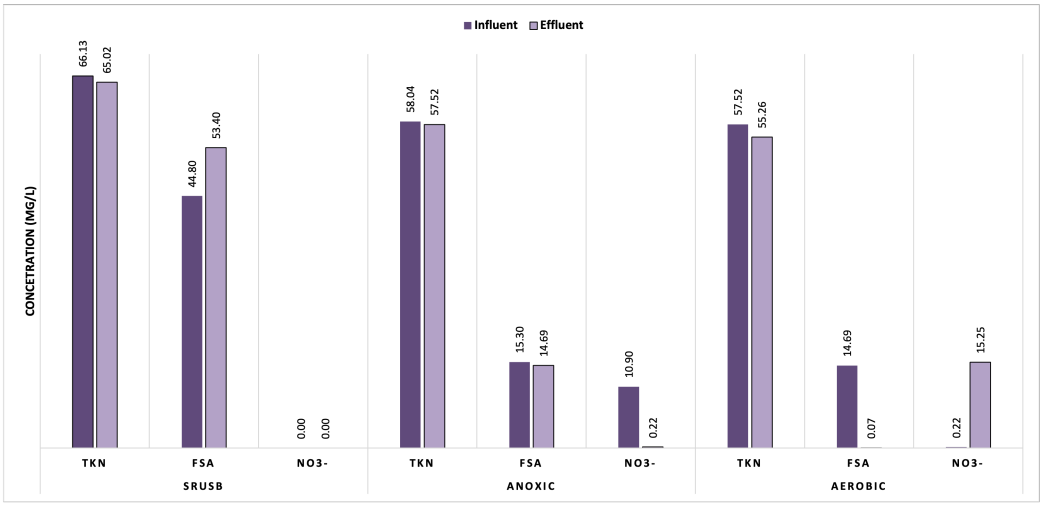


Figure 4.8 Nitrogen distribution across the three reactors of the PWM_SA: Influent and effluent TKN, $NH_4^+$ and $NO_3^-$ Concentrations.

This indicates effective physical and biological treatment processes, with the aerobic reactor playing a crucial role in final solids removal. The COD also exhibits significant

reductions, particularly for unfiltered COD, which drops from 439.22 mgCOD/L in the SRUSB influent to 42.42 mgCOD/L in the aerobic effluent.

Phosphorus removal is limited, as evidenced by the minor reductions in TP across the three reactors, with the concentration decreasing from 7.80 mgP/L in the SRUSB influent to 6.52 mgP/L in the aerobic reactor effluent. This is in line with the expected results as P removal processes are not a major focus of the current system.

### 4.4.1 Mass Balances

Table 4.11 presents the predicted and measured data mass balances of the overall system, and Figure 4.10 illustrates the distribution and transformations of COD, N, S, and P throughout the entire system. The influent COD mainly consisted of BO and UO COD, and a small fraction of COD from $H_2S$. During the treatment process, most of the BO COD was effectively broken down and used for biomass growth, and transformed into $H_2S$ during BSR in the SRUSB, resulting in a very small predicted BO COD in the effluent. The UO COD remained largely unchanged, with UO COD effluent concentrations closely matching the influent, confirming that this fraction was not degraded and exits the system with the effluent. The effluent COD then contains COD conserved in biomass, a large portion of COD from $H_2S$, and UO COD. The COD mass balance is 100% as shown in Table 4.11, which means that the system is internally consistent in tracking COD.

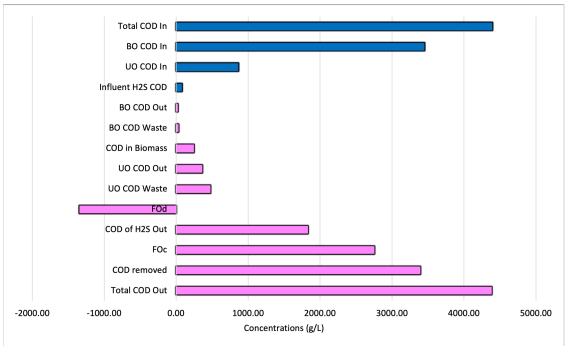


(a) COD tracking

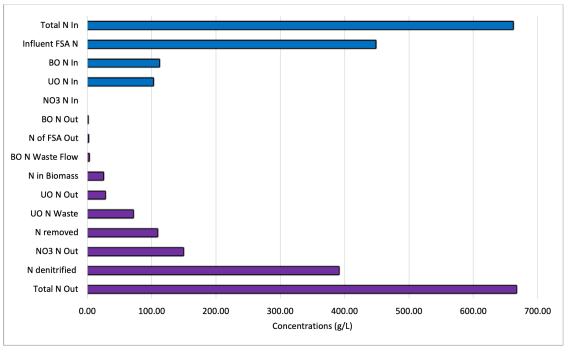


(b) N tracking.

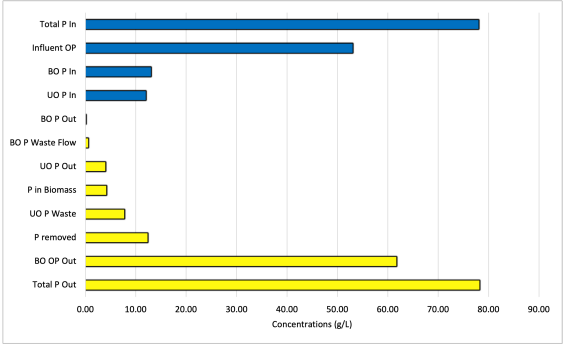


(c) P tracking

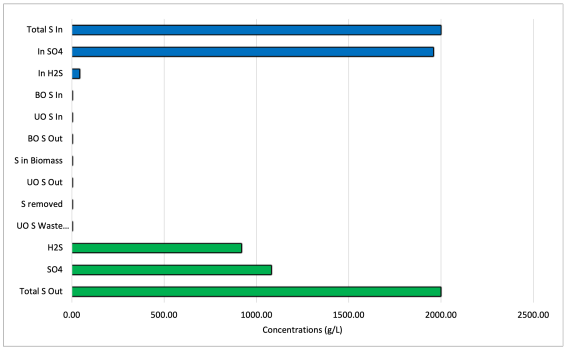


(d) S tracking

Figure 4.9 Comprehensive tracking of COD, N, S, and P throughout the entire system.

Figure 4.9b illustrates N tracking throughout the system, where the total influent N consists of FSA, BO, and UO N, with no $NO_3^-$ present initially. During nitrification, nearly all the FSA was oxidized to $NO_3^-$ in the aerobic reactor, as evidenced by the very low FSA concentration in the effluent and the presence of $NO_3^-$. Additionally, a significant portion of the $NO_3^-$ was reduced to $N_2$ through denitrification, reflected by the substantial amount of N denitrified in the effluent.

The BO N was utilized for biomass growth, while the UO N remained unchanged and exited in the effluent. The N mass balance for the entire system is 100%, as all influent N is accounted for in the effluent—either as $NO_3^-$, denitrified N, released N, or unchanged UO N.

With regard to S, the total influent into the system primarily consisted of $SO_4^{2-}$, along with a small amount of $H_2S$ and trace concentrations of BO and UO S. The majority of the $SO_4^{2-}$ is reduced to $H_2S$ during BSR in the SRUSB, resulting in a significant amount of $H_2S$

being released in the effluent as shown in Figured 4.9d. Additionally, a substantial portion of the $SO_4^{2-}$ is also found in the effluent due to the oxidation of $H_2S$ back to $SO_4^{2-}$ during autotrophic denitrification in the anoxic reactor. The S mass balance is 100%, indicating that all influent S is accounted for either as $H_2S$ released or $SO_4^{2-}$ remaining in the effluent, reflecting complete tracking of S transformations within the system.

The changes in TP and OP in each reactor have remained relatively stable. The TP in the overall system predominantly consisted of OP, with smaller contributions from BO and UO P. The UO P remained unchanged and exited with the effluent, while the BO P was degraded, with a portion being utilized in biomass and the remainder released as OP. This is reflected by a slight increase in the OP concentration in the effluent as shown in Figure 4.9c. The P mass balance shows that all influent P is fully accounted for in the effluent, achieving a 100% balance.

The overall mass balances of COD, N, S, and P across the three reactors demonstrate the model's efficacy in replicating the processes observed in the SANI pilot plant. The total influent COD that entered the system was 4392 gCOD/d, comprising 3449 gCOD/d from BO, 863 gCOD/d from UO, and an additional 80 gCOD/d attributed to $H_2S$ in the SRUSB reactor. The effluent data reveal a total COD outflow of 3536 gCOD/d, with 22 gCOD/d from BO and 365 gCOD/d from UO. Additionally, 3397 gCOD/d was effectively removed throughout the system, indicating successful treatment. The model achieves a 100% COD mass balance, confirming its ability to accurately track COD transformations and removals. In contrast, the actual SANI pilot plant reported only 71%, suggesting potential discrepancies in measurement.

Table 4.11 Comparison of predicted and measured data mass balances of the overall system.

| Parameters | Biodegradable Organics (BO) | Unbiodegradable Organics (UBO) |
|---|---|---|
| COD (gCOD/d) | COD In = 3449<br>Influent $H_2S$ COD = 80<br>BO COD Out = 22<br>BO COD Waste = 30<br>COD removed = 3397<br>COD of $H_2S$ Out = 14<br>COD in Biomass = 305<br>FOc = 4493<br>FOd = -1327<br>Total COD out = 3536 | COD In = 863<br>COD Out = 365<br>COD Waste = 510 |
| **COD Mass Balance %** | **100%** | |
| **SANI Pilot Plant** | **71%** | |
| N (gN/d) | BO N In = 111<br>NO3 N In = 0<br>Influent FSA N = 448<br>BO N out = 0.55<br>N Waste Flow = 1.99<br>N removed = 109<br>N of FSA Out = 1.13<br>N in Biomass = 32<br>NO3 N out = 152<br>Total N out = 579 | N In = 102<br>N Out = 28<br>N Waste = 72 |
| **N Mass Balance %** | **100** | |
| **SANI Pilot Plant** | **97%** | |
| S (gS/d) | BO S In = 0.329<br>$H_2S$ and $SO_4$ In = 1997.05<br>BO S Out = 0.0016<br>BO S Waste Flow = 0.00<br>S removed = 0.32<br>$H_2S$ and $SO_4$ Out = 1996.85<br>S in Biomass = 0.0229<br>Total S out = 1996.90 | UO S In = 0.085<br>UO S Out = 0.036<br>UO S Waste Flow = 0.05 |
| **S Mass Balance %** | **100** | |
| **SANI Pilot Plant** | **86%** | |
| P (gP/d) | BO P In = 12.99<br>Influent OP = 52.99<br>BO P Out = 0.09<br>P Waste Flow = 0.49<br>P removed = 12.42<br>OP Out = 60.59<br>P in Biomass = 0.028<br>Total P out = 66.31 | UO P In = 11.99<br>P Out = 3.95<br>P Waste = 7.76 |
| **P Mass Balance %** | **100** | |
| **SANI Pilot Plant** | **79%** | |

In terms of N, the total influent comprised 661 gN/d, which included 111 gN/d from

BO, 102 gN/d from UO, and 448 gN/d from influent FSA. The system's effluent N totals 568 gN/d, predominantly in the form of $NO_3^-$, with an N removal of 109 gN/d primarily attributed to autotrophic denitrification and nitrification. The model maintains a 100% N mass balance, showcasing its capability to accurately replicate the N processes present in the SANI system. The SANI pilot plant closely mirrors this performance, achieving a 97% N balance.

Regarding S, the total influent included 1997.05 gS/d, predominantly from $SO_4^{2-}$ and $H_2S$. The effluent reflects 1996.85 gS/d remaining as $H_2S$ and $SO_4^{2-}$, with only 0.32 gS/d of S removed across the reactors. The model achieves a 100% S mass balance, indicating effective replication of sulfate reduction processes within the SRUSB reactor. While the SANI pilot plant reports an 86% S balance, it suggests potential losses or transformations that the model may not fully account for.

In summary, the comprehensive tracking of COD, N, S, and P mass balances across all three reactors demonstrates the model's efficiency in replicating the internal dynamics of the SANI pilot plant. The achievement of 100% mass balances in the model emphasizes its accuracy in reflecting the biological processes involved. While the actual SANI system shows some discrepancies, the model's performance offers a reliable framework for understanding and optimizing treatment processes, reinforcing its utility in future research and application. The mass balance of 100% does not necessarily imply that the system is performing well. It simply showcases how well the components being tracked in the system are accounted for, whereby a good mass balance shows that they are well accounted for and hence confidence can be placed in the results. In mathematical models the mass balance must be at 100% because the confidence in the capability for the model to predict an outcome is based on this principle.

# Chapter 5: Conclusions

The primary objectives of this study focused on extending and verifying the PWM _SA to incorporate the unique bioprocesses of the SANI system. This integration required the inclusion of sulfate reduction, autotrophic denitrification, and nitrification processes, tailored to reflect the complex reactions occurring within the SRUSB, anoxic, and aerobic reactors. The study also aimed to ensure the model's internal consistency by conducting comprehensive mass balance checks on key elements, including COD, N, P, and S, as well as on COD and ionic charges, to verify that each bioprocess maintained a complete elemental balance. Additionally, a detailed characterization of the influent parameters and operational conditions from the Hong Kong SANI pilot plant was conducted, establishing a foundational dataset for rigorous verification of the model's performance under real-world conditions.

The research demonstrated that integrating the SANI processes into the PWM _SA was both feasible and effective. This integration allowed the model to simulate the essential treatment processes and successfully capture complex biochemical interactions within the SANI system, aligning closely with real-world data from the Hong Kong pilot plant, thereby validating its utility in representing saline wastewater treatment dynamics.

The model achieved a high degree of mass balance accuracy across crucial parameters, including COD, N, P, and S, confirming its reliability. With a COD mass balance reaching 100%, the model effectively tracked organic matter transformations, while N and S also demonstrated complete mass balances.

A significant outcome of the model was its ability to predict reductions in effluent contaminants effectively. The model simulated substantial decreases in $H_2S$ concentrations, attributed to the efficient sulfate reduction processes within the SRUSB. Furthermore, the aerobic reactor successfully facilitated nitrification, converting nearly all influent FSA to $NO_3^-$, which aligns with observed treatment outcomes and verifies the model's predictive

capabilities regarding N transformations. The findings underscore the importance of reliable experimental data for accurate modelling and calibration, especially in systems where competitive microbial processes, such as sulfate reduction and methanogenesis, play significant roles. Overall, this research contributes to the refinement of saline wastewater treatment models and lays a foundation for future studies aimed at improving the predictive accuracy of process simulations and enhancing resource recovery strategies in decentralized systems.

Finally, this study verified the extended PWM _SA model as a promising tool for addressing saline wastewater treatment challenges in South Africa. These findings establish the model as a valuable framework for advancing saline wastewater treatment practices within the unique environmental context of South Africa.

# Future recommendations

- The kinetics of autotrophic and heterotrophic denitrifiers (which collaborate to remove nitrates) could be explored in further studies towards calibration of the model to predict anoxic solids concentrations while accounting for varying sources and concentration of carbon and $H_2S$ in the anoxic influent.

- The absence of experimental OUR data hindered the accuracy of the COD balance in this study. It is recommended that future work includes comprehensive OUR measurements alongside other key parameters such as TSS, which are critical for calculating accurate SRTs.

- The current steady-state model, though effective for calibration, could be further refined to provide instantaneous results and explicit links between variables and parameters. A refined MS Excel model would allow for quicker calibration and adjustments, offering a more streamlined approach to steady-state and dynamic modelling of the SANI system.

- Given the limitations in available kinetic data for sulfide-reducing biomass in anaerobic digesters, future research should focus on acquiring and validating kinetic parameters specific to sulfidogenic organisms in saline wastewater environments. Comparative studies with existing data could help fine-tune these kinetics for a more accurate model. Future studies should focus on refining dynamic simulation models using more accurate solvers, such as the Runge-Kutta method. While slower, this approach would enhance simulation accuracy and better capture the complex kinetics of sulfate reduction and methanogenesis in anaerobic environments. Furthermore, more studies should be conducted to gather kinetic data specific to the competition between sulfide-reducing and methanogenic microorganisms in anaerobic digesters.[56,18]

- The incorporation of seawater flushing into decentralized sanitation systems presents a unique opportunity for resource recovery in South Africa. Future studies should explore the feasibility of scaling up this approach in both rural and urban settings, focusing on the potential for reusing treated seawater and groundwater for non-potable applications such as toilet flushing. Additionally, research should assess the economic and environmental benefits of resource recovery from saline wastewater, particularly in the context of circular economy initiatives.

By addressing these recommendations, future research can enhance the robustness and applicability of saline wastewater treatment models, ultimately leading to more sustainable and efficient wastewater management solutions in both coastal and inland communities in South Africa.

# References


1. Ahmadian, F., Rahmani Sani, A., Soltani, S. and Kowsari, M. H. 2022, 'Study of wastewater treatment efficiency by trickling filter method using solar power energy', *Journal of Sabzevar University of Medical Sciences* **29**(2), 303–317.

2. Batstone, D. J., Keller, J., Angelidaki, I., Kalyuzhnyi, S., Pavlostathis, S., Rozzi, A., Sanders, W., Siegrist, H. a. and Vavilin, V. 2002, 'The iwa anaerobic digestion model no 1 (adm1)', *Water Science and technology* **45**(10), 65–73.

3. Brouckaert, C., Ikumi, D. and Ekama, G. 2010, Modelling of anaerobic digestion for incorporation into a plant-wide wastewater treatment model, *in* 'WISA Biennial Conference', pp. 18–22.

4. Brun, R., Kühni, M., Siegrist, H., Gujer, W. and Reichert, P. 2002, 'Practical identifiability of asm2d parameters—systematic selection and tuning of parameter subsets', *Water research* **36**(16), 4113–4127.

5. Bryers, J. 1985, 'Structured modeling of the anaerobic digestion of biomass particulates', *Biotechnology and bioengineering* **27**(5), 638–649.

6. Cao, S., Sun, G., Zhang, Z., Chen, L., Feng, Q., Fu, B., McNulty, S., Shankman, D., Tang, J., Wang, Y. et al. 2011, 'Greening china naturally', *Ambio* **40**, 828–831.

7. Chen, G.-H., van Loosdrecht, M. C., Ekama, G. A. and Brdjanovic, D. 2020, *Biological wastewater treatment: principles, modeling and design*, IWA publishing.

8. Chrispim, M. C., Scholz, M. and Nolasco, M. A. 2019, 'Phosphorus recovery from municipal wastewater treatment: Critical review of challenges and opportunities for developing countries', *Journal of environmental management* **248**, 109268.

9. Corominas, L., Rieger, L., Takács, I., Ekama, G., Hauduc, H., Vanrolleghem, P. A., Oehmen, A., Gernaey, K. V., van Loosdrecht, M. C. and Comeau, Y. 2010, 'New framework for standardized notation in wastewater treatment modelling', *Water Science and Technology* **61**(4), 841–857.

10. Daelman, M. R., van Voorthuizen, E. M., van Dongen, U. G., Volcke, E. I. and van Loosdrecht, M. C. 2012, 'Methane emission during municipal wastewater treatment', *Water research* **46**(11), 3657–3670.

11. Daelman, M., van Voorthuizen, E. M., Van Dongen, L., Volcke, E. and Van Loosdrecht, M. 2013, 'Methane and nitrous oxide emissions from municipal wastewater treatment–results from a long-term study', *Water Science and technology* **67**(10), 2350–2355.

12. Daigger, G. T. 2014, 'Oxygen and carbon requirements for biological nitrogen removal processes accomplishing nitrification, nitritation, and anammox', *Water Environment Research* **86**(3), 204–209.

13. Dold, P., Ekama, G. et al. 1981, A general model for the activated sludge process, *in* 'Water pollution research and development', Elsevier, pp. 47–77.

14. Droste, R. L. and Gehr, R. L. 2018, *Theory and practice of water and wastewater treatment*, John Wiley & Sons.

15. du Plessis, A. and du Plessis, A. 2019, 'Evaluation of southern and south africa's freshwater resources', *Water as an Inescapable Risk: Current Global Water Availability, Quality and Risks with a Specific Focus on South Africa* pp. 147–172.

16. Eastman, J. A. and Ferguson, J. F. 1981, 'Solubilization of particulate organic carbon during the acid phase of anaerobic digestion', *Journal (Water Pollution Control Federation)* pp. 352–366.

17. Ekama, G. A. 2015, 'Recent developments in biological nutrient removal', *Water SA* **41**(4), 515–524.

18. Ekama, G. A. 2021, 'Optimizing water and resource recovery facilities (wrrf) for energy generation without compromising effluent quality', *Water SA* **47**(2), 141–153.

19. Ekama, G. A. and Wentzel, M. C. 2008*a*, 'Nitrogen removal', *Biological wastewater treatment: principles, modelling and design* pp. 87–138.

20. Ekama, G. A. and Wentzel, M. C. 2008*b*, 'Organic matter removal', *Biological Wastewater Treatment: Principles, Modelling and Design. IWA Publishing, London* pp. 53–86.

21. Ekama, G. and Wentzel, M. 2004, 'A predictive model for the reactor inorganic suspended solids concentration in activated sludge systems', *Water Research* **38**(19), 4093–4106.

22. Ekama, G. and Wentzel, M. n.d., 'Aerobic digestion of waste activated and primary sludges'.

23. Eliosov, B. and Argaman, Y. 1995, 'Hydrolysis of particulate organics in activated sludge systems', *Water Research* **29**(1), 155–163.

24. Flores-Alsina, X., Ramin, E., Ikumi, D., Harding, T., Batstone, D., Brouckaert, C., Sotemann, S. and Gernaey, K. V. 2021, 'Assessment of sludge management strategies in wastewater treatment systems using a plant-wide approach', *Water Research* **190**, 116714.

25. Foladori, P., Andreottola, G. and Ziglio, G. 2010, *Sludge reduction technologies in wastewater treatment plants*, IWA publishing.

26. Ghoor, T. 2019, 'Developments in anaerobic digestion modelling'.

27. Gujer, W. and Zehnder, A. J. 1983, 'Conversion processes in anaerobic digestion', *Water science and technology* **15**(8-9), 127–167.

28. Gupta, A. K., Majumder, A. and Ghosal, P. S. 2022, 'Introduction to modular wastewater treatment system and its significance', *Modular Treatment Approach for Drinking Water and Wastewater* p. 81–106.

29. Han, Y.-L., Zhang, X.-Z., Liu, H.-B., Rittmann, B. E. and Zhao, H.-P. 2023, 'Novel sulfate reduction coupled to simultaneous nitrification and autotrophic denitrification process for removing nitrogen and organics from saline wastewater', *Environmental Science & Technology* **57**(29), 10733–10744.

30. Hauduc, H., Rieger, L., Takács, I., Héduit, A., Vanrolleghem, P. and Gillot, S. 2010, 'A systematic approach for model verification: application on seven published activated sludge models', *Water Science and Technology* **61**(4), 825–839.

31. Henze, M., Gujer, W., Mino, T., Matsuo, T., Wentzel, M. and Marais, G. 1995, 'Wastewater and biomass characterization for the activated sludge model no. 2: biological phosphorus removal', *Water Science and Technology* **31**(2), 13–23.

32. Henze, M. and Harremoës, P. 1983, 'Anaerobic treatment of wastewater in fixed film reactors–a literature review', *Water science and technology* **15**(8-9), 1–101.

33. Henze, M., van Loosdrecht, M. C., Ekama, G. A. and Brdjanovic, D. 2008, *Biological wastewater treatment*, IWA publishing.

34. Ikumi, D. and Harding, T. 2020, 'Kinetics of biological and chemical processes in anoxic-aerobic digestion of phosphorus rich waste activated sludge', *Water Research* **170**, 115333.

35. Ikumi, D. S. 2011, 'The development of a three phase plant-wide mathematical model for sewage treatment'.

36. Jenicek, P., Koubova, J., Bindzar, J. and Zabranska, J. 2010, 'Advantages of anaer-

obic digestion of sludge in microaerobic conditions', *Water Science and Technology* **62**(2), 427–434.

37. Jenkins, D. and Wanner, J. 2014, *Activated sludge-100 years and counting*, IWA publishing.

38. Kalyuzhnyi, S., Fedorovich, V., Lens, P., Hulshoff Pol, L. and Lettinga, G. 1998, 'Mathematical modelling as a tool to study population dynamics between sulfate reducing and methanogenic bacteria', *Biodegradation* **9**, 187–199.

39. Khan, N. A., Ullah Khan, S., Ahmed, S., Farooqi, I. H., Hussain, A., Vambol, S. and Vambol, V. 2020, 'Smart ways of hospital wastewater management, regulatory standards and conventional treatment techniques: A short review', *Smart and Sustainable Built Environment* **9**(4), 727–736.

40. Levenspiel, O. 1972, 'Experimental search for a simple rate equation to describe deactivating porous catalyst particles', *Journal of Catalysis* **25**(2), 265–272.

41. Loubser, C., Chimbanga, B. M. and Jacobs, H. 2021, 'Intermittent water supply: a south african perspective', *Water SA* **47**(1), 1–9.

42. Lu, H. 2011, *Evaluation of the sulfate reduction-autotrophic denitrification-nitrification integrated (SANI) process for saline wastewater treatment*, Hong Kong University of Science and Technology (Hong Kong).

43. Lu, H., Ekama, G. A., Wu, D., Feng, J., Van Loosdrecht, M. C. and Chen, G.-H. 2012, 'Sani® process realizes sustainable saline sewage treatment: steady state model-based evaluation of the pilot-scale trial of the process', *water research* **46**(2), 475–490.

44. Lu, H., Wang, J., Li, S., Chen, G.-H., van Loosdrecht, M. C. and Ekama, G. A. 2009, 'Steady-state model-based evaluation of sulfate reduction, autotrophic denitrification and nitrification integrated (sani) process', *water research* **43**(14), 3613–3621.

45. Lu, H., Wu, D., Jiang, F., Ekama, G. A., Van Loosdrecht, M. C. and Chen, G.-H. 2012, 'The demonstration of a novel sulfur cycle-based wastewater treatment process: Sulfate reduction, autotrophic denitrification, and nitrification integrated (sani®) biological nitrogen removal process', *Biotechnology and Bioengineering* **109**(11), 2778–2789.

46. Lu, H., Wu, D., Tang, D. T., Chen, G., van Loosdrecht, M. C. and Ekama, G. 2011, 'Pilot scale evaluation of sani® process for sludge minimization and greenhouse gas reduction in saline sewage treatment', *Water Science and Technology* **63**(10), 2149–2154.

47. McCarty, P. and Mosey, F. 1991, 'Modelling of anaerobic digestion processes (a discussion of concepts)', *Water science and technology* **24**(8), 17–33.

48. Monod, J. 1949, 'The growth of bacterial cultures', *Annual review of microbiology* **3**(1), 371–394.

49. Moosbrugger, R., Wentzel, M., Ekama, G. and Marais, G. v. R. 1993, 'A 5 ph point titration method for determining the carbonate and scfa weak acid/bases in anaerobic systems', *Water Science and Technology* **28**(2), 237–245.

50. Musingafi, M. C. C. 2014, 'Fresh water sources pollution: a human related threat to fresh water security in south africa'.

51. Nkosi, M., Mathivha, F. I. and Odiyo, J. O. 2021, 'Impact of land management on water resources, a south african context', *Sustainability* **13**(2), 701.

52. Ødegaard, H. 2006, 'Innovations in wastewater treatment:–the moving bed biofilm process', *Water science and technology* **53**(9), 17–33.

53. Parkin, G. F. and McCarty, P. L. 1981, 'A comparison of the characteristics of soluble organic nitrogen in untreated and activated sludge treated wastewaters', *Water Research* **15**(1), 139–149.

54. Pavlostathis, S. and Giraldo-Gomez, E. 1991, 'Kinetics of anaerobic treatment: a critical review', *Critical Reviews in Environmental Science and Technology* **21**(5-6), 411–490.

55. Pérez-Elvira, S., Nieto Diez, P. and Fdz-Polanco, F. 2006, 'Sludge minimisation technologies', *Reviews in Environmental Science and Bio/Technology* **5**, 375–398.

56. Poinapen, J. and Ekama, G. 2010, 'Biological sulphate reduction with primary sewage sludge in an upflow anaerobic sludge bed reactor–part 6: Development of a kinetic model for bsr', *Water Sa* **36**(3), 203–214.

57. Preisner, M., Neverova-Dziopak, E. and Kowalewski, Z. 2020, 'An analytical review of different approaches to wastewater discharge standards with particular emphasis on nutrients', *Environmental Management* **66**(4), 694–708.

58. Pronk, M., De Kreuk, M., De Bruin, B., Kamminga, P., Kleerebezem, R. v. and Van Loosdrecht, M. 2015, 'Full scale performance of the aerobic granular sludge process for sewage treatment', *Water research* **84**, 207–217.

59. Qian, J., Jiang, F., Chui, H. K., van Loosdrecht, M. C. and Chen, G. 2013, 'Industrial flue gas desulfurization waste may offer an opportunity to facilitate sani® application for significant sludge minimization in freshwater wastewater treatment', *Water science and technology* **67**(12), 2822–2826.

60. Qian, J., Wei, L., Liu, R., Jiang, F., Hao, X. and Chen, G.-H. 2016, 'An exploratory study on the pathways of cr (vi) reduction in sulfate-reducing up-flow anaerobic sludge bed (uasb) reactor', *Scientific reports* **6**(1), 23694.

61. Ramin, E., Flores-Alsina, X., Gaszynski, C., Harding, T., Ikumi, D., Brouckaert, C., Brouckaert, B., Modiri, D., Al, R., Sin, G. et al. 2022, 'Plant-wide assessment of alternative activated sludge configurations for biological nutrient removal under uncertain influent characteristics', *Science of The Total Environment* **822**, 153678.

62. Rao, D. G., Senthilkumar, R., Byrne, J. A. and Feroz, S. 2012, *Wastewater treatment: advanced processes and technologies*, CRC Press.

63. Rojas, M. R., Leung, C., Bonk, F., Zhu, Y., Edwards, L., Arnold, R. G., Sáez, A. E. and Klečka, G. 2013, 'Assessment of the effectiveness of secondary wastewater treatment technologies to remove trace chemicals of emerging concern', *Critical reviews in environmental science and technology* **43**(12), 1281–1314.

64. S.Ahmed, A. 2013, 'Additional processes in prearation tank and primary settling tank for wastewater treatment using laboratory unit', *Engineering and Technology Journal* **31**(4 B), 410–418.

65. Shahot, K., Idris, A., Omar, R. and Yusoff, H. M. 2014, 'Review on biofilm processes for wastewater treatment', *Life Sci J* **11**(11), 1–13.

66. Siebritz, I., Ekama, G. and Marais, G. v. R. 1983, 'A parametric model for biological excess phosphorus removal', *Water Science and Technology* **15**(3-4), 127–152.

67. Sonune, A. and Ghate, R. 2004, 'Developments in wastewater treatment methods', *Desalination* **167**, 55–63.

68. Sotemann, S., Ristow, N., Wentzel, M. and Ekama, G. 2005, 'A steady state model for anaerobic digestion of sewage sludges', *Water SA* **31**(4), 511–528.

69. Sotemann, S., Van Rensburg, P., Ristow, N., Wentzel, M., Loewenthal, R. and Ekama, G. 2005, 'Integrated chemical/physical and biological processes modelling: part 2-anaerobic digestion of sewage sludges', *Water Sa* **31**(4), 545–568.

70. Stumm, W. and Morgan, J. 1996, 'Water chemistry', *Encyclopedia of Environmental science* **3**, 1142–1161.

71. Subtil, E. L., Cassini, S. T. A. and Gonçalves, R. F. 2012, 'Sulfate and dissolved sulfide variation under low cod/sulfate ratio in up-flow anaerobic sludge blanket (uasb) treating domestic wastewater', *Revista Ambiente & Água* **7**, 130–139.

72. Tillman, G. M. 1991, *Primary treatment at wastewater treatment plants*, CRC Press.

73. Vaiopoulou, E. and Aivasidis, A. 2008, 'A modified uct method for biological nutrient removal: Configuration and performance', *Chemosphere* **72**(7), 1062–1068.

74. Van Loosdrecht, M. C., Ekama, G. A., Wentzel, M., Brdjanovic, D. and Hooijmans, C. M. 2008, 'Modelling activated sludge processes', *Biological Wastewater Treatment. Principles, Modelling and Design, eds M. Henze, MC M. van Loosdrecht, GA Ekama, MC Wentzel, D. Brdjanovic (ondon: IWA Publishing)* **361**.

75. Van Zyl, P., Wentzel, M., Ekama, G. and Riedel, K. 2008, 'Design and start-up of a high rate anaerobic membrane bioreactor for the treatment of a low ph, high strength, dissolved organic waste water', *Water Science and Technology* **57**(2), 291–295.

76. Vanhooren, H., Meirlaen, J., Amerlinck, Y., Claeys, F., Vangheluwe, H. and Vanrolleghem, P. A. 2003, 'West: modelling biological wastewater treatment', *Journal of Hydroinformatics* **5**(1), 27–50.

77. Vanrolleghem, P. A., Benedetti, L. and Meirlaen, J. 2005, 'Modelling and real-time control of the integrated urban wastewater system', *Environmental Modelling & Software* **20**(4), 427–442.

78. Wang, J., Lu, H., Chen, G.-H., Lau, G. N., Tsang, W. and Van Loosdrecht, M. C. 2009, 'A novel sulfate reduction, autotrophic denitrification, nitrification integrated (sani) process for saline wastewater treatment', *Water research* **43**(9), 2363–2372.

79. Wu, D., Ekama, G. A., Chui, H.-K., Wang, B., Cui, Y.-X., Hao, T.-W., van Loosdrecht, M. C. and Chen, G.-H. 2016, 'Large-scale demonstration of the sulfate reduction au-

totrophic denitrification nitrification integrated (sani®) process in saline sewage treatment', *Water research* **100**, 496–507.

80. Xiaoxin, Z., Jin, H., Ling, L., Shuming, L., Yueping, W. and Xinheng, Z. 2019, Research on standards and regulations of the operation of wastewater treatment plants, *in* 'IOP Conference Series: Earth and Environmental Science', Vol. 267, IOP Publishing, p. 032028.

81. Zhou, S., Wang, J., Peng, S., Chen, T. and Yue, Z. 2021, 'Anaerobic co-digestion of landfill leachate and acid mine drainage using up-flow anaerobic sludge blanket reactor', *Environmental Science and Pollution Research* **28**, 8498–8506.

# Supplementary Data

The supplementary data accompanying this study provides detailed insights into the modelling framework and analyses underpinning the research. The file includes comprehensive datasets across several sheets. The "Introduction and Model Components" sheet outlines the foundational elements of the PWM_SA model, while the ADM3P and ASM2-3P sheets provide detailed parameter definitions, stoichiometric and kinetic parameters, processes, and mass balance verification, as well as values critical for anaerobic digestion and activated sludge modelling. Additionally, the "Preprocessor" sheet presents the modelling results, including flow rates, effluent concentrations, and other key measurements. This supplementary data supports and verifies the findings of this study.

The supplementary data for this study can be accessed at the following link: UCT PWM _SA SANI model Gujer matrix.